Journal of Energy Storage 160 (2026) 121797

Contents lists available at ScienceDirect

Journal of Energy Storage

journal homepage: www.elsevier.com/locate/est

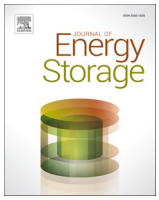

Review Article

A comparative study of the modified high voltage olivine-phosphate $LiMPO_4$ (M = Fe, Mn, Co, Ni) as promising cathode materials for next-generation rechargeable batteries

Theodore Azemtsop Manfo [a,*], Hannu Laaksonen [a]

[a] Department of Electrical Engineering and Energy Technology, School of Technology and Innovations, University of Vaasa, Wolffintie 32, 65200, Vaasa, Finland

ARTICLE INFO

Keywords:
$LiMPO_4$
Olivine cathodes
Lithium-ion batteries
High-voltage energy storage
Surface engineering
Solid-state batteries

ABSTRACT

The growing demand for energy storage has driven extensive research into advanced cathode materials for lithium-ion batteries (LIBs), where cathode chemistry critically governs safety, cost, and electrochemical performance. Olivine lithium metal phosphates ($LiMPO_4$) are promising cathode candidates due to their structural robustness and thermal stability. Rietveld refinement confirms an orthorhombic olivine structure (Pnma), with lithium occupying octahedral sites and Mn^{2+} and Co^{2+} substituting for Fe^{2+}. Cell parameters and unit-cell volume increase with Mn substitution; while $LiFePO_4$ (LFP) exhibits favorable electrochemical stability, $LiMnPO_4$ (LMP) offers higher operating potential but suffers from sluggish lithium intercalation kinetics. Recent studies demonstrate that partial substitution with Co and Ni can significantly enhance electrochemical performance by modifying lithium diffusion pathways and energetics within the olivine framework. This paper summarizes recent progress on olivine cathodes, including $LiCoPO_4$ (LCP) and $LiNiPO_4$ (LNPO), which exhibit operating potentials exceeding 5.0 V versus Li^+/Li. Strategies to overcome intrinsic limitations, such as particle size reduction, surface modification, and cation doping, are critically discussed, highlighting clear correlations between structure and electrochemical behavior. Key material descriptors, including cohesive energy, lithium intercalation energetics, and electrochemical stability, are examined. Finally, emerging opportunities and remaining challenges for olivine phosphates in solid-state and aqueous energy storage systems are outlined, providing a forward-looking perspective for next-generation LIB development.

1. Introduction

Progress in LIB technology is closely tied to understanding the electronic, chemical, and structural evolution of battery components during charge–discharge cycling [1]. Improvements in energy density are primarily achieved through the development of high-voltage cathodes, advanced anode materials, and optimized electrodes. Since Sony commercialized the first LIB nearly three decades ago, these batteries have come to dominate the advanced energy storage market due to their widespread use in electronics, electric vehicles, and grid-scale systems [2–4]. Owing to lithium's high reduction potential and low atomic mass, LIBs deliver exceptionally high energy density, as the stored energy scales with both voltage and charge [5]. As a result, LIBs are regarded as a clean and efficient alternative to fossil fuel–based technologies, offering superior power density, cycle life, and reliability compared to conventional rechargeable batteries [6,7]. Despite these advantages, traditional energy storage systems still face challenges such as slow charging rates and limited lifetimes [8]. Rechargeable batteries store energy via reversible electrochemical reactions, providing a cost-effective and practical solution compared to mechanical, electromagnetic, or other electrochemical storage technologies. LIBs are the most efficient and adaptable technology available, with outstanding energy and current density, increased voltage, and prolonged life cycles of up to 1000 cycles [9]. The growing demand for portable electronics and electric and hybrid vehicles continues to drive the development of advanced battery materials with enhanced performance and durability. In recent years, renewed interest in olivine phosphate cathodes has been driven by escalating safety concerns, cost volatility of Co- and Ni-rich layered oxides, and the rapid expansion of electric vehicle and stationary storage markets [10–12]. In particular, the demand for thermally stable, cobalt-lean, and high-voltage cathode materials has positioned $LiMPO_4$-based systems as strategic candidates for next-generation LIBs

* Corresponding author.
E-mail address: Theodore.AzemtsopManfo@uwasa.fi (T.A. Manfo).

https://doi.org/10.1016/j.est.2026.121797
Received 9 December 2025; Received in revised form 2 February 2026; Accepted 23 March 2026
Available online 1 April 2026

[10–12].

Commercial 4 V-class cathodes such as $LiCoO_2$ (LCO), $LiNi_{1/3}Mn_{1/3}Co_{1/3}O_2$ (NMC), and $LiMn_2O_4$ (LMO) dominate current LIB technology, motivating the exploration of doped olivine materials to enhance electrochemical performance. Olivine $LiMPO_4$ (M = Fe, Mn, Co, Ni) cathodes offer high structural stability and a theoretical capacity of ~170 mAh g^{-1} [13–16]. LFP operates at ~3.5 V vs. Li/Li^+, while LMP and LNPO exhibit higher working potentials of ~4.1 V and ~5.2 V, respectively [16,17]. Owing to its higher voltage, LMP provides ~20% greater theoretical energy density than LFP [18]. Recent advances in high-voltage electrolytes, including fluorinated carbonate systems, localized high-concentration electrolytes, and solid-state electrolytes, have partially mitigated oxidative instability above 4.5 V, thereby renewing interest in high-voltage olivine phosphates such as LCP and LNPO [19–21].

The charge–discharge process in LMP involves a two-phase transformation between LMP and $MnPO_4$, where strong P—O bonding stabilizes the Mn^{2+}/Mn^{3+} redox couple; however, poor electronic conductivity and instability of the Mn^{3+} state upon delithiation limit its practical performance [22]. LNPO, despite its high voltage, suffers from antisite defects that hinder Li extraction. To overcome these limitations, mixed-metal phospho-olivines are being actively investigated as high-energy cathode materials. Since LIB performance is cathode-limited, high-capacity and high-voltage cathodes can reduce excess material usage, lower cost and weight, and simplify cell and module design. Nevertheless, balancing energy density, safety, and cost remains challenging, and while capacity enhancement is widely studied, voltage upliftment strategies remain comparatively underexplored. Fig. 1 summarizes the average discharge voltage and specific capacity ranges of LIB cathode materials [16].

Materials with olivine-type crystal structures are widely investigated as cathodes for rechargeable LIBs owing to their high theoretical capacity, thermal stability, and favorable redox potentials versus Li/Li^+ [23–25]. Among them, olivine phosphate cathodes such as $LiMPO_4$ (M = Fe, Mn) have attracted considerable attention for electric and hybrid vehicle applications due to their low cost and intrinsic safety. However, their practical performance is limited by poor electronic conductivity. To address this, various strategies, including particle size reduction [26], cation doping [27], carbon coating [28], and $LiMPO_4$/carbon composite formation [27,29], have been extensively explored. LFP, with a redox potential of 3.45 V and a theoretical capacity of 170 mA h g^{-1}, has been successfully commercialized [30–35] and remains the most widely studied member of the olivine family [23,36–38]. Higher-voltage olivine phosphates, such as LCP with a redox potential of ~4.8 V, were first reported by Amine et al. [39–42], offering increased energy density but also introducing challenges related to mechanical degradation, diffusion-induced stress, and interfacial instability during cycling [43–45]. Owing to its low cost, high safety, and long cycle life, nanoscale carbon-coated LFP continues to be a leading candidate for large-scale LIB applications, outperforming other $LiMPO_4$ compositions while reducing reliance on critical raw materials [46].

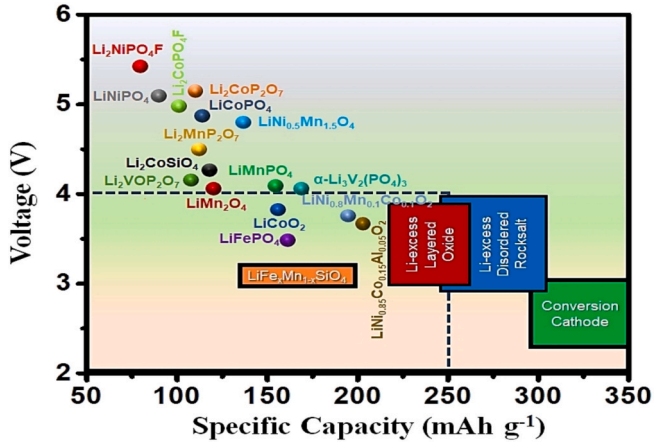

Fig. 1. The approximate range of average discharge voltage and specific capacity for LIB cathode materials provides key insights into their performance characteristics. Olivine structures, such as those of $LiMPO_4$ (M = Fe, Mn, Ni, Co), are chosen to be discussed in this review.

The Pnma space group's olivine $LiMPO_4$ material family encompasses some of the most promising cathodes for LIB applications, as well as commercially accessible compounds (such as LFP and LCP) [47]. Much research has lately been conducted to optimize the relevant material properties of various $LiMPO_4$ materials, with first-principles calculations remaining at the forefront of such research. Theoretical analysis of Li diffusion in various olivine phosphate structures revealed that the diffusivity is often overestimated compared to actual results [48]. Olivine-based positive electrode materials have been extensively investigated as lithium-ion battery cathodes due to their structural stability, safety, and favorable electrochemical properties [49]. LFP is a commonly used commercial product as an active component of cathodes for lithium batteries. LFP-based lithium batteries are increasingly preferred for commercial applications due to their affordability, safety, and reduced toxicity compared to LCO and other cobalt-containing lamellar compounds. The demand for batteries is predicted to rise annually in the 2020s, owing primarily to the global adoption of electric vehicles [50]. As a result, demand for LFP has risen. Until recently, layered oxide positive electrodes (such as lithium nickel manganese cobalt oxides, lithium nickel cobalt aluminum oxides, and others) were the norm in the EV market in terms of energy density [51]. However, as the prices of transition metal resources like cobalt and nickel grow, the resource-rich LFP is regaining popularity. LFP demand for light-duty EV batteries has surged dramatically, from 7% in 2020 to nearly 30% in 2022, primarily due to increased $LiFePO_4$ uptake by Chinese manufacturers [52].

Most research has focused on the commercially available LFP phase [53–55]. Other transition metal systems may yield greater cell voltages than LFP, prompting more research [56–60]. Unfortunately, these materials have constraints that must be addressed before they can be considered viable rivals to LFP. LMP has lower Li-ion conductivity than LFP, while LCP and LNPO require breakthroughs in electrolyte chemistry for application [58,59]. Lithium nickel phosphate (LNP) exhibits intrinsically poor electronic conductivity and therefore delivers limited charge–discharge capacity [58]. The application of olivine-type $LiMPO_4$ (M = Mn, Fe, Co, Ni) cathodes remains challenging because of their low inherent electronic conductivity. To overcome this drawback, combined synthesis strategies are commonly employed, including nanoscale particle formation and surface coating with electronically conductive phases such as carbon [54,61,62]. Early studies on supervalent cation-doped LFP reported conductivity enhancements spanning several orders of magnitude [61]. Nevertheless, the electrochemical performance of $LiMPO_4$ cathodes prepared using these approaches still does not satisfy the demands of commercial lithium-ion batteries.

In recent years, significant research has focused on improving LFP [63], while parallel efforts have explored other isostructural olivine materials, particularly LMP and related transition-metal phosphates. Replacing Fe with other transition metals increases the M^{3+}/M^{2+} redox potential relative to Li^+/Li, thereby enhancing the achievable energy density compared with LFP. The redox behavior of transition-metal ions is governed by the inductive effects of neighboring counter-cations [64]. Furthermore, differences in metal–oxygen bonding and metal–oxygen–metal interactions contribute to variations in redox potential [65]. Fig. 2 illustrates the capacity/discharge potential curves of olivine frameworks used in lithium batteries, highlighting the positions of $M^{2+/3+}$ redox energy [66]. As shown in Fig. 2, the discharge profile of $LiFe_{0.5}Mn_{0.5}PO_4$ differs markedly from those of single-metal LFP and LMP cathodes. While LFP and LMP exhibit well-defined voltage plateaus at approximately 3.45 V and 4.1 V, respectively, the mixed-metal

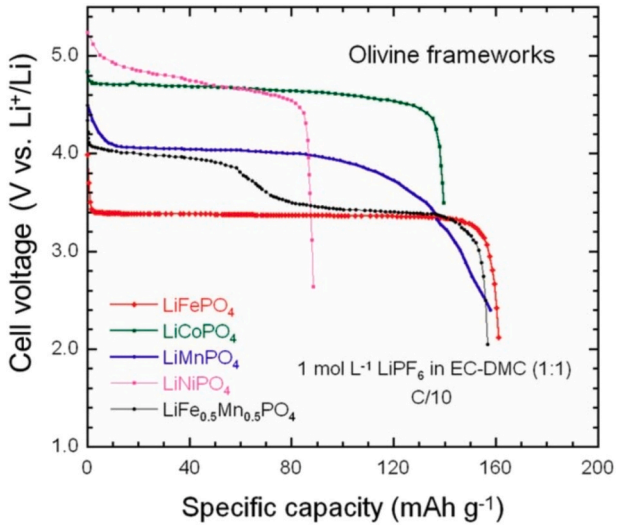

Fig. 2. Comparison of olivine $LiMPO_4$ and $LiFe_{0.5}Mn_{0.5}PO_4$ solid solutions as cathodes for LIBs. Half-cells were compared with lithium metal to measure voltages.

$LiFe_{0.5}Mn_{0.5}PO_4$ system displays a broadened and intermediate discharge potential. This behavior reflects the regulatory effect of Fe^{2+}/Fe^{3+} and Mn^{2+}/Mn^{3+} redox couples coexisting within the same olivine framework, leading to partial overlap and electronic interaction between redox processes. Such a cation modifies the local electronic environment, reduces voltage polarization, and enables more continuous lithium extraction and insertion. As a result, $LiFe_{0.5}Mn_{0.5}PO_4$ achieves a balanced combination of operating voltage and reversible capacity, demonstrating the effectiveness of mixed-metal substitution as a strategy for tuning redox potential and enhancing energy density in olivine phosphate cathodes.

Several review articles have addressed individual olivine phosphate cathodes or modification strategies such as carbon coating and doping. However, a unified comparative analysis that correlates crystal structure, lithium transport pathways, morphology evolution, and electrochemical behavior across the entire $LiMPO_4$ family (M = Fe, Mn, Co, Ni) remains limited [67–69]. This review distinguishes itself by systematically comparing modified high-voltage olivine phosphates using a structure–property–performance framework, with particular emphasis on lithium diffusion anisotropy, voltage scalability, and electrolyte compatibility constraints relevant to next-generation rechargeable batteries. Accordingly, this review provides a comprehensive framework linking materials chemistry to practical energy storage performance.

2. Crystal structures of $LiMPO_4$ (M = Fe, Mn, Co, Ni)

Cathode materials for lithium-ion batteries are commonly categorized according to their crystallographic structure [70,71]. Among these, layered transition-metal oxides with the general composition $LiMO_2$ (M = Co, Mn) have been widely investigated. These compounds typically adopt an α-$NaFeO_2$-type layered framework and crystallize in the $R\bar{3}m$ space group [72,73]. Their structure is characterized by the alternate stacking of lithium and transition-metal layers within an oxygen framework, where the cations occupy octahedral coordination sites. Spinel oxides such as LiM_2O_4 crystallize in the $Fd\bar{3}m$ space group and feature lithium and transition-metal ions distributed among tetrahedral and octahedral sites within a close-packed oxygen lattice [74]. In this configuration, edge-sharing MO_6 octahedra are confined to the transition-metal sublattice, forming an interconnected network of lithium tetrahedra. In addition to oxides, polyanionic cathodes including olivine phosphates, silicates, and tavorite-type materials have attracted considerable interest [75,76,78]. Olivine-structured $LiMPO_4$ crystallizes in the orthorhombic Pnma space group and is composed of corner- and edge-sharing MO_6 octahedra and PO_4 tetrahedra, together with LiO_6 octahedra, as schematically shown in Fig. 3 for the three major lithium insertion compound families.

Electrode materials are classified based on the dimensionality of Li^+-ion penetration and the activation energy that allows Li-ion to pass [79]. The archetypes of $Li[M]O_2$ include two-dimensional $Li[M]O_2$ with M = Co, Ni, three-dimensional $Li[X]_2O_4$ with Mn, and unidimensional $Li[M']PO_4$ with M′ = Fe, Mn, Ni, Co, or $FeyMn_{1-y}$ [80].

Emerging technologies require increased voltage/energy density, stability, and long-term operation, necessitating further performance enhancements. Advancements in battery system components, including the anode, cathode, electrolyte, and separator, are crucial for progress [81,82]. Positive electrodes with high specific capacity or operating potential can achieve higher energy densities [83,84] and are commercialized cathode materials, as mentioned in Table 1.

Numerous iron phosphates exist naturally. The possibility that lithium in the olivine structure, LFP, may be removed and cause the iron to oxidize to the ferric state is what has aroused their current attention. Olivine occurs naturally as a manganese/iron combination, Li (MnFe)PO_4. Other iron phosphates found in nature, including lipscombite, giniite, strengite, and phosphosiderite, have been observed to exhibit redox behavior [88]. These compounds are diverse, which makes studying them difficult; the lattice tends to produce amorphous or glassy structures, and protons can easily incorporate into it. Most iron phosphates have FeO_6 octahedra and PO_4 octahedra. The tunnel structure in Fig. 3 illustrates the olivine form of LFP, where octahedra join to form a ring-like structure. Tunnels along the b-axis are not connected, making it difficult for lithium ions to move between them. Lithium-ion diffusion in tunnels is dimensional, affecting the electrochemical performance of iron-containing materials [85]. Doping should focus on iron sites instead of lithium sites. Lithium is completely removed from this phase with minimal structural changes. Padhi et al. [86] discovered that $LiMPO_4$ (M = Fe, Mn) can be reversibly cycled at voltages of 3.4–4.0 V due to the inductive action of the phosphate group. Additional research has been conducted on several metal phosphate compounds to determine their suitability as cathodes for improved lithium batteries. The inexpensive cost and apparent thermodynamic and kinetic stability of these materials make them very appealing.

Determining the structure of compounds is crucial, especially when synthesized at low or high temperatures with potential for lattice instability. A simple analysis of lattice parameters can indicate the presence of a disorder, as explained below. In most circumstances, X-ray powder diffraction and Rietveld refinement (with site occupancy) are sufficient. Protons may be integrated into aqueous medium structures during hydrothermal or other reactions. LMP(OH) is formed when the hydroxyl group is lost when heated in oxygen to 500 °C, as confirmed by X-ray diffraction. Rietveld method refinements of Pnma (a = 6.1028(2) Å, b = 10.4465(3) Å, and c = 4.7437(2) Å) are like those that have been documented in previous research [91]. LMP synthesized hydrothermally has the same cell parameters as those synthesized by chemical means. The hydrothermal sample forms more ordered LFP when heated in nitrogen at 500–700 °C [87,88]. Alternatively, performing the synthesis at 190 °C arranges the cations, resulting in less than 1% iron on lithium sites [89]. The lithium-free samples exhibit minor lattice expansion/contraction and a reduced overall volume, which corresponds to the smaller ferric ions. $FePO_4$ is a heterosite in LFP, an olivine form [89], with no direct experimental evidence for additional compositions except for the two end members; nonetheless, the comparatively quick diffusion of lithium would imply that a very low vacancy concentration is permitted on lithium sites. Otherwise, diffusion would necessitate the coordinated transit of all ions in a single tunnel. The diffusion of lithium does not cease after a surface layer is depleted of lithium. The lithium diffusion coefficient at very low x values in Li_xFePO_4 has not been measured. If lithium is not soluble in $FePO_4$, a grain of LFP must delithiate, resulting in pure $FePO_4$ in its center.

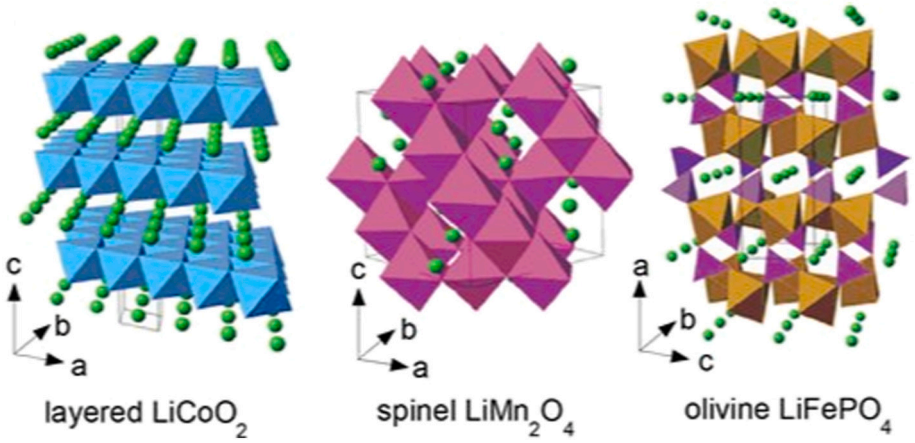

Fig. 3. Crystal structures of several cathode materials [77,78].

Table 1
An overview of commercial cathode materials, including their structure and electrochemical properties.

Cathode materials	Types of structures	Potential (V)	Theoretical capacity (mAh g^{-1})
$LiMO_2$	Layered		
$LiCoO_2$		3.7	274
$LiMnO_2$			285
$LiNiO_2$		4.0	274
$LiNi_{1-x-y}Co_xM_yO_2$	Layered		
$LiNi_{1-x-y}Co_xAl_yO_2$, NCA		~4.4	195
$LiNi_{1-x-y}Co_xMn_yO_2$, NCM		~4.5	200
$LiMn_2O_4$	Spinel	4.0	148
$LiMPO_4$	Olivine		
$LiFePO_4$		3.5	170
$LiMnPO_4$		4.1	170
$LiCoPO_4$		4.8	167
$LiNiPO_4$		5.2	170

$LiMPO_4$ phosphate materials display olivine structures and are orthorhombic [90,91]. Li (Li) is bonded to six oxygen (O) atoms in these three-dimensional structures to form LiO_6 octahedra. They have four equivalent MO_6 octahedra and four equivalent PO_4 tetrahedra at their corners and, as shown in Fig. 3, two equivalent LiO_6 octahedra, two equivalent MO_6 octahedra, and two equivalent PO_4 tetrahedra as edges. Based on a closer look at its crystal structure, $LiMPO_4$ is made up of LiO_6 octahedra embedded in PO_4 tetrahedra that are connected parallel to the B-axis, forming a Li channel on this axis. Although the specific mechanism of lithium-ion mobility in olivine-type formations is unknown, conductivity measurements provide a rough notion of its magnitude. Two proposed lithium (Li) diffusion pathways exist within the B- and A-crystallographic axes [92]. Theoretical analyses indicate that Li diffusion along the channels of the B-crystallographic axis in $LiMPO_4$ materials is more favorable compared to diffusion characterized by inter-channel hopping along the C-crystallographic axis [67,93–97,99]. Fig. 4 illustrates the olivine-type crystal structures of $LiMPO_4$ (M = Fe, Mn, Co, Ni), emphasizing the one-dimensional lithium-ion diffusion pathways along the [010] direction and the role of the rigid PO_4^{3-} polyanion framework in enhancing structural stability [49]. Variations in lattice parameters and transition-metal environments significantly influence lithium transport kinetics and electrochemical behavior.

As illustrated in Fig. 4, lithium ions reside within LiO_6 octahedra that are edge-shared and continuously connected along the crystallographic b-axis of the olivine $LiMPO_4$ structure. This specific connectivity creates a one-dimensional diffusion channel that enables lithium-ion migration with relatively low activation energy along the b-axis. In contrast, the

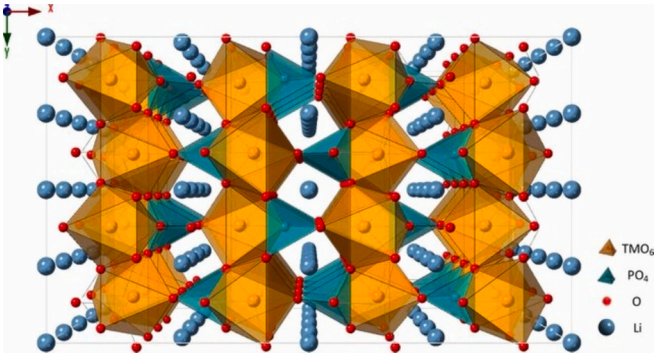

Fig. 4. Crystal structures of olivine $LiMPO_4$ (M = Fe, Mn, Co, Ni) highlighting Li^+ diffusion channels and MO_6 octahedra.

LiO_6 octahedra are separated in the a- and c-directions by corner-sharing PO_4 tetrahedra, whose rigid covalent framework effectively blocks lithium-ion transport in these directions. Consequently, lithium diffusion in olivine phosphates is highly anisotropic, with the b-axis representing the most favorable and energetically accessible pathway. This structural feature underpins both the intrinsic rate limitations of $LiMPO_4$ cathodes and the effectiveness of strategies aimed at shortening diffusion lengths or enhancing electronic conductivity.

The synthesized LFP, LMP, and LCP were achieved through a sol-gel reaction [98]. Fig. 5 shows the XRD data for LFP, LMP, and LCP olivine compounds [98]. The XRD patterns of the LMP and LCP showed no noticeable structural changes; the cell characteristics determined from Rietveld refinement are provided in Table 2 [98]. An orthorhombic system was discovered using XRD analysis of the LFP [99]. Observable changes in lattice parameters of different axes can be observed. The lattice parameters can be organized in decreasing size as follows: LMP < LFP < LCP, and the volume of the cells decreases in this order as well. Neither an amorphous peak nor any indication of crystalline carbon was discovered. The amount of carbon in all materials is represented by crystallites measuring roughly 200 nm. A tiny coating of carbon exists on $LiMPO_4$ (M = Fe, Mn, and Co), which is most likely the cause of this.

Elemental analysis determined that all materials contained approximately 4% ± 0.3% carbon. After the carbon gel was applied, the olivine structure was maintained, and impurity phases were not detected. Consequently, the carbon source inhibits the formation of M^{3+} ions [100,107]. The study found that LCP crystallites were larger than LFP and LMP, as indicated by their higher diffraction intensities.

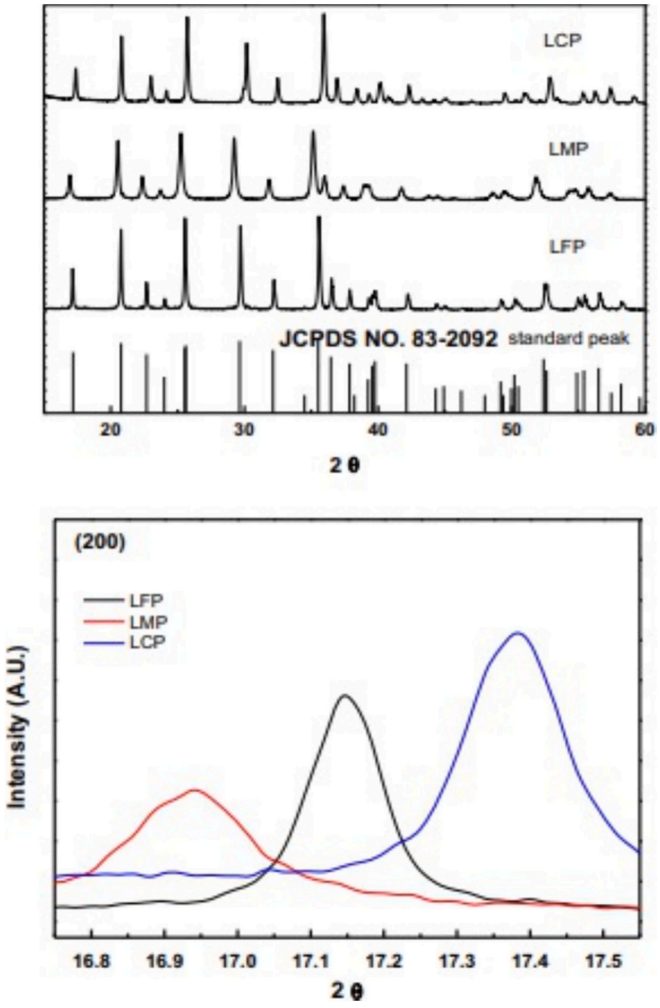

Fig. 5. The XRD analysis data for LFP, LMP, and LCP olivine compounds.

Table 2
Rietveld structure refinement of phosphate materials unit cell parameters.

Sample no.	LFP	LMP	LCP
a (Å)	10.3307 (2)	10.4478 (4)	10.2026 (3)
b (Å)	6.0087 (1)	6.1036 (3)	5.9235 (2)
c (Å)	4.6946 (1)	4.7443 (2)	4.7004 (1)
V (Å^3)	291.42 (1)	302.54 (2)	284.07 (2)

2.1. Summary and perspective

Olivine $LiMPO_4$ cathodes exhibit a robust polyanion framework that ensures high structural stability and safety; however, lattice distortions and anisotropic lithium-ion diffusion strongly influence electrochemical performance. Future progress will depend on precise control of crystal chemistry and defect engineering to optimize lithium transport without compromising structural integrity.

3. Morphology studies of the olivine $LiMPO_4$

Managing morphology is critical for overcoming the inherent kinetic constraints of olivine $LiMPO_4$ cathodes with low electrical conductivity and one-dimensional lithium-ion diffusion channels. Changing particle size, shape, and surface design directly affects lithium diffusion length, electrode-electrolyte contact area, and strain accommodation while cycling. As a result, microstructural engineering, which includes technologies like nanostructuring, controlled crystal growth, and morphology-directed synthesis, has emerged as a critical tool for increasing rate capability, capacity utilization, and cycling stability. This section investigates the correlation between morphology-controlled $LiMPO_4$ materials and their electrochemical performance.

The LFP and LCP operate across a wide voltage range, with notable values of 3.5 vs Li^+/Li and 4.8 vs Li^+/Li [101,109]. Upon decreasing the particle size, carbon coatings are applied, and surface changes are made; these materials are capable of significantly improved electrochemical performance [102–104,112]. As a result of shorter Li-ion path lengths and smaller Particle sizes, LFP can cycle at high rates [105]. It inhibits structural rearrangements during phase transitions by forming a non-equilibrium solid solution phase [106,107]. Nanosizing electrode materials can reduce tap density and volumetric energy density. Porous materials and extended nanostructured architectures have been designed to reduce these effects via template-assisted and solvothermal synthesis [108–112]. Low-temperature solvothermal techniques can be impeded by crystal structure antisite defects, which can block 1D Li-ion pathways [113,114]. We discovered a straightforward method for generating LMP phases (M = Fe, Co) from lithium-rich $LiPO_3$ at low temperatures while keeping significant control over the final shape. To create a nanostructured $LiPO_3$-type material, heat a tetra glyme solution of phosphorus pentasulfide to 200 °C while heating lithium tert-butoxide in a microwave [113].

K. Kim et al. utilized the sol-gel process to create olivine-like compounds with a $LiMPO_4$ structure [98], using Scanning Electron Microscopy (SEM) imaging performed on a FE-SEM (Philips XL30 S FEG). The LFP, LMP, and LCP powders comprise polycrystalline grains with varied size distributions, as illustrated in Fig. 6 [98]. Particles above 50 mm and smaller crystallites around 200 nm are found. All materials appear spongy and porous on a low-scale micrograph. Porous particles improve lithium transport and influence liquid electrolyte dynamics, impacting electrochemical performance [99,100,114].

A more extensive study reveals that the bigger particles are agglomerates of smaller sintered grains. The LFP sample has the largest and smallest grain compared to the other two samples, while the LCP sample has the smallest grain. The particles have a circular shape and well-defined grain boundaries, consistent with extensive heat treatment. Sintering at 700 °C yielded well-well-crystallized powders. Analysis using transmission electron microscopy (TEM) found that all LMPs feature a uniform carbon covering of 4–6 nm thick. The thickness is comparable to the published value, which corresponds to the carbon content [115,116].

Fig. 7 depicts the SEM images of LNPO samples [117]. Fig. 7a (annealed samples) demonstrates that a network of homogenous particle sizes results in a compact morphology with a large surface area, and Fig. 7b shows the non-annealed sample. Fig. 7c (higher magnification) shows the orthorhombic structure of grains in annealed samples, which is absent in unannealed samples. Although post-annealing treatments at high temperatures can help, they often result in unwanted particle development. Talebi-Esfandarani et al. employed graphite crucibles heated to 1100 °C to react $LiPO_3$ with iron ore concentrate, producing olivine LFP [118].

While these SEM observations provide valuable insight into particle morphology and agglomeration behavior, a complete understanding of electrochemical performance also requires examination of the underlying atomic-scale structure, including metal-oxygen bond lengths and polyhedral connectivity within the olivine lattice. Fig. 8 depicts the different transition metals located on the MO_6 octahedra [98]. MO_6 octahedra site bond lengths depend on the transition metal and show regular and significant changes. LCP compositions have slightly shorter M—O distances than other samples on average. High-spin Mn^{2+} (0.97 Å), Fe^{2+} (0.92 Å), and Co^{2+} (0.88 Å) have different ionic radii, which explains this [118]. The angles of O_1-M-O_2, O_1-M-O_3, and O_2-M-O_3 in LMP are approximately 180°, 90°, and 90°, respectively, with O_3-M-O_3 [118,119] having the smallest angle, causing structural distortion in PO_4 tetrahedra and MO_6 octahedra.

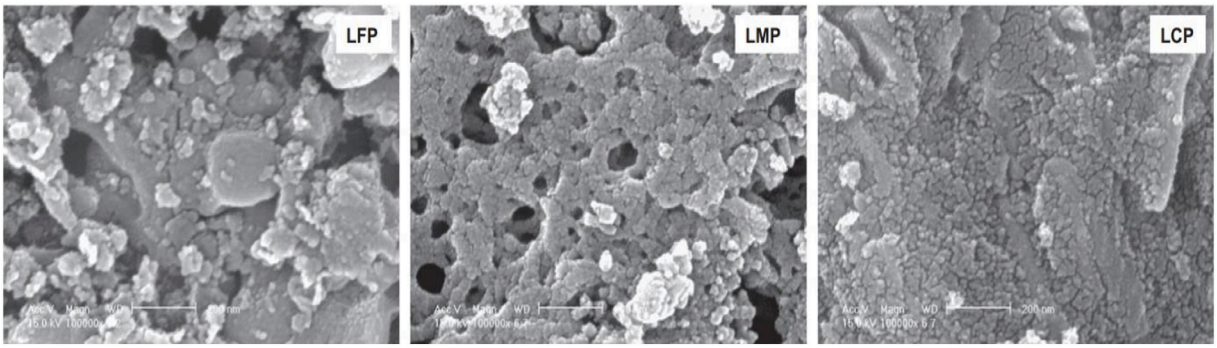

Fig. 6. SEM pictures of LFP, LMP, and LCP olivine chemicals generated by the sol-gel technique [98].

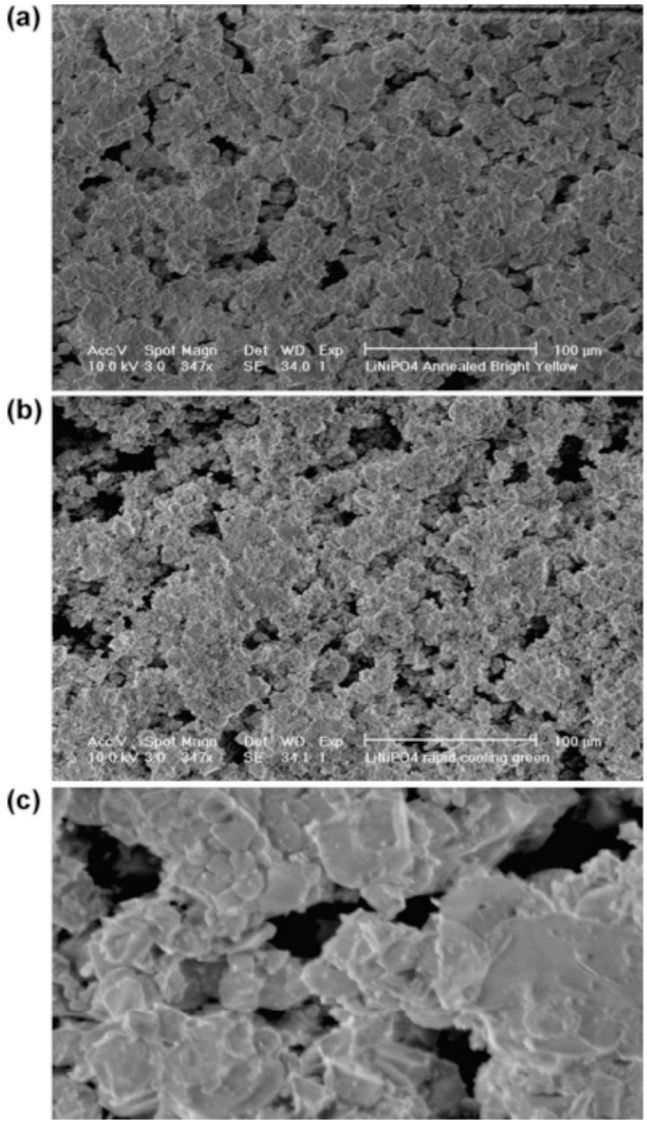

Fig. 7. SEM images of LNPO olivine (a), non-annealed (b), and annealed (c) samples at higher magnification (4× of Fig. 6a) reveal an orthorhombic structure [117].

Olivine-structured $LiMPO_4$ materials are regarded as promising cathodes for next-generation high-power lithium-ion batteries; however, their practical application is hindered by intrinsically low electronic conductivity and sluggish lithium-ion transport along the [010] crystallographic direction. To address these limitations, Xianhong R. et al. developed ultrathin $LiMPO_4$ nanosheets by combining a liquid-phase exfoliation strategy with a solvothermal lithiation process conducted under high-pressure, high-temperature (HPHT) supercritical fluid conditions [120]. In contrast to conventional high-temperature solid-state synthesis, which typically produces large crystalline particles and severe nanosheet agglomeration, the HPHT solvothermal lithiation route yielded uniformly dispersed, monodisperse nanosheets. The resulting nanosheets provide an enlarged electrode–electrolyte interfacial area and facilitate rapid lithium-ion transport, achieving diffusion times below 25, 2.5, and 250 μs for LFP, LMP, and LCP nanosheets, respectively, as estimated using the relation $t = L^2 / D$. Among these, LFP nanosheets demonstrated outstanding electrochemical performance, delivering high rate capability and energy density values of 18 kW kg^{-1} and 90 Wh kg^{-1} at 80 °C, which are markedly superior to those of bulk counterparts. The synthesis pathway for carbon-coated LFP nanosheets based on liquid-phase exfoliation and HPHT solvothermal lithiation is schematically illustrated in Fig. 9 [120].

XRD analysis was used to investigate the crystal structures of LMP/C, LCP/C, and LNPO/C nanosheets produced during HPHT solvothermal lithiation of PVP-capped $NH_4MnPO_4.H_2O$, NH_4CoPO_4, and $NH_4NiPO_4{\cdot}H_2O$ nanosheets [120]. The reflections in Fig. 10A–C are orthorhombic olivine structures composed of LMP, LCP, and LNPO. Conventional cards, such as LMP, LCP, and LNPO, have high I (020)/I (200) ratios, which promote ac-plane orientation. The Raman spectra show an amorphous carbon coating layer with distinct D-band (~1350 cm^{-1}) and G-band (~1590 cm^{-1}). TEM images (Fig. 10D–F) show that the lithiated products retain the nanosheet form. SAED patterns (insets in Fig. 10D–F) from individual nanosheets exhibit single-crystalline properties and correspond to the [010] projection of orthorhombic olivine-type reciprocal lattices, showing the exposure of (010) faces. These HRTEM images of Fig. 10G–I show interlayer spacings of 0.21, 0.23, and 0.21 nm, which coincide well with the d-spaces of LMP, LCP, and LNPO. Fig. 10G–I also demonstrates that the LMP, LCP, and LNPO nanosheets are coated with a thin carbon layer (0.5–1.5 nm thick). AFM measurements show that the 3.7 nm thick LMP/C, LCP/C, and LNPO/C nanosheets had thicknesses of 3.7, 4.6, and 4.0 nm, respectively [120].

Depending on the synthesis conditions, LFP can also have different morphologies depending on its performance [121]. Spherical architectures have been successfully realized through the construction of interpenetrating conductive networks, including coralloid nitrogen-doped carbon frameworks [122], nanofiber-based microspheres [123], and self-assembled LFP nanorods with lengths of 2–3 μm and diameters of 30–50 nm [124]. In addition, alternative morphologies such as bow-tie-shaped nanocrystals [125], hollow nanoparticles [126], as well as nanoplates and nanorods [127], have demonstrated comparable electrochemical behavior. It was reported that LFP/C nanorods containing 9 wt% carbon delivered a discharge capacity of 120 mAh g^{-1} at a high rate of 10 C while retaining 83% of their initial capacity after 2000 charge–discharge cycles [128]. These nanorods were synthesized via a solvothermal route, and their discharge capacity ranged from 155 to 124

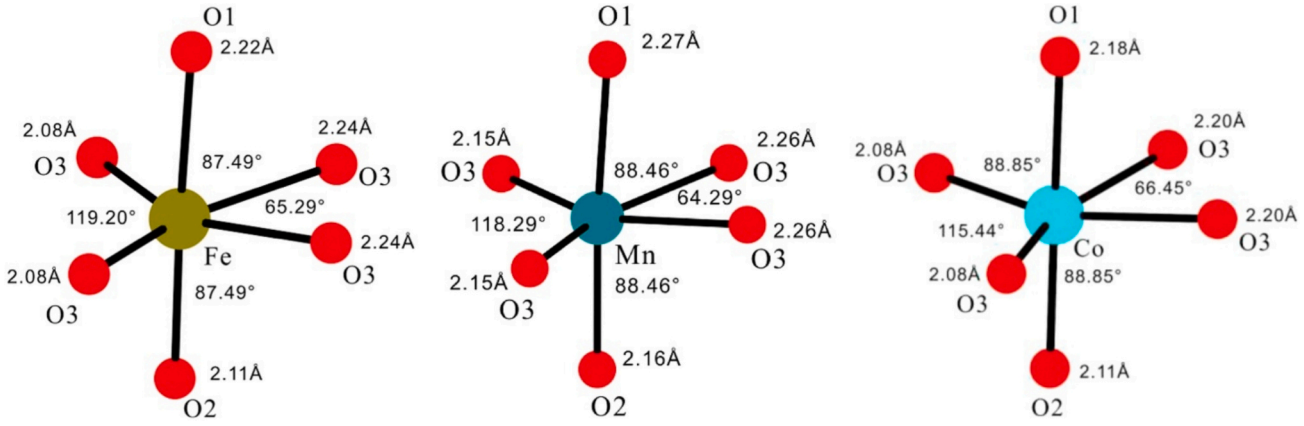

Fig. 8. M—O bonding in LFP, LMP, and LCP olivine compounds: local geometry, lengths, and angles [98].

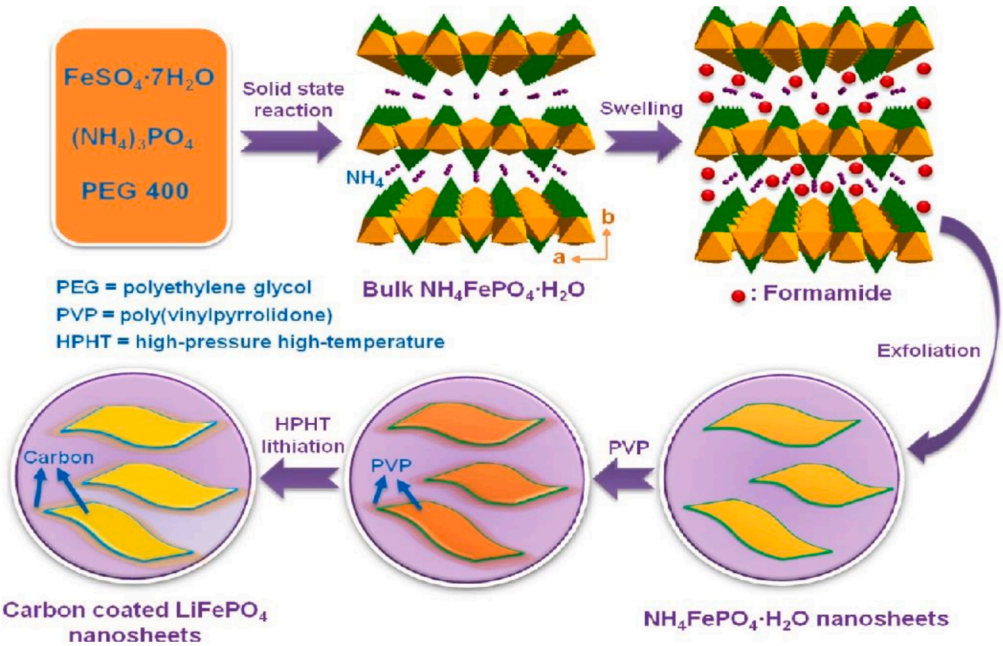

Fig. 9. The carbon-coated LFP nanosheets were obtained via a liquid-phase exfoliation strategy combined with an HPHT solvothermal lithiation process.

mAh g^{-1} depending on the operating temperature. Furthermore, LFP/C nanorods prepared using tetraethylene glycol as a surfactant and incorporating 10 wt% conductive additives achieved capacities of 160 mAh g^{-1} at 0.1 C and 55 mAh g^{-1} at an ultrahigh rate of 200 C, along with a power density of 95 kW g^{-1} [129]. Similarly, a sol–gel-derived synthesis of carbon-coated LFP nanonetworks resulted in favorable electrochemical performance and long-term cycling stability, delivering 120 mAh g^{-1} at 20 C [130].

Electrospinning of LFP/C nanofibers [131–136] using polyacrylonitrile (PAN) and carbon [133] showed significantly better capacity of 162 mAh g^{-1} at 0.1 C rate and 139 mAh g^{-1} at 1 C. LFP (001) nanorods with carbon coating showed improved performance, delivering 173 mAh g^{-1} at 0.1 C, 117 mAh g^{-1} at 10 C, and 113 mAh g^{-1} after 500 cycles, indicating 96.5% capacity retention due to lithium path reduction [137]. The reduced particle size (100 nm) is crucial for achieving good rate capability [138]. Synthesized LFP/C nano pillows employing ethylene glycol as a reaction medium solvent demonstrated much greater rate capability at 30 C, achieving an outstanding rate capability [139]. Based on prior discoveries [140–142] on LFP nanoplates created via a solvothermal technique, this result marks a substantial advancement. However, as stated by the authors in [139], LFP/C nanorods have better prospects for practical application, at least if they are synthesized at a speed that facilitates industrial production of nanorods at about the economic cost [152].

The results reported here are largely about lab-scale synthesis and electrochemical performance. However, because LFP is a commercial product, we decided it was appropriate to report on marketable methods for LFP synthesis. Recent papers [143] address advancements and challenges in LIB materials for automotive applications, including cost and industrial synthesis methodologies. Current industrial strategies for LFP include hydrothermal and solid-state technologies. Hydrothermal synthesis is more expensive than solid-state processes due to its high pressure and energy-intensive nature. Benedek et al. discovered a low-temperature hydrothermal technique that reduces synthetic energy by 30%, comparable to solid-state reactions [133]. The hydrothermal synthesis process is attractive for commercial processing because particle sizes and shapes can be regulated more easily than in solid-state synthesis.

The scalable synthetic approach was performed to synthesize $LiMPO_4$ nanostructures (M = Fe and/or Mn), revealing the material's electrochemical properties [144]. Phosphate-based cathode materials synthesized by the soft template method assisted by the high-energy ball

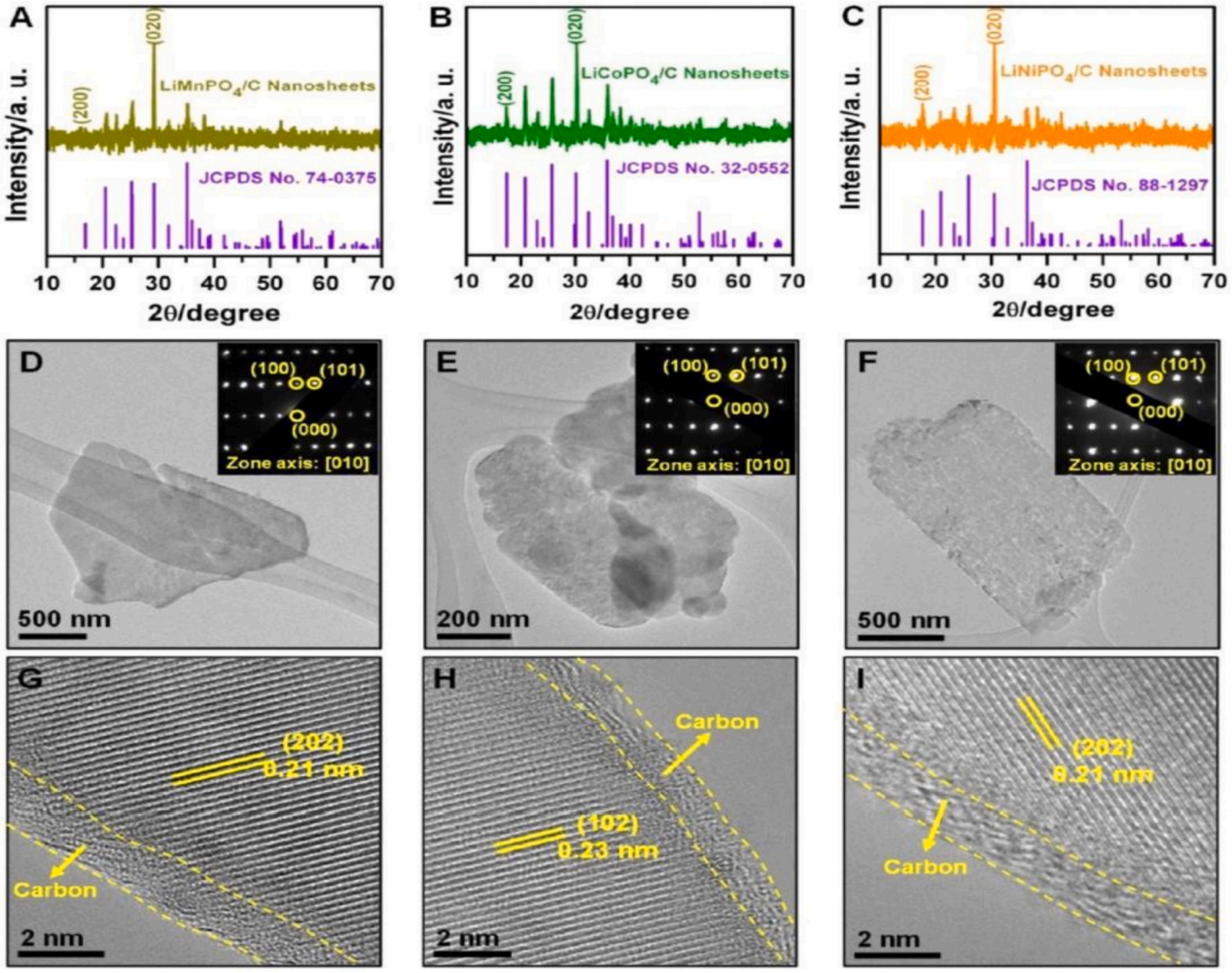

Fig. 10. The study examines XRD (A–C), TEM (D–F), and HRTEM images (G–I) of LMP/C, LCP/C, and LNPO/C nanosheets, with SAED patterns insets in panels D–F [120].

milling method with carbon black attain reduced particle size and enhanced carbon wiring formation as described in our earlier reports [145–147]. Lithium storage properties can be further enhanced by nanostructures with divalent cation substitution. Lithium storage properties can be further enhanced by nanostructures with divalent cation substitution. Fig. 11 shows how nanostructuring can improve an inorganic electrode's electrochemical characteristics.

Fig. 11 presents the nanostructuring strategies employed to improve lithium storage performance in $LiMPO_4$ (M = Fe and/or Mn) cathode materials. The resulting particles consist of interconnected

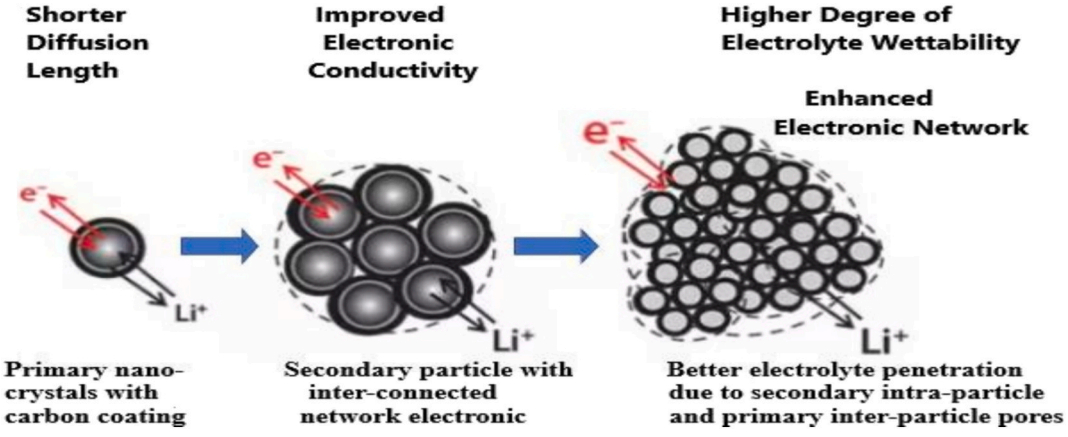

Fig. 11. A design showing how nanostructuring can improve an inorganic electrode's electrochemical properties [144].

nanocrystalline building blocks and mesoporous features, all encapsulated within a conductive carbon layer. These structures were fabricated using a soft-template-assisted high-energy ball milling technique [144]. The strong connectivity between primary nanocrystals and secondary aggregated particles enables several performance benefits, including shortened lithium-ion diffusion pathways, enhanced electronic conductivity, and the formation of an efficient electron transport network. In addition, the presence of an interconnected pore system facilitates electrolyte infiltration, thereby accelerating lithium-ion insertion and extraction processes within the electrode material.

Morphology control, including particle size reduction, shape engineering, and hierarchical structuring, effectively addresses the inherent kinetic limits of olivine $LiMPO_4$ cathodes. Optimized microstructures decrease lithium-ion diffusion routes and improve electrode-electrolyte contact, resulting in higher rate capability and cycle stability. However, there are still issues in obtaining consistent morphological control at scale while retaining structural integrity over lengthy cycles. Future studies should concentrate on scalable synthesis pathways, in situ monitoring of morphology evolution, and combining morphology control with complementary tactics such as surface coating and multi-cation doping.

4. Electrochemical performance comparison

The electrochemical performance of olivine phosphates is limited by their electronic conductivity [148]. Recent studies have shown that Li-ion diffusion can be helpful [149]. Li is transported along the b-axis in olivine structures via 1D channels (refer to Fig. 4) [150]. To investigate Li diffusion, a single Li-ion vacancy was introduced into pure (doped) $LiMnPO_4$ supercells, and a single Mn ion was added to pure (doped) $MnPO_4$ supercells to compute activation energies. Table 3 [151] displays the computed activation barriers.

The enhanced lithium insertion potentials of doped systems, particularly $LiMn_{3/4}Ni_{1/4}PO_4$, could improve electrochemical performance, particularly for producing cathodes for LIBs, as nickel is less environmentally harmful than cobalt. The activation barriers in $LiMn_{3/4}Ni_{1/4}PO_4$ are similar because substituting an Mn atom does not materially change the crystal structure. However, $LiMn_{3/4}Ni_{1/4}PO_4$ has a greater variation in activation energy due to enhanced Pauli repulsion between Li ions and MO_6 octahedrons. The expected lithium diffusion coefficients for LMP and doped materials are similar, indicating that carbon coating could be used to improve LFP conductivity [152].

Increasing the discharge capacity or operating voltage of cathode materials improves energy density [153,154]. Researchers are working to develop effective cathodes for high-potential lithium-ion batteries [155]. $LiMPO_4$ is a good electrode material for LIBs due to its high specific capacity (~170 mAh g^{-1}), appropriate operating voltage, and stability during lithium insertion/extraction [155–159]. LMP cathode materials have a high theoretical specific energy and lithium-ion intercalation potential, making them a better choice than commercial LFPs due to their superior discharge voltage platform, specific energy density, safety, and low cost. However, their low ionic and electronic conductivity limits their application in high-performance LIBs. As summarized in Fig. 12, LFP exhibits the most balanced electrochemical performance with excellent cycling stability, while LMP and LCP offer higher operating voltages at the expense of slower kinetics and interfacial instability. LNPO provides the highest theoretical voltage but remains challenging due to electrolyte oxidation and poor reversibility. Obtaining practical capacity close to theoretical values poses challenges due to electrochemical durability issues [160,161] (Fig. 12a). Spinel-structured $LiMn_2O_4$ has a theoretical capacity of 148 mAh g^{-1} but can only achieve 120 mAh g^{-1} in practice, thereby limiting the energy density in Li-ion batteries [162]. Moreover, manganese depletion is a concern due to its reducing nature. In contrast, olivine-structured LFP exhibits a theoretical capacity of 170 mAh g^{-1} with 97–98% retention over 1000 cycles [163], ensuring a long cycle life and efficiency due to effective lithium-ion management during lithiation and delithiation (Fig. 12b).

Table 3
The barrier activation energies (E_a) in eV for pristine and doped systems are denoted as Li vacancy diffusion in lithiated structures and Li-ion diffusion in delithiated structures.

Material	E_a (eV)
$LiMnPO_4$	0.40
$MnPO_4$	0.44
$LiMn_{3/4}Ni_{1/4}PO_4$	0.49
$Mn_{3/4}Ni_{1/4}PO_4$	0.44
$LiMn_{3/4}Co_{1/4}PO_4$	0.43

Enhanced electronic conductivity and improved diffusion of Li^+ can improve $LiMnPO_4$ rate performance [164] with a carbon coating surface layer [165], doped or substituted with guest ions [166], reducing particle size and controlling particle morphology [165,177] to enhance the performance of LMP. LMP doped with ions enhances its electronic conductivity and electrochemical performance, providing high discharge capacity and good rate capability [167,168]. Doping elements modify the lattice structure and alter the length of the Li—O bonds in doped LMP. Li-ions diffuse faster through nanoparticles because of their shorter diffusion lengths, but electron transfer occurs at higher surface areas [169,170]. Furthermore, nanoparticles have low tapping density because of their enormous surface areas, and electrodes have a poor loading of active materials [171]. Micro-sized LMP particles have a tap density of 1.79 g mL^{-1} and deviate from the sphere form as they grow; their tap densities decrease [172,173]. The tap density of spheres is the highest, while needle-shaped particles have the lowest because of the high aspect ratio [91]. Regularly shaped particles have higher tap density, crucial for electrode material transition from laboratory to industry [174].

Doi et al. [175] synthesized LMP using long-chain Oleic acids at 300 °C. As shown in Fig. 13, the non-heat-treated LMP particles exhibit sloping charge–discharge profiles without distinct voltage plateaus. This behavior can be attributed to a high concentration of crystal defects and structural disorder arising from insufficient thermal treatment. Defects such as antisite Li/M disorder, lattice distortion, and partial amorphization disrupt the well-defined two-phase reaction mechanism characteristic of olivine phosphates, leading to a broad distribution of redox potentials. In contrast, heat-treated samples with improved crystallinity display more pronounced voltage plateaus, indicating enhanced structural order and more uniform lithium-ion insertion and extraction processes. Fig. 13(a) indicates that the initial charge capacity was 30 mAh g^{-1}, significantly lower than the theoretical 171 mAh g^{-1}. The discharge capacity was 6 $mAhg^{-1}$, with a monotonous decrease in voltage, unlike LMP powder's clear plateau. Fig. 13(b) displays the charging-discharging characteristics of LMP particles after heat treatment in Ar, which had initial capacities of 118 and 65 mAh g, respectively. Zhong Sheng-Kui et al. [176] developed LMP/C using citric acid's sol-gel method, suggesting its carbon source and chelating agent can reduce particle size and maintain Mn^{2+} stability. Sol-gel technique demonstrated good electrochemical reversibility, with LMP/C achieving maximum initial discharge capacity and capacity retention over 30 cycles at 0.05 C as illustrated in Fig. 13c, d.

The electrochemical characteristics of olivine phosphate $LiMPO_4$ (M = Fe, Mn, Co, Ni), as summarized in Fig. 13, are strongly influenced by intrinsic electronic conductivity, anisotropic lithium-ion diffusion, and interfacial stability. Among the olivine family, $LiFePO_4$ exhibits the most balanced performance in terms of cycling stability, safety, and practical rate capability, whereas higher-voltage materials such as LNP, LCP, and LNPO offer enhanced energy density but suffer from pronounced kinetic limitations and polarization effects. These challenges highlight the necessity of targeted materials engineering to bridge the gap between theoretical potential and practical performance. Accordingly, the following subsections focus on modification strategies, beginning with

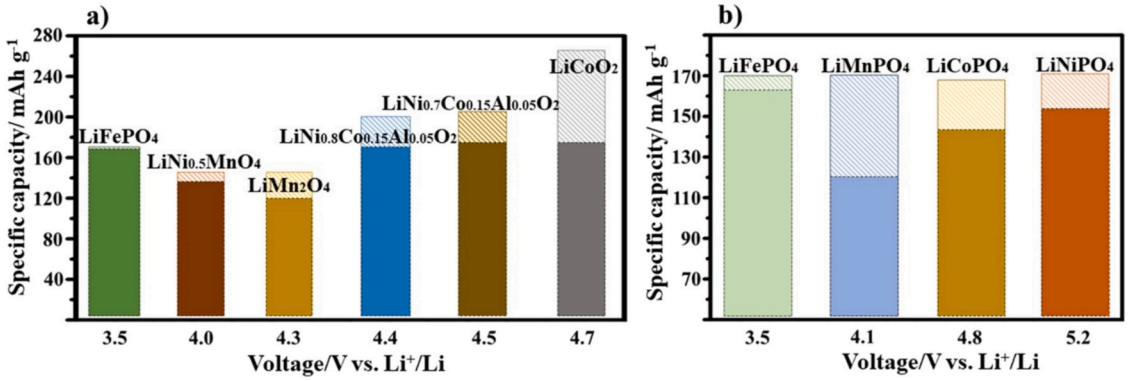

Fig. 12. Comparison of redox potentials, theoretical capacities, and electrochemical performance of $LiMPO_4$ (M = Fe, Mn, Co, Ni).

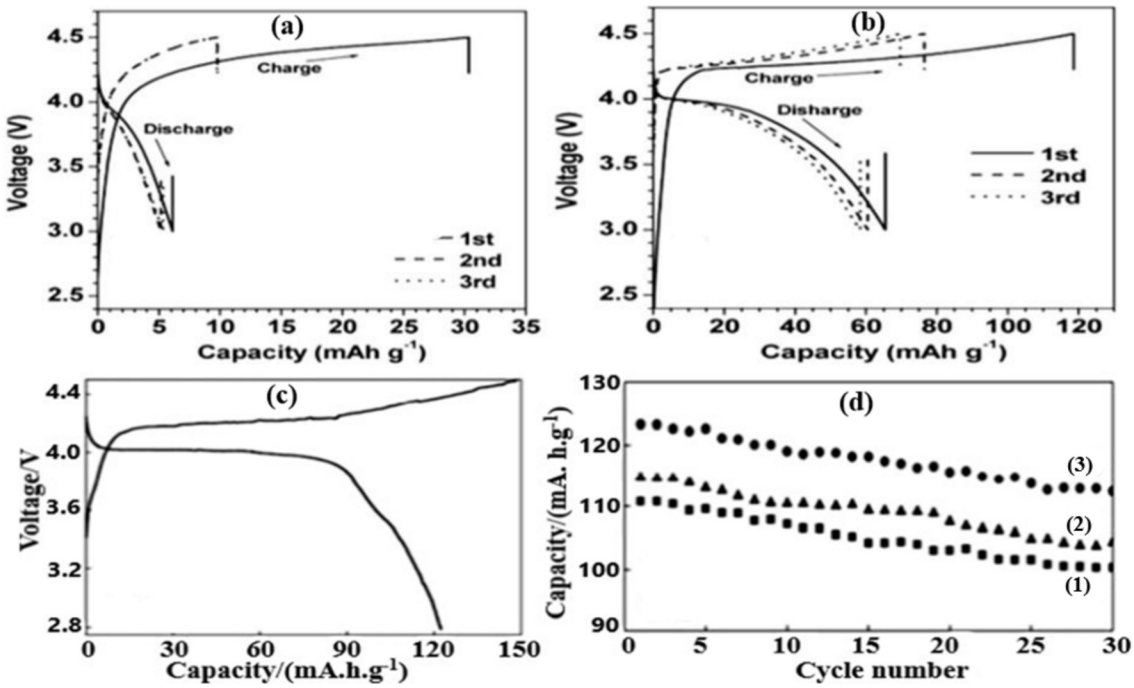

Fig. 13. The electrochemical properties of $LiMnPO_4$ particles: (a) shows the charge and discharge curves during the first three cycles; (b) depicts the curves for particles treated with Ar at 500 °C for one hour; (c) presents the initial charge-discharge curves; and (d) details the electrochemical cycling performance of LMP/C samples calcined for 10 h at temperatures of (1) 400 °C, (2) 500 °C, and (3) 600 °C [177].

carbon coating, which have proven effective in mitigating transport limitations and improving the electrochemical performance of olivine phosphate cathodes.

4.1. *Surface coating and interfacial engineering strategies*

The conductivity of the carbon coating increases with an increase in the coating temperature [178]. It is important to reach a compromise between increasing this temperature and not forming impurities. LFP has a melting point of 650–700 °C [179]. The same applies to $LiMnPO_4$. As far as the carbon precursor is concerned, LMP and LFP differ primarily. Since iron binds to carbon, any type of carbon precursor can be used with little impact on C-LFP electrochemical performance. The only requirement is that the carbon supply includes hydrogen, which serves as a reducing agent [180]. The electrochemical properties of LMP are influenced by the choice of precursor [181,182], with the degree of carbon layer graphitization varying depending on the precursor. Li et al. [182] demonstrated that the effectiveness of carbon incorporation strongly depends on the formation of a uniform surface coating, as evidenced by high-resolution transmission electron microscopy observations and electrochemical impedance spectroscopy analysis. In their work, the electrode was fabricated by blending carbon-coated $LiMnPO_4$ (C-LMP) nanorods with acetylene black and PVdF binder in *N*-methyl-2-pyrrolidinone using a mass ratio of 75:15:1. The introduction of β-cyclodextrin enabled stable electrochemical behavior, delivering capacities of 153, 153, 143, 90, and 57 mAh g^{-1} over 50 cycles, indicative of favorable cycling performance [152]. In another approach, C-LMP nanoparticles with diameters below 40 nm and uniform carbon shells of approximately 2–3 nm were synthesized using oleylamine as both the solvent and carbon precursor. When evaluated as a cathode material, this sample achieved a discharge capacity of 168 mAh g^{-1} at 0.1C and 105 mAh g^{-1} at 5 C, while exhibiting an initial capacity of 135 mAh g^{-1} at 1 C with 81% retention after 50 cycles [183]. These electrochemical results exceeded those reported for C-LMP prepared via alternative routes such as high-energy ball milling [184], solid-state synthesis [185], microwave-assisted methods [186], spray pyrolysis [187], and chemical vapor deposition [188]. Subsequent studies further enhanced rate performance by producing nearly spherical C-LMP nanoparticles

with ultra-small sizes of 8–12 nm through a solvothermal method employing sucrose as the carbon source [189]. Electrodes assembled using PVDF binder and Timcal Super P conductive carbon in a 7:1 weight ratio exhibited capacities comparable to those previously reported [184], with capacity values increasing at higher C-rates and stabilizing near 130 mAh g^{-1} after 35 cycles at 0.5 C, primarily due to the reduced particle dimensions.

Yu et al. investigated LCP nanocomposites with different carbon-coating architectures, including single-layer, double-layer, and dual carbon-shell configurations [190]. For single-layer coatings, LCP was combined separately with 3 wt% acetylene black (AB), 5 wt% phenol–formaldehyde resin, and 10 wt% glucose. In contrast, the double-layer coating strategy involved forming an initial carbon shell using 10 wt% glucose, followed by a secondary coating composed of 1 wt% AB and 3 wt% polyacrylic sodium salt (PAS). Electrochemical evaluation revealed discharge capacities of 120.92, 107.0, and 138.06 mAh g^{-1} for the different coating configurations, with the glucose–PAS-derived carbon layers exhibiting more homogeneous surface coverage. At a rate of 0.1 C, LCP/C_PAS and LCP/C_AB electrodes delivered capacities of 143.51 and 147.12 mAh g^{-1}, respectively, although capacity retention after 50 cycles was limited to 21.6% and 11.9%, as shown in Fig. 14a and b. In a related study, Maeyoshi et al. compared various organic carbon precursors, including carboxymethyl cellulose (CMC), glucose, and ascorbic acid, against carbon-free LCP samples [191]. Their results indicated that ascorbic acid-derived coatings formed continuous carbon layers with large interparticle gaps, whereas glucose resulted in discontinuous carbon islands, while carbon-free LCP achieved the most uniform surface morphology. The corresponding initial discharge capacities were 108.5, 112.9, 107.9, and 135.0 mAh g^{-1}, respectively (Fig. 14c). Furthermore, synthesized LNP exhibited a high initial discharge capacity of 150.2 mAh g^{-1} with negligible capacity degradation over 100 cycles, underscoring the critical role of reaction-facilitating solvents in stabilizing electrochemical performance [192]. Effective interaction between organic precursors and LNP at relatively low temperatures was found to be essential for achieving strong carbon adhesion, with partial carbon formation occurring at 200–250 °C and becoming more uniformly distributed at elevated temperatures [193]. The resulting electrochemical behavior was analyzed through charge–discharge profiles (Fig. 14d), cyclic voltammetry curves (Fig. 14e), and cycling stability plots for LNP synthesized using different solvents (Fig. 14f).

The influence of different reaction solvents on the structural and electrochemical characteristics of LNP/C was systematically investigated. Among the tested media, the isopropyl alcohol (IPA)–based

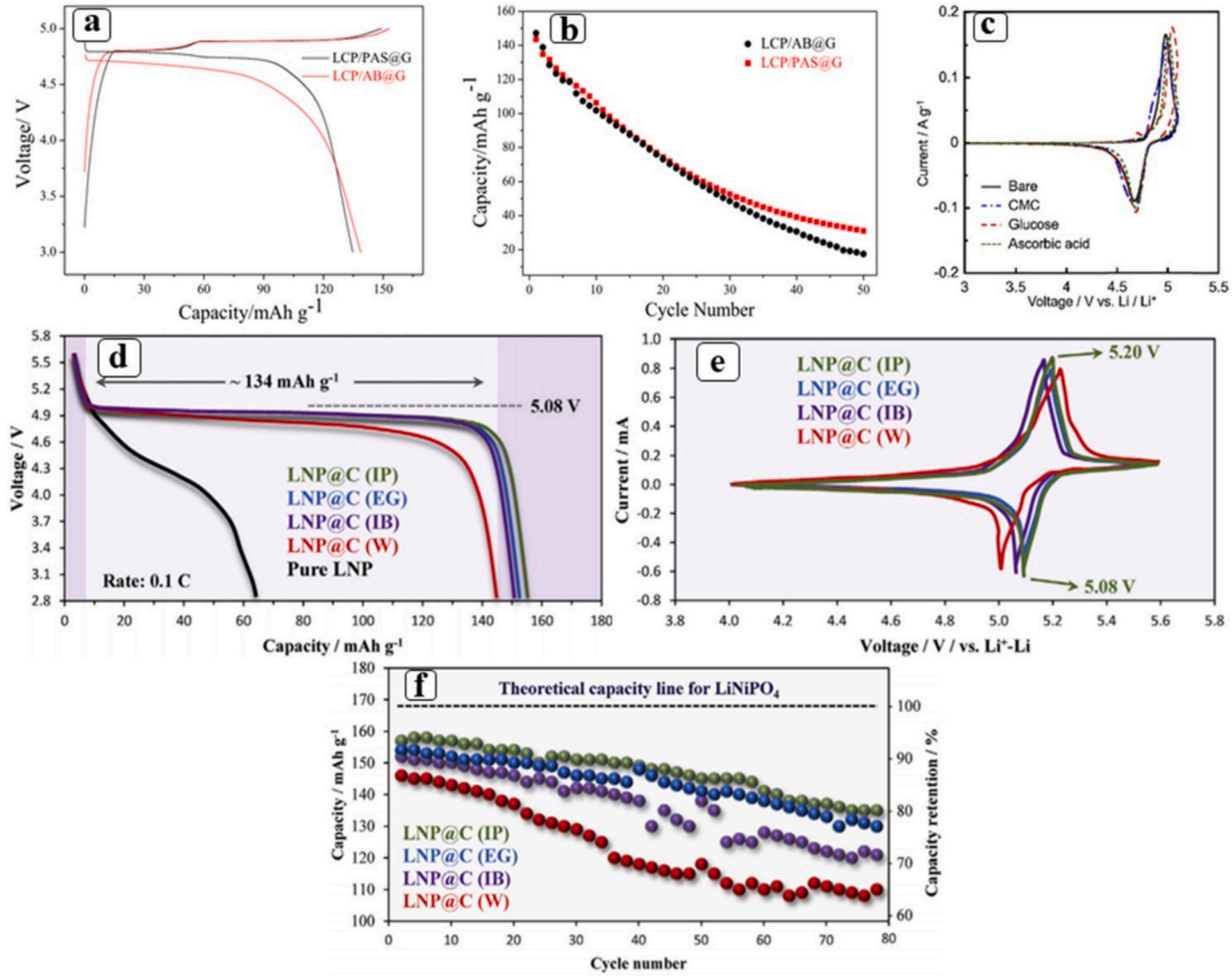

Fig. 14. Carbon coating improves LCP and LNP. Charge and discharge curves (a) and cycle performance (b) of a 0.1 °C double carbon-coated LCP composite [190]. CV profile of LCP with various carbon coatings (c) [191]. Charge and discharge curves (d), CV profile (e), and cycling stability profiles of LNP with various solvents (f) [192].

system delivered the highest initial discharge capacity of 157 mAh g^{-1} at a 0.1 C rate, although a capacity decay of about 19% was observed after 80 charge–discharge cycles. Transmission electron microscopy revealed that the carbon layer formed on the LNP particles had a thickness of approximately 5–6 nm [193]. In a related approach, Zang et al. [194] employed glucose as a carbon precursor using a combined solvothermal and solid-state reaction route in a biphasic water–benzyl alcohol solvent system. This strategy effectively suppressed particle coarsening during the annealing step, reducing the size of LNP particles that would otherwise reach diameters of ~2 μm. As a result, the LNP/C cathode demonstrated superior rate capability relative to bare LNP, achieving a notably high initial specific capacity of 220 mAh g^{-1} at a low current density of 0.05 C.

Carbon coating significantly improves high-voltage olivine cathode performance by increasing electronic conductivity and decreasing particle size. In situ techniques show outstanding electrochemical performance, achieving a discharge capacity close to theoretical values. The carbon layer should be less than 6 nm thick to ensure strong electronic conductivity and sufficient lithium-ion conduction, as thick layers prevent lithium-ion motion.

Carbon coating enhances the electronic conductivity and interfacial stability of $LiMPO_4$ cathodes, leading to improved electrochemical performance. Despite significant improvements, exact control of carbon thickness, homogeneity, and graphitization remains difficult, especially in high-voltage olivine phases. Future research should investigate advanced coating topologies such as hybrid carbon-inorganic layers and conductive polymers, as well as their long-term durability under high-voltage and solid-state battery conditions.

Beyond Carbon: Advanced Surface Coating Strategies for Olivine $LiMPO_4$ Cathodes.

Carbon coating is often employed to increase the electronic conductivity of olivine $LiMPO_4$ cathodes, although its efficiency may be limited by interfacial side reactions and insufficient chemical passivation during high-voltage operations. As a result, different surface coatings have gained popularity as supplemental or replacement solutions for stabilizing the cathode-electrolyte interface while maintaining favorable charge-transport kinetics.

Oxide-based coatings like Al_2O_3, TiO_2, and ZrO_2 operate as chemically durable interfacial barriers, reducing electrolyte oxidation and transition-metal dissolution. Although these coatings are normally electrically insulating, their performance is heavily dependent on thickness and uniformity; ultrathin oxide layers can maintain lithium-ion transport while greatly improving cycling stability at high voltages.

Phosphate-based coatings, such as Li_3PO_4 and metal phosphate layers, have better chemical compatibility with olivine cathodes due to their common polyanion framework. Coatings can minimize interfacial impedance and increase structural coherence, especially in high-voltage systems like LCP and LNPO, where electrolyte instability is a major concern.

Conductive polymer coatings, such as polyaniline and polypyrrole, on the other hand, serve two purposes: they improve electronic conductivity while also producing flexible, conformal interfacial layers. Their mechanical plasticity allows them to accommodate volume variations during cycling, but long-term chemical stability under harsh electrochemical conditions is still a worry.

More recently, hybrid coating topologies that combine carbon with oxide or polymer components have developed as a viable method for decoupling electrical conduction from interfacial protection. These multilayer or composite coatings combine the high conductivity of carbon frameworks with the chemical passivation of inorganic or polymeric layers to improve rate capability, cycling stability, and interfacial durability.

From a design perspective, the effectiveness of surface coatings in olivine $LiMPO_4$ cathodes is governed by a delicate balance between ionic permeability, electronic connectivity, and chemical stability. Future progress will require coating strategies that are not only electrically conductive but also chemically compatible with high-voltage electrolytes and scalable for practical electrode manufacturing. To illustrate the distinct roles of different surface engineering strategies, Fig. 15 schematically compares conventional carbon coatings with oxide-based and hybrid coating architectures applied to olivine $LiMPO_4$ cathode materials.

4.2. Particle size effect

Furthermore, this study shows that small LMP particles are particularly fascinating. Several methods can be used to do this, including phosphate-formate precursor [195], ultrasonic spray pyrolysis [196], antisolvent precipitation [197], and hydrothermal processes [198]. The LMP/C nanorods (thin <50 nm) had a capacity of 168 mAh at 0.05 C and 110 mAh at 10 C, with 94.5% capacity retention after 100 cycles at 0.5 C [199]. As indicated in the LFP section, some commercialization barriers exist for nanoparticles. First, such nanoparticles are difficult to handle [200]. Limiting tap density to 0.3–0.8 g cm^{-3} lowers the product's volumetric energy density [201]. The solution, like the LFP, was to use hierarchical structures. According to [202], a mechanochemical liquid-phase activation method successfully coupled nano-sized crystallites (20–50 nm) with micron-sized secondary particles. The use of nano primary particles and micron-sized secondary particles in Li (Mn, Fe) PO_4 resulted in similar capacities and enhanced rate capability, proving its efficacy in maximizing tap density [152].

4.3. Kinetic limitations and conductivity challenges

Atomistic modeling approaches can investigate multiple diffusion pathways in lithium-conducting materials, with particular emphasis on the relaxation of the surrounding lattice as an ion migrates across the structure [203]. Fig. 16 displays the lithium-ion migration paths in olivine-structured phosphates ($LiMPO_4$). Path A (migration between adjacent Li sites in the [010] direction), Path B (migration in the [001] direction), and Path C (migration across lithium channels in the [95] direction). The energy profiles of these mechanisms can be determined by calculating the energy of the migrating ion along the diffusion path, with the maximum potential energy representing the activation energy (Table 4) [203].

According to the study, the lowest energy path for lithium-ion migration in all four materials is through the [010] channel, path A. Other channels (B and C) have significant barriers of over 2.2 eV, preventing lithium ions from freely moving between them. The rapid oxide ion conductor constructed of 8 mol% yttria-stabilized zirconia (YSZ) [204] has identical activation energies for both oxide ion migration (0.9 eV) and cation migration (2.3 eV), confirming the very anisotropic nature of Li-ion migration in $LiMPO_4$. The study found that the migration of Li-ion in $LiMP0_4$ is significantly anisotropic, which is consistent with electronic structure estimations and experimental activation energies [150]. Molecular dynamics simulations can give a thorough examination of Li pathways, which are distinguished by complex particle translocation events and intersite Li^+ jumps in competitive pathways [216]. The predicted activation energies for LFP and LMP are consistent with the previously reported activation energy of 0.63 eV for both LFP and $LiFe_{0.45}Mn_{0.55}PO_4$ [205].

Recent LFP surface simulations [206] demonstrate that the (010) surface is prevalent in crystal morphology. This correlates to the desired [010] conduction channel [207]. The migrating ion moves in a curved way between lithium sites [220], deviating from a linear path by approximately 0.5 Å at its midpoint (Fig. 17). The observed lattice deformation surrounding the diffusing lithium-ion, as it travels through PO_4 and MO_6 polyhedra, highlights the importance of the (010) surface in nanoparticle behavior. Yamada et al. [208] confirmed the one-dimensional diffusion of Li^+ along a curved migration channel between adjacent lithium sites, agreeing with simulation results and predictions [220]. Magnetic susceptibility and X-ray absorption

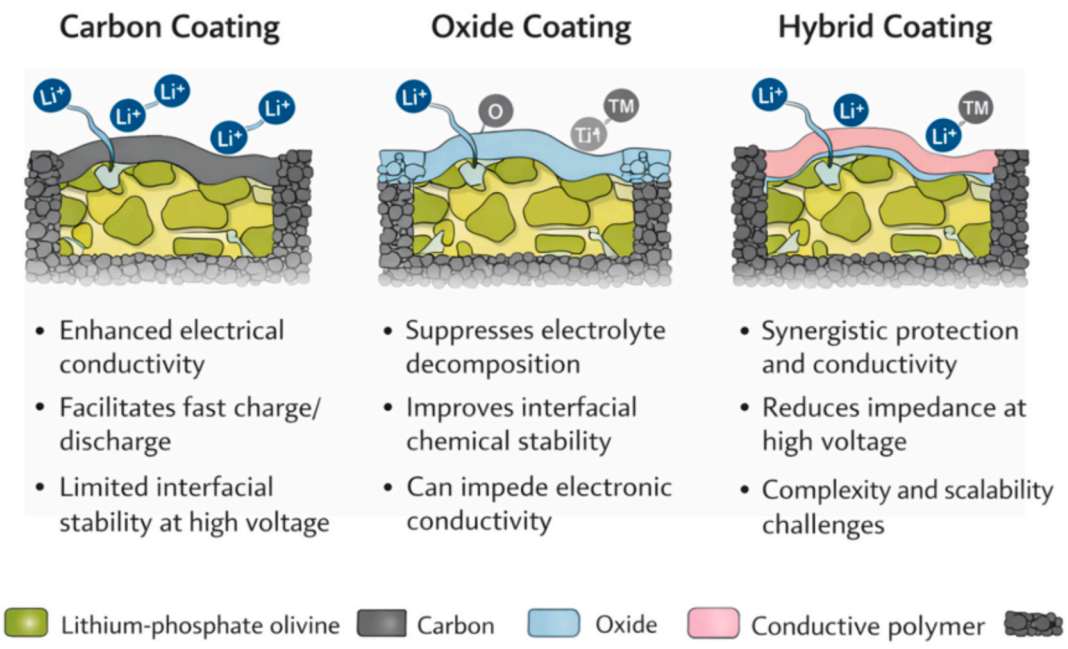

Fig. 15. Schematic illustration of representative surface coating strategies for olivine $LiMPO_4$ cathodes, including (a) conductive carbon coatings that enhance electronic transport, (b) inorganic oxide coatings that improve interfacial chemical stability and suppress electrolyte decomposition, and (c) hybrid coating architectures combining conductive and protective layers to synergistically enhance charge-transfer kinetics and cycling stability.

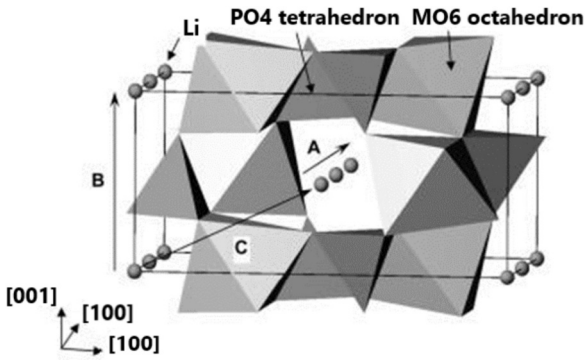

Fig. 16. Lithium-ion migration paths in olivine-structured phosphates ($LiMPO_4$) comprise components such as M = Mn, Fe, Co, and Ni [203].

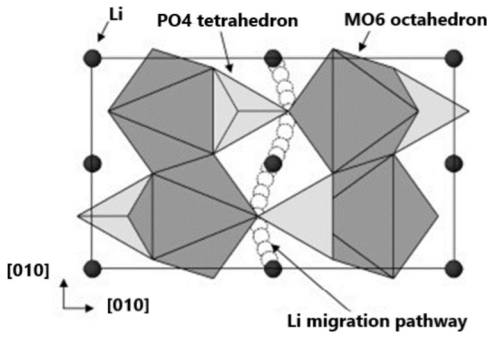

Fig. 17. A curved migration channel for lithium-ion migration pathway in olivine compounds $LiMPO_4$ (M = Mn, Fe, Co, and Ni) [203].

Table 4
Mechanisms and energies of Li migration in $LiMPO_4$ (Mn, Fe, Co, and Ni).[a]

Path	Migration	Energy, Emin (eV)	Co	Ni
	Mn	Fe		
A [010]	0.62	0.55	0.49	0.44
B [001]	2.83	2.89	3.28	3.49
C [101]	2.26	3.36	3.41	3.99

[a] Illustrated in Fig. 16.

spectroscopy experiments reveal distinct magnetic characteristics and electronic structures of single-crystal LFP in three axial directions [209].

The study discovered that lithium-ion diffusion in LFP crystals is two-dimensional, in contrast to the one-dimensional concept described previously [210]. The anisotropic character of the orthorhombic olivine structure is challenging to reconcile, as the Li—Li jump distances are extremely different. Furthermore, tracer diffusion investigations of Fe_2SiO_4 revealed distinct Fe diffusion along the three major axes [211]. Fig. 18 schematically illustrates the one-dimensional lithium-ion diffusion pathways in olivine $LiMPO_4$ and the associated kinetic limitations arising from low electronic conductivity. Modification strategies such as particle downsizing, conductive carbon coating, and hetero-ion doping are shown to effectively shorten diffusion lengths and improve the charge transport.

4.3.1. Summary and perspective

Carbon coating, particle size reduction, and hetero-ion doping address distinct yet interconnected limitations of olivine $LiMPO_4$ cathodes and therefore tend to exhibit synergistic effects when judiciously combined. Carbon coatings enhance surface electronic conductivity and interparticle charge transport, while particle downsizing shortens lithium-ion diffusion pathways and improves interfacial kinetics. In parallel, appropriate cation doping can modulate lattice parameters and defect concentrations, lowering lithium-ion migration barriers within the bulk structure. The simultaneous optimization of these strategies enables concurrent enhancement of electronic and ionic transport, leading to improved rate capability and cycling stability. Nevertheless, excessive carbon loading, extreme nanoscaling, or high dopant levels may compromise structural integrity or energy density, highlighting the importance of balanced materials design.

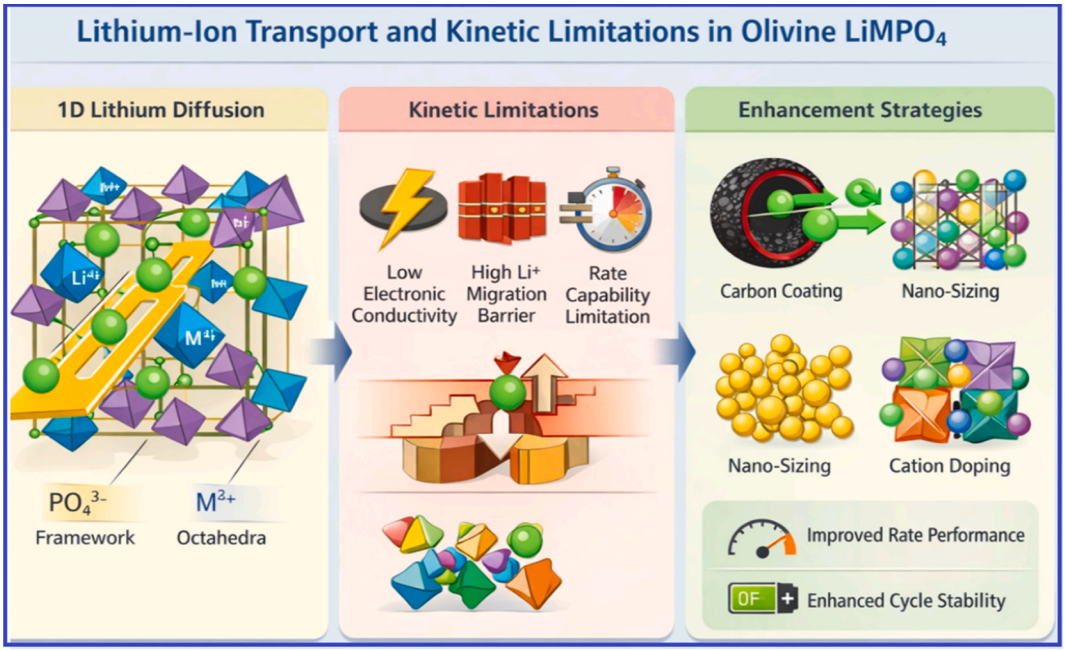

Fig. 18. Graphical illustration of lithium-ion transport pathways and kinetic limitations in olivine $LiMPO_4$ cathodes, highlighting intrinsic one-dimensional diffusion, electronic conductivity constraints, and the role of modification strategies such as carbon coating, nanosizing, and cation substitution in enhancing electrochemical performance.

4.4. Doping and compositional engineering

Introducing small amounts of aliovalent cations such as Al^{3+}, Zr^{4+}, and Nb^{5+} into $LiFePO_4$ has been reported to markedly enhance its electronic conductivity [225], leading to ongoing discussion regarding the underlying mechanism. Key questions include whether the dopants truly substitute into the olivine lattice, the identity of the charge-carrying species, and whether the observed conductivity improvements arise instead from indirect effects such as carbon impurities or the formation of phosphide phases [212–215]. To clarify these issues, Fisher et al. employed atomistic modeling approaches capable of quantitatively evaluating the relative energies associated with different dopant incorporation pathways, thereby offering systematic insight into site preference and dopant solubility trends. Their study extended the analysis of dopant behavior in $LiMPO_4$ systems beyond the range previously explored experimentally.

The primary objective was to determine the dominant charge-compensation mechanisms associated with aliovalent substitution, such as Na^+ replacing Li^+ or Mg^{2+} occupying M^{2+} sites; however, experimental validation of these mechanisms remained inconclusive. Possible compensation routes considered included the formation of lithium vacancies, transition-metal vacancies, oxygen vacancies, or electronic compensation effects [203]. To assess these scenarios, total substitution energies were calculated for different compensation schemes by examining Na^+ and Zr^{4+} dopants introduced at Li and M sites, respectively, and comparing multiple incorporation reactions.

Substitution and solution energies were obtained by combining defect formation energies with lattice energy contributions for each modeled reaction. Interatomic potential methods were applied to simulate dopant incorporation in binary oxides containing the relevant cations, following a systematic modeling framework that has previously been extended to other oxide and silicate materials [216,217]. As illustrated in Fig. 19, dopant incorporation energies for monovalent, divalent, and trivalent cations with energetically favorable charge-compensation mechanisms are plotted as a function of ionic radius. All calculations were performed in the dilute doping limit to represent low dopant concentrations. The calculated solution energies for tetravalent and pentavalent dopants in olivine phosphate structures are summarized in Table 5, where A^{4+} and A^{5+} species are reported separately [203]. The results indicate that Nb^{5+} substitution at the M^{2+} site in LMP and LNPO is energetically unfavorable, suggesting limited dopant stability in these systems.

The researchers discovered that all four $LiMPO_4$ materials had the lowest isovalent substitution energies, with Na doping for Li^+ and divalent doping for M^{2+} being the most successful. This is compatible with the mutual solubility observed in other $LiMPO_4$ systems [218–223,232,234] but does not necessitate charge compensation, reducing the number of charge carriers. Roberts et al. [224] found that Mg^{2+} is soluble at Fe sites in LFP but not at Li sites. The $LiFe_{0.9}Mg_{0.1}PO_4$ system is more resistant to capacity fading than the undoped LFP [222]. However, adding redox-inactive Mg^{2+} reduces the effective electrochemical capacity.

Aliovalent substitution with tetravalent and pentavalent cations is energetically unfavorable across the $LiMPO_4$ family, indicating that A^{4+} and A^{5+} dopants are thermodynamically unstable within the olivine lattice and therefore unlikely to be incorporated in significant amounts [220]. As the valence mismatch between the dopant and the host ion increases, the energy required for dopant incorporation rises accordingly, highlighting the dominant role of electrostatic interactions in governing dopant energetics in olivine-structured $LiMPO_4$ materials.

Among the examined donor dopants, Ti^{4+} and Nb^{5+} exhibit the poorest compatibility with both Li and transition-metal sites, with charge compensation primarily occurring through the formation of M^{2+} vacancies or changes in oxidation states. Despite numerous reports of enhanced electronic conductivity following supervalent doping, the fundamental mechanism responsible for such improvements remains unclear. Maier and Amin [225] reported that even trace levels of supervalent dopants can alter the valence state of transition-metal ions, potentially decreasing, rather than increasing, the concentration of intrinsic electronic charge carriers. Their findings also showed that undoped LFP and LCP can achieve electronic conductivities in the range of 10^{-4} to 10^{-2} S cm^{-1} [212,214,215]. Experimental studies further indicate limited dopant solubility and effectiveness: Butt et al. [226] observed that Ti^{4+} does not dissolve into the LNPO lattice, while Wolfenstine [218] demonstrated that the presence of a conductive Co_2P surface layer does not substantially improve the electronic conductivity

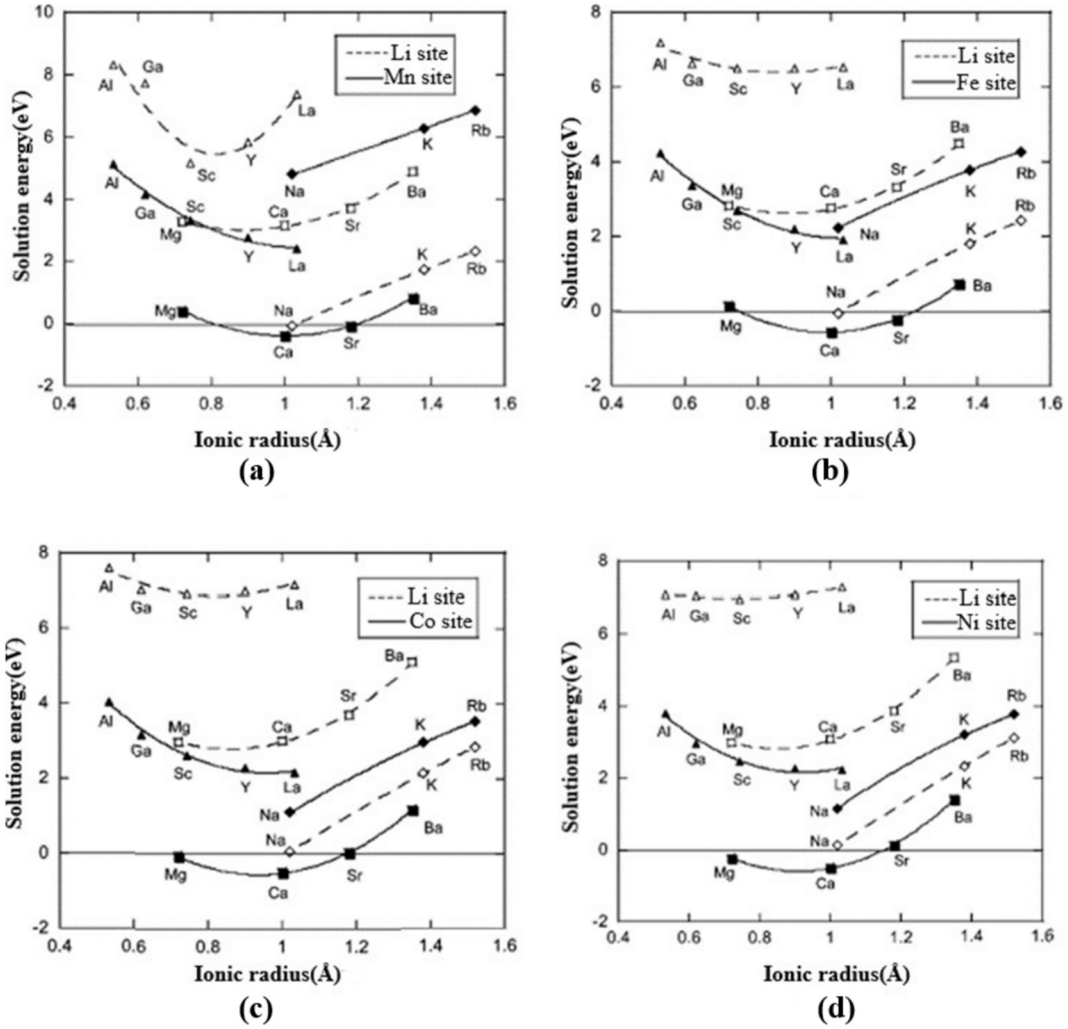

Fig. 19. Solution energies vs dopant ionic radius for (a) LMP, (b) LFP, (c) LCP, (d) LNPO. Lines are purely visual guidelines [203].

Table 5
Solution energies of tetravalent and pentavalent dopants in olivine phosphates.

Solution energy (eV/dopant)			
Site	Ti^{4+}	Zr^{4+}	Nb^{5+}
LMP			
Li	11.0	12.6	17.9
Mn	7.6	6.8	NC[a]
LFP			
Li	10.7	10.6	13.5
Fe	6.0	5.7	7.7
LCP			
Li	11.6	11.5	14.8
Co	6.3	7.3	12.5
LNPO			
Li	11.8	11.7	14.8
Co	6.2	5.8	NC[a]

[a] NC = nonconverge of calculation.

of LCP. Similarly, Delacourt et al. [212] were unable to successfully introduce Nb^{5+} into $LiFePO_4$, and Ellis et al. [214] concluded that aliovalent dopants such as Al, Y, Cr, and Zr do not lead to enhanced conductivity in $LiMPO_4$ materials synthesized under carbothermal reduction conditions.

The stability of hypervalent dopants like Zr^{4+} and Nb^{5+} in olivine $LiMPO_4$ cathodes is influenced by thermodynamic and kinetic factors. Thermodynamically, substituting higher-valence cations at the M^{2+} site creates charge imbalances and lattice strain, necessitating the formation of lithium or oxygen vacancies and mixed-valence states for charge compensation. This process increases defect formation energy and may lead to destabilization of the olivine structure, resulting in phase separation when the energetic cost of defects outweighs the stabilization benefits of substitution.

Kinetically, the PO_4^{3-} framework inhibits long-range cation diffusion, promoting dopant segregation at grain boundaries and forming metastable structures during electrochemical cycling. Consequently, hypervalent doping remains stable primarily at low concentrations, with detrimental effects at higher levels, despite short-term enhancements in transport properties. Table 6 presents a benchmarking analysis of single-metal olivine phosphates, summarizing key performance metrics and characteristics relevant to their application in various contexts. All tabulated data presented in this section are derived from published literature and are intended for comparative benchmarking.

Cation doping and mixed transition-metal substitution have emerged as powerful tools to tune lattice parameters, electronic structure, and lithium-ion migration kinetics in $LiMPO_4$ materials. While performance enhancements have been widely reported, the thermodynamic stability and defect chemistry of heavily or hypervalent-doped systems are not yet fully understood. Future studies combining first-principles modeling

Table 6
Benchmark electrochemical performance of representative single-metal olivine $LiMPO_4$ cathodes. Data are compiled from recent literature reports (2021–2025) under comparable testing conditions.

Cathode material	Primary modification strategy	Average operating voltage (V vs. Li/Li^+)	Practical capacity (mAh g^{-1})	Rate capability	Cycling stability	Key performance characteristics
$LiFePO_4$	Pristine	~3.4–3.5	150–165	Moderate	Excellent (>2000 cycles)	Enhanced electronic conductivity and power capability
$LiFePO_4$	Carbon coating	~3.4–3.5	155–170	High (up to several C)	Excellent	Higher voltage but sluggish kinetics
$LiMnPO_4$	Pristine	~4.0–4.1	110–130	Low	Moderate	Higher voltage but sluggish kinetics
$LiMnPO_4$	Nanosizing/surface modification	~4.0–4.1	125–140	Moderate	Improved	Reduced diffusion length and polarization
$LiCoPO_4$	Carbon coating/ doping	~4.7–4.8	140–155	Low-moderate	Limited	High voltage benefits offset by interfacial and kinetic challenges
$LiNiPO_4$	surface engineered	~4.9–5.1	150–165	Low	Poor–moderate	Very high voltage, severe kinetic and interfacial limitations

with operando characterization are needed to establish rational doping limits and design multi-cation olivine cathodes with optimized structure–property–performance relationships.

4.5. *Mixed transition-metal olivine phosphates: structure–property–performance relationships*

Beyond single-metal olivine phosphates, mixed transition-metal Li$(TM_1TM_2)PO_4$ and Li$(TM_1TM_2TM_3)PO_4$ systems have emerged as an effective strategy to balance voltage, capacity, and kinetic limitations inherent to individual $LiMPO_4$ compositions. Partial substitution of Fe^{2+} with Mn^{2+}, Co^{2+}, or Ni^{2+} has been shown to introduce multiple redox couples, leading to broadened operating voltage windows and tunable electrochemical profiles [227]. For example, $LiFe_{1-x}Mn_xPO_4$ exhibits a synergistic combination of the structural stability of Fe-based olivines and the higher redox potential of Mn-based counterparts.

From a structural perspective, multi-cation substitution induces controlled lattice distortion and local symmetry breaking, which can reduce lithium-ion migration barriers along the one-dimensional b-axis diffusion channels [67]. First-principles and experimental studies indicate that appropriately designed cation disorder can mitigate antisite defect formation while enhancing percolative lithium diffusion pathways. However, excessive compositional complexity may also introduce local strain and phase heterogeneity, underscoring the need for optimized stoichiometry.

Electrochemically mixed-TM olivines often display smoother voltage profiles and improved rate capability compared to single-metal analogues, particularly when combined with nanostructuring and conductive carbon architectures [228]. Recent work on ternary olivine compositions such as Li(Fe, Mn, Co)PO_4 demonstrates that rational compositional tuning enables simultaneous optimization of energy density, cycling stability, and thermal safety. These findings highlight multi-cation olivines as a promising material platform for high-performance and application-specific LIBs. Table 7 presents a comparative analysis of mixed and multi-cation olivine phosphates, likely outlining their properties, performance metrics, or applications as benchmarks within the relevant scientific field.

To quantitatively benchmark these trends, a Ragone plot comparing representative single-metal and mixed-metal olivine phosphate cathodes under different optimization strategies is presented in Fig. 20.

Overall, while individual optimization strategies improve either energy density or power capability, mixed transition-metal olivine systems combined with surface and morphological engineering demonstrate the most balanced electrochemical performance.

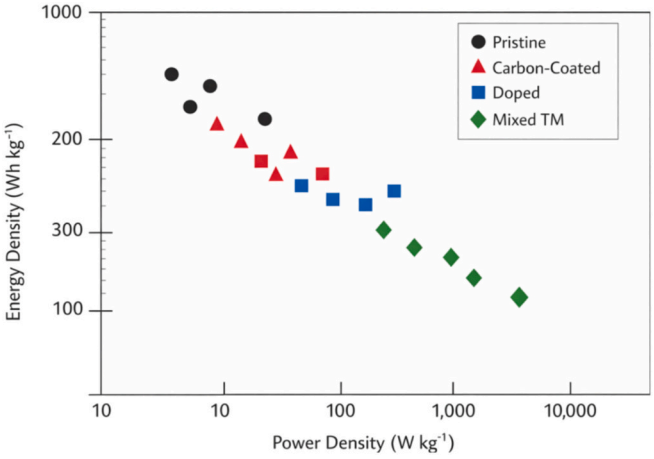

Fig. 20. Ragone plot comparing representative single-metal and mixed-metal olivine phosphate cathodes with different optimization strategies. Energy and power densities are calculated from reported capacity and voltage values at specified C-rates. Markers reflect (●) pristine, (▲) carbon-coated, (■) doped, and (◆) mixed transition-metal systems.

Table 7
Comparative performance of mixed transition-metal olivine phosphate cathodes and their dominant optimization strategies. Values represent typical ranges reported in the literature.

Composition	Dominant redox couples	Voltage range (V vs. Li/Li^+)	Practical capacity (mAh g^{-1})	Rate performance	Cycling stability	Structure–property–performance insight
$LiFe_{1-x}Mn_xPO_4$	Fe^{2+}/Fe^{3+}, Mn^{2+}/Mn^{3+}	~3.6–4.1	140–155	Moderate	Good	Balanced voltage and stability with improved kinetics over $LiMnPO_4$
Li(Fe,Mn)PO_4 (optimized ratios)	Fe/Mn	~3.7–4.0	145–160	Moderate–high	Good	Smoother voltage profile and reduced polarization
Li(Fe,Mn,Co)PO_4	Fe/Mn/Co	~3.8–4.7	150–165	Moderate	Moderate	Enhanced energy density with manageable structural stability
Li(Fe,Co,Ni)PO_4	Fe/Co/Ni	~3.9–4.9	~155–165	Moderate	Limited	High voltage benefits offset by interfacial and kinetic challenges
Multi-cation $LiMPO_4$ with carbon networks	Multiple	Composition-dependent	150–170	High	Good	Synergistic effects from compositional tuning and conductive frameworks

4.6. High-voltage olivine phosphates and electrolyte challenges

The sol-gel process was utilized to create olivine-type compounds with the structural formula $LiMPO_4$, which has a sponge-like particle shape appropriate for cathode materials [98]. The composite consists of an orthorhombic olivine structure, with lithium occupying the octahedral sites while Mn^{2+} and Co^{2+} replace Fe^{2+}. LFP has excellent electrochemical characteristics, but LCP has limited reversible capacity and unpredictable cycle performance.

Fig. 21 illustrates the initial charge–discharge behavior and cycling stability of the synthesized sponge-like olivine powders and presents the galvanostatic profiles of LFP, LMP, and LCP composite cathodes measured at room temperature under identical current density conditions. As shown in Fig. 21a, LFP delivers discharge capacities of 136.9 and 136.0 mAh g^{-1}, LMP achieves 109.1 and 107.7 mAh g^{-1}, and LCP exhibits 134.6 and 83.4 mAh g^{-1} during the first cycles. The LFP electrode displays a well-defined and flat charge–discharge voltage plateau across different compositions, characteristic of a two-phase redox mechanism [86,229]. In contrast, the charge–discharge profiles of LMP and LCP exhibit two distinct voltage plateaus corresponding to their respective redox reactions. While both LFP and LMP exhibit nearly 100% reversible capacity, LCP's reversibility is limited to about 62%, primarily due to electrolyte decomposition at its higher operating voltage. Cycling performance over 30 cycles, presented in Fig. 21b, further confirms the excellent stability of LFP, whereas LMP and LCP undergo noticeable capacity fading during repeated cycling. LFP cells have 100%, 78%, and 59% capacity retention rates, respectively. The capacity loss in LMP cells may be due to Mn dissolution and electrolyte decomposition [196]. LCP has unpredictable cycle performance and significant capacity reduction due to electrolyte breakdown. LFP cells have a higher rate capability.

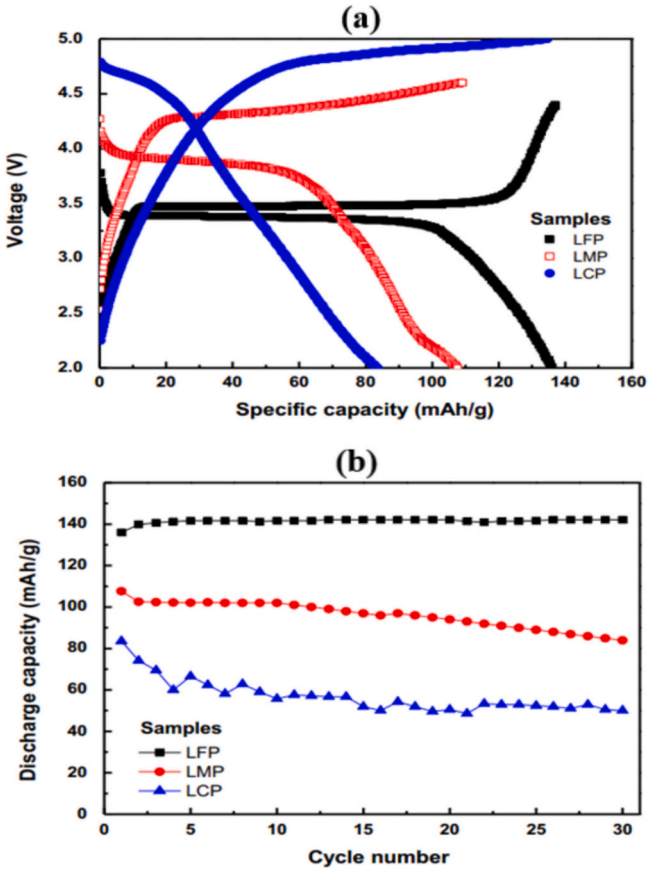

Fig. 21. Initial charge-discharge performance (a) and cycle stability (b) of lithium cells at 0.5 C-rate using cathodes made from three materials (RT) [98].

Sol-gel synthesis resulted in pure powders of LFP, LMP, and LCP, with LMP having the biggest unit cell. The lattice properties and cell volumes of the composite altered as the transition metal changed, particularly in MO_6 octahedra. The deformation of PO_4 tetrahedra occurs solely in LMP. LFP has good electrochemical characteristics; however, LCP has low cycle stability because of electrolyte breakdown at high voltages. Fig. 22 highlights recent advances in electrolyte engineering that extend oxidative stability beyond 4.5 V, thereby enabling improved cycling of high-voltage olivine phosphates. The development of high-voltage and functional electrolytes has renewed interest in $LiCoPO_4$ and $LiNiPO_4$ for high-energy LIBs. Table 8 compares the electrochemical characteristics of LFP and high-voltage olivine cathodes.

The high operating voltages of LMP, LCP, and LNPO are due to strong electrostatic repulsions between M and P ions, resulting in lower covalence of M—O bonds. The P—O covalent bond provides high structural stability, making it ideal for large-scale applications such as electric and hybrid vehicles, where battery safety is a crucial factor [246]. These phosphates have discharge capacities similar to those of $LiFePO_4$, resulting in higher theoretical energy densities. $Li_3V_2(PO_4)_3$ represents another high-voltage phosphate cathode and exists at room temperature in two polymorphic forms: a rhombohedral NASICON-type β phase and a monoclinic α phase [244]. In contrast, orthorhombic olivine phosphates generally suffer from inherently sluggish kinetics, which originate from their very low electronic conductivity caused by the separation of MO_6 octahedra by insulating PO_4 tetrahedra, as well as from one-dimensional lithium diffusion pathways within the crystal framework. In the case of $LiMnPO_4$, both electronic and ionic conductivities are particularly poor, resulting in practical capacities that fall well below the theoretical limit. Moreover, during delithiation, the presence of Mn^{3+} induces pronounced Jahn–Teller distortions, leading to structural instability in LMP [247–250,266]. Despite this, parasitic interfacial reactions with conventional electrolytes are relatively minor, since EC-based electrolytes remain stable at operating voltages around 4.1 V. This behavior contrasts with that of LCP and LNPO, which operate at much higher voltages and therefore suffer from severe electrolyte oxidation, like high-voltage spinel systems such as $LiNi_{0.5}Mn_{1.5}O_4$ (~4.7 V), albeit with somewhat improved transport properties [251]. Approaches to enhance lithium transport and electrochemical reversibility in high-voltage olivine phosphates and α-$Li_3V_2(PO_4)_3$ largely mirror those developed for LFP, including particle downsizing, conductive carbon coatings, and elemental substitution. However, aliovalent doping has not been shown to intrinsically enhance the electronic conductivity of LFP, a limitation that likely extends to other $LiMPO_4$ compounds. Instead, dopant incorporation often generates cation vacancies at lithium and/or transition-metal sites, which can indirectly facilitate lithium-ion diffusion within the structure [252]. High-voltage phosphates have shown inferior half-cell electrochemical performance compared to LFP, especially for Co- and V-based compositions. Future considerations should focus on long-term cycling behavior and graphite anodes. Further research is required to gain a deeper understanding of the impact of elemental substitution on high-voltage phosphates.

Recent studies have further advanced the understanding and performance optimization of olivine $LiMPO_4$ cathodes through integrated structural design, interfacial engineering, and compositional tuning. For instance, systematic investigations have demonstrated that controlled surface modification and conductive network construction can significantly enhance electronic conductivity and lithium-ion diffusion kinetics, leading to improved rate capability and cycling stability in olivine phosphate cathodes [253,254]. In parallel, targeted cation substitution and defect regulation have been shown to modulate lattice parameters and redox behavior, enabling improved electrochemical reversibility and energy density without compromising structural stability [255,256]. Moreover, emerging work has highlighted the adaptability of olivine-based cathodes to advanced battery systems, including high-voltage and solid-state configurations, by addressing interfacial compatibility and transport limitations through rational materials and

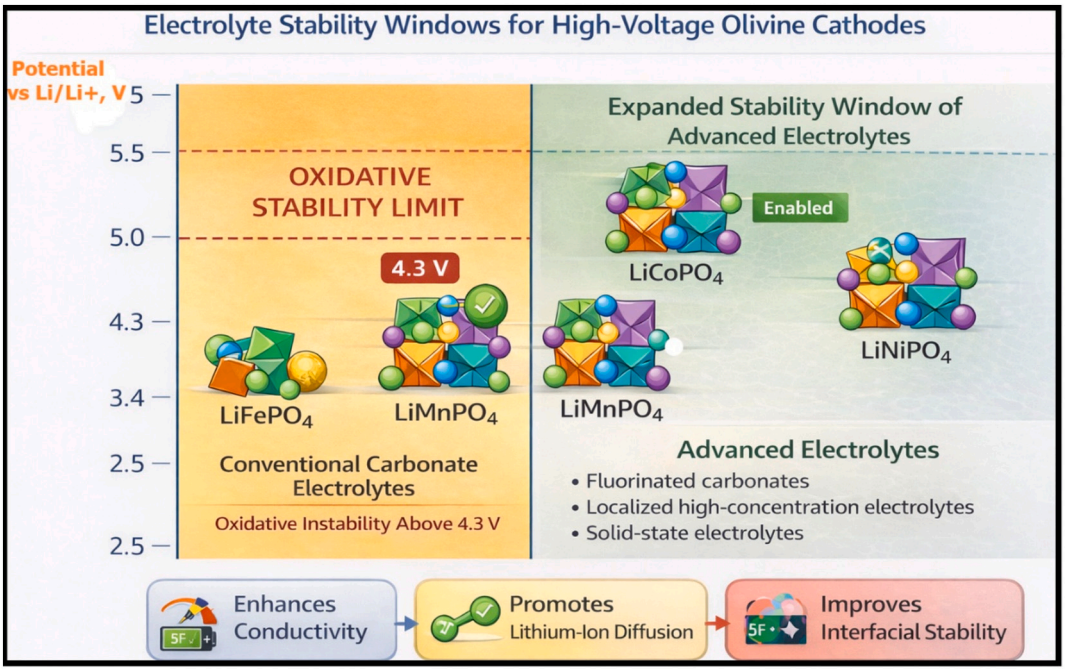

Fig. 22. Graphical comparison of electrochemical stability windows of conventional and advanced electrolytes relative to the operating voltages of olivine $LiMPO_4$ cathodes, illustrating the electrolyte constraints and opportunities for high-voltage LCP and LNPO systems.

Table 8
Electrochemical characteristics of high-voltage olivine and monolithic α-$Li_3V_2(PO_4)_3$ with LFP.

	LFP	LMP	LCP	LNPO	α-Li3V2(PO_4)3
Average voltage (V, vs. Li^+/Li)	3.45	4.1	4.8	5.1	4.0[b]
Theoretical capacity (mA h g^{-1})	170	171	167	169	197
Reversible capacity (mA h g^{-1})	>160	160	>120	>75	170
Theoretical energy density (Wh kg^{-1})	586	701	801	862	788
Electrical conductivity (S cm^{-1})	10^{-9}	10^{-11}	10^{-9}	10^{-7}[c]	108
Apparent Li diffusivity (cm^2 s^{-1})[a]	10^{-14}–10^{-16}	10^{-17}	10^{-13}–10^{-14}	10^{-14}–10^{-15}	10^{-9}–10^{-10}
Reference	[86,230,231]	[86,232–234]	[235–237]	[238–241]	[242–245]

[a] Based on empirical rather than computational data. The latter often suggests values that are several orders of magnitude greater [150,156].
[b] $V^{3+/4+}$ ranges between 3.6 and 4.0 V, whereas $V^{4+/5+}$ exceeds 4.5 V [243].
[c] This data was gathered at 716 K.

interface design [257]. These recent advances reinforce the relevance of $LiMPO_4$-based materials as versatile and robust cathodes for next-generation rechargeable batteries.

High-voltage olivine phosphates offer substantial energy-density gains but remain constrained by electrolyte oxidative stability and interfacial degradation. Emerging electrolyte formulations and solid-state systems provide promising pathways toward stable high-voltage operation, though long-term reliability remains a critical research focus.

4.7. Advanced characterization of electrochemical mechanisms

Recent advances in operando and in situ characterization techniques have provided critical insights into the electrochemical mechanisms governing olivine $LiMPO_4$ cathodes. Operando X-ray diffraction (XRD) studies have clarified the phase evolution during lithium insertion and extraction, revealing a transition from classical two-phase behavior in LFP to more complex solid-solution or mixed-phase mechanisms in Mn-, Co-, and Ni-based olivine phosphates, particularly under non-equilibrium or high-rate conditions [258]. These findings underscore the strong coupling between crystal chemistry, lithium diffusion anisotropy, and electrochemical response.

Complementary X-ray absorption spectroscopy (XAS) investigations have enabled direct probing of transition-metal redox states and local coordination environments, demonstrating that cation substitution not only shifts redox potentials but also alters metal–oxygen covalency and polyanion inductive effects [259]. In several $LiMPO_4$ systems, XAS results further indicate partial irreversibility of transition-metal redox at elevated voltages, contributing to voltage hysteresis and long-term capacity degradation [259,260].

Furthermore, in situ and operando TEM and spectroscopic techniques have revealed nanoscale degradation pathways, including anti-site defect accumulation, microcrack formation, interfacial reconstruction, and localized amorphization during prolonged cycling or high-voltage operation [261]. These observations demonstrate that electrochemical performance is governed not only by bulk lithium diffusion kinetics but also by defect chemistry and electrode-electrolyte interfacial stability. Collectively, these advanced characterization studies provide a comprehensive mechanistic framework for guiding the rational design of high-performance and high-voltage olivine phosphate cathodes [262].

Electrochemical investigations reveal that the performance of olivine $LiMPO_4$ cathodes is governed by a complex interplay between crystal structure, microstructure, and surface chemistry. Although LFP has reached commercial maturity, higher-voltage members remain limited by kinetic barriers and electrolyte instability. Future research should prioritize operando diagnostics to elucidate degradation mechanisms

and guide the design of next-generation high-voltage olivine cathodes with improved durability and energy density.

5. Technological prospects and applications

From an application standpoint, the balance between energy and power density is critical, as illustrated by the Ragone comparison shown in Fig. 21. Olivine phosphate cathode materials have demonstrated strong potential for a wide range of lithium-ion battery applications due to their intrinsic safety, structural robustness, and long-term cycling stability. Among them, LFP has already achieved large-scale commercial success in electric vehicles, grid-level energy storage, and stationary backup systems, owing to its low cost, environmental benignity, and excellent thermal stability. These attributes make LFP particularly attractive for applications where safety, longevity, and cost-effectiveness outweigh the need for ultra-high energy density.

Higher-voltage olivine phosphates, including LMP, LCP, and LNPO, offer significantly increased operating voltages and theoretical energy densities, positioning them as promising candidates for next-generation LIBs targeting extended driving range and compact energy storage. However, their practical deployment remains limited by challenges such as sluggish lithium-ion transport, low electronic conductivity, and electrolyte instability at elevated voltages (see Sections 3–4). Recent advances in materials engineering, such as the design of nanoscale particles, conductive carbon architectures, and hetero-ion substitution, have partially mitigated these limitations, leading to improved rate capability and cycling stability. Lithium transition metal phosphates (Co, Ni) are investigated as cathode materials for high-voltage lithium-ion batteries due to their ability to undergo full lithiation and delithiation. Despite advancements, materials like LCP and LNP have only achieved around 80% specific capacity, and their discharge capacity remains limited to 10–20 cycles at lower rates. Fig. 23 illustrates the status of high-voltage olivine-structured $LiMPO_4$ cathode materials used in energy storage applications. Advancements in battery technology indicate that olivine-structured cathodes, with high potentials of 4.8 and 5.2 V, are promising for implementation in all-solid-state battery systems for large-scale applications, particularly in electric vehicles (EVs) and hybrid vehicles (HVs). Research by Okumura et al. demonstrated the use of LCP-LATP composite cathodes in all-solid-state LIBs using the spark plasma sintering (SPS) method to evaluate their electrochemical performance [263].

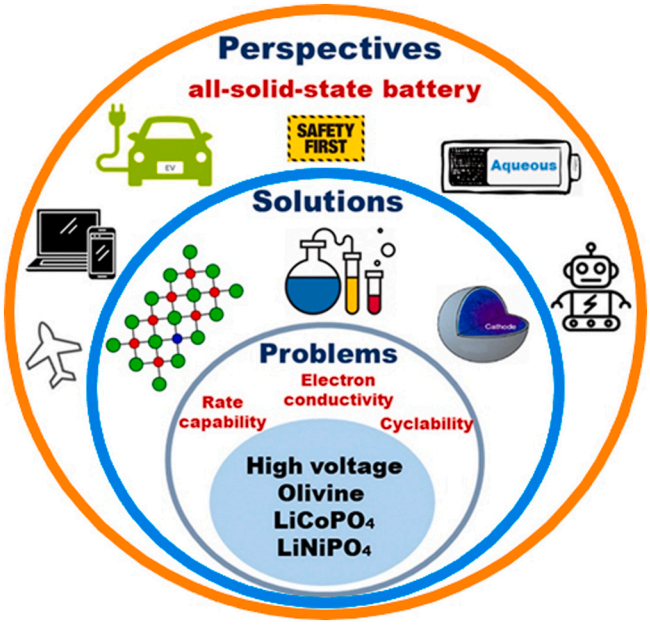

Fig. 23. The present state of high voltage olivine structured $LiMPO_4$ cathode materials for energy storage applications.

Recent developments in energy storage have highlighted aqueous batteries utilizing lithium-ion conduction mechanisms [264]. An experimental study reported the use of a high-potential electrode, LCP, as a cathode in these batteries [265]. From a system-level perspective, the compatibility of high-voltage olivine cathodes with advanced electrolytes has emerged as a critical factor for technological adoption. Developments in high-voltage electrolyte systems, including fluorinated carbonate formulations and localized high-concentration electrolytes, have expanded the electrochemical stability window beyond 4.5 V, thereby enabling more stable operation of LCP- and LNPO-based cells. These electrolyte innovations not only enhance oxidative stability but also improve interfacial robustness, which is essential for long-term cycling under high-voltage conditions.

The development of solid electrolytes, including polymer [266–269] and inorganic ceramic types [270,271], facilitates the creation of new high-power cells with stable lithium metal anodes. Despite significant research into high-voltage olivine-structured cathodes like LCP and LNPO, challenges remain in meeting current energy storage system demands. To address these issues, detailed computational studies are necessary to better understand the weaknesses of these cathodes, integrating theoretical calculations with experimental work for future advancements. Beyond conventional LIBs, olivine phosphate cathodes are also being explored for emerging energy-storage platforms, including solid-state batteries and hybrid battery–capacitor systems. The rigid polyanion framework and thermal resilience that characterize olivine structures are particularly advantageous in solid-state configurations, where mechanical and chemical stability at electrode–electrolyte interfaces is paramount. As research continues to integrate advanced materials design with scalable manufacturing and electrolyte optimization, olivine phosphates are expected to play an increasingly important role in future safe, sustainable, and high-performance energy-storage technologies. The suitability of olivine $LiMPO_4$ cathodes for solid-state batteries is closely related to their favorable interfacial behavior with solid electrolytes. The rigid PO_4^{3-} polyanion framework confers excellent structural and thermal stability, while the small volume change associated with lithium insertion and extraction minimizes mechanical stress at the cathode–electrolyte interface. These characteristics help preserve interfacial contact and suppress the formation of resistive interphases during cycling, which are common challenges in solid-state battery systems.

Furthermore, $LiMPO_4$ cathodes exhibit good chemical compatibility with a range of inorganic solid electrolytes, reducing the likelihood of parasitic interfacial reactions. Surface engineering strategies, including carbon coating, nanoscale morphology control, and the introduction of thin interfacial buffer layers, have been shown to further decrease interfacial impedance by improving electronic percolation and facilitating lithium-ion transport across the solid–solid interface. As a result, olivine phosphate cathodes represent promising candidates for solid-state lithium batteries, particularly in applications where safety, interfacial stability, and long-term cycling reliability are critical.

5.1.1. *Summary and perspective*

Olivine phosphate cathodes have already proven their technological relevance through the commercial success of LFP, while higher-voltage analogues present compelling opportunities for next-generation lithium-ion batteries. Continued progress will depend on coordinated advances in materials modification, electrolyte engineering, and system-level design to bridge the gap between laboratory-scale performance and commercial viability, particularly in high-voltage and solid-state applications.

6. Commercial prospects and market readiness of $LiMPO_4$-based batteries

Olivine phosphate cathodes, particularly LFP, represent one of the most commercially successful lithium-ion battery chemistries to date due to their exceptional thermal stability, long cycle life, and low material cost. LFP-based batteries have achieved large-scale commercialization in electric vehicles, grid-scale energy storage, and backup power systems, driven by their intrinsic safety, cobalt-free composition, and tolerance to abusive operating conditions. The mature supply chain and scalable synthesis routes for LFP further enhance its economic competitiveness in comparison with layered oxide cathodes.

Beyond LFP, other LMP materials such as LMP, LCP, and LNP offer higher operating voltages and the potential for increased energy density, positioning them as candidates for next-generation applications where safety and voltage scalability are simultaneously required. Although challenges related to electronic conductivity, lithium-ion transport kinetics, and electrolyte compatibility currently limit their widespread commercialization, recent advances in nanostructuring, carbon coating, doping, and electrolyte engineering have significantly narrowed the performance gap. These developments suggest that high-voltage olivine phosphates could find niche commercial adoption in high-power, high-safety, and solid-state battery systems.

Olivine phosphate cathodes, especially LFP, showcase strong scalability and industrial viability due to their utilization of abundant, low-cost raw materials and compatibility with established manufacturing processes. These cathodes present a more stable cost structure and lower environmental impact compared to cobalt- and nickel-rich layered oxides, such as NMC and NCA. Their robust structure allows for high-temperature processing and resilience under aggressive operating conditions, resulting in enhanced thermal safety and more straightforward safety management in battery packs. Consequently, LFP has gained traction in electric vehicles, grid-scale energy storage, and stationary backup systems.

Nevertheless, LMP's lower gravimetric energy density, stemming from moderate operating voltage and limited lithium-ion diffusion compared to layered oxides, poses a challenge. High-voltage variants like LCP and LNP could improve energy density, but face hurdles such as electrolyte instability and manufacturing complexity beyond 4.7 V.

Therefore, the competitiveness of LMP cathodes depends on application, excelling in areas where safety and cost efficiency are prioritized, while layered oxides dominate high-energy applications. Advancements in surface engineering, mixed transition-metal composition, and electrolyte compatibility may enhance performance and support the broader acceptance of advanced olivine cathodes in future lithium-ion and solid-state battery technologies.

Overall, the combination of cost-effectiveness, environmental sustainability, and robust safety characteristics ensures that $LiMPO_4$-based cathodes will continue to play a central role in the lithium-ion battery market. Continued progress in materials engineering and interface optimization is expected to further expand their commercial footprint, particularly in applications demanding long service life and high reliability.

7. Modification strategies and outlook

Cathode materials significantly influence lithium battery energy density, enhancing its efficiency, power density, and safety. Cathode materials should have high specific capacities, excellent performance rates, structural stability, and optimal charge/discharge voltage windows. Moreover, large-scale commercial applications require cathode materials that are eco-friendly and economical. This article presents a comparative analysis of the structural, morphological, and electrochemical features of various structured olivine phosphates and evaluates their impact as promising cathode materials for energy storage devices in general and high-performance LIBs in particular. Recent research has shown that multiple synthetic techniques can be employed to generate $LiMPO_4$ electrode materials via a soft chemical route while retaining the original $LiPO_3$ nanostructured morphology. The scalable approach allows for the control of metal content in $LiMPO_4$ nanoparticles with large surface areas, offering a viable alternative to traditional polycrystalline and glass forms. The method also shows potential for producing carbon-based olivine with superior battery performance and cycling stability.

Sol-gel synthesis resulted in pure powders of LFP, LMP, and LCP, with LMP having the biggest unit cell. The lattice properties and cell volumes of the composite altered as the transition metal changed, particularly in MO_6 octahedra. The deformation of PO_4 tetrahedra occurs solely in LMP. LFP has good electrochemical characteristics; however, LCP has low cycle stability because of electrolyte breakdown at high voltages.

Previous investigations of the olivine family have consistently shown that LFP exhibits outstanding electrochemical behavior, delivering experimental discharge capacities that approach its theoretical limit. Enhancing the conductivity of the carbon coating through the incorporation of graphene sheets or carbon nanotubes has further improved its electrochemical performance, enabling the use of LFP not only as a battery cathode but also as an active material in hybrid supercapacitor systems. Nevertheless, the limited scalability of carbon nanotube growth and the current challenges associated with large-scale graphene production hinder their widespread industrial adoption, indicating that further technological progress is required.

Lithium transition-metal phosphates based on cobalt and nickel are being actively explored as potential cathode materials for high-voltage lithium-ion batteries because they can reversibly accommodate lithium ions during repeated charge–discharge processes. Despite various optimization strategies, these materials typically achieve only about 80% of their theoretical capacity and suffer from rapid capacity decay over 10–20 cycles at low current densities. Continued improvements could enable their application in all-solid-state battery architectures for large-scale energy storage, particularly given their high operating voltages (approximately 4.8–5.2 V) and structurally robust olivine frameworks, which are attractive for electric and hydrogen-powered vehicles. Among them, olivine-type LCP is especially promising due to its exceptionally high redox potential. It has been synthesized using multiple approaches, including solid-state reactions, hydrothermal or solvothermal methods, and sol–gel techniques; however, the development of a synthesis route that is simple, rapid, controllable, and scalable for industrial production remains a key challenge.

Recent research efforts increasingly target next-generation lithium-ion batteries operating above 5 V versus Li/Li^+ to significantly boost energy density, building upon decades of progress in cathode materials with high specific capacities [271]. Compared with conventional systems operating below 4 V, such high-voltage batteries offer clear performance advantages. Strategies commonly employed to improve the electronic and ionic transport properties of phosphate polyanion cathodes include surface modification, particle downsizing, elemental doping, and deliberate control of morphology. In this context, evaluating the relationship between processing conditions and resulting material properties is essential to clarify the strengths and limitations of different synthesis routes and to tailor materials for targeted functionalities. Overall, the discussed approaches provide a roadmap for advancing high-voltage phosphate polyanion cathodes, which are expected to enable lithium-ion batteries with higher operating voltages and enhanced gravimetric energy densities. Fig. 24 summarizes the principal modification strategies applied to olivine $LiMPO_4$ cathodes, including particle-size reduction, surface carbon coating, cation substitution, and composite formation. These approaches collectively aim to enhance electronic conductivity, lithium-ion transport, and interfacial stability.

Research on high-voltage olivine-structured cathodes, such as LCP and LNPO, is striving to fulfill current energy storage requirements. To

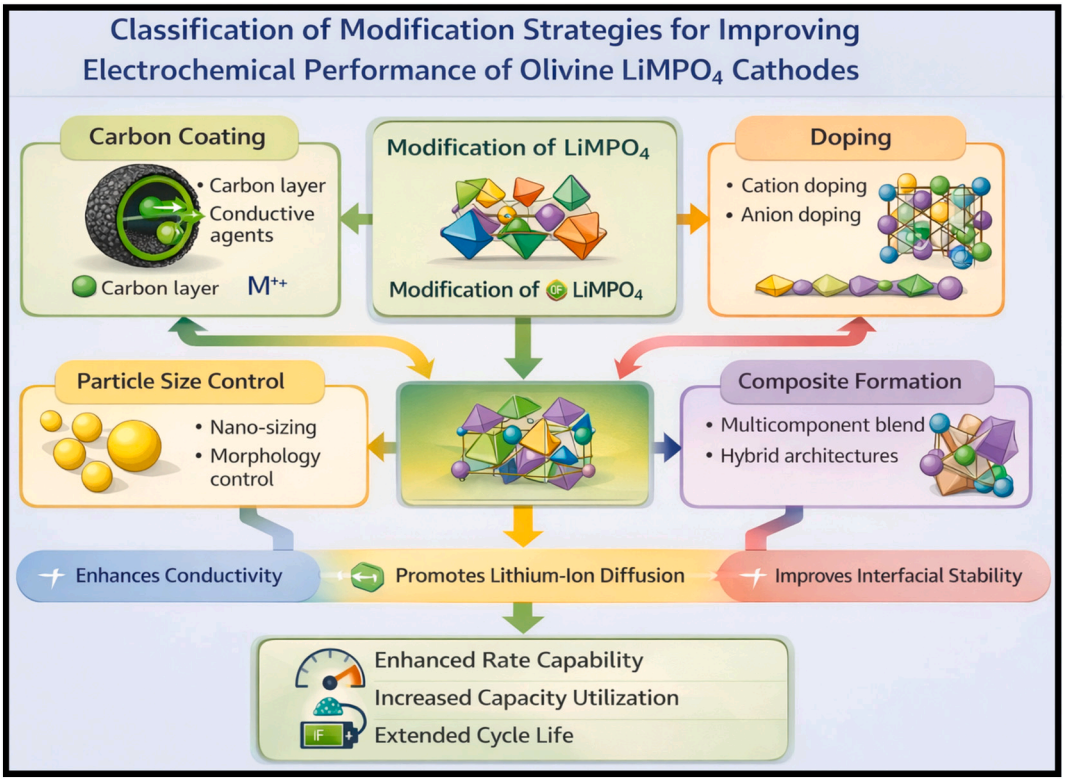

Fig. 24. Classification of modification strategies for improving the electrochemical performance of olivine $LiMPO_4$ cathodes.

comprehend these flaws, a computational study is required. These cathodes should be evaluated in real-world scenarios to help build next-generation energy storage devices. These cathodes have the potential to accelerate the development of all-solid-state batteries while also impacting environmentally friendly, non-hazardous aqueous energy storage. Despite these advances, there is still room for further development in all-solid-state and aqueous energy storage.

From the authors' perspective, the future of olivine phosphate cathodes lies not in incremental modification of single-metal systems, but in rationally designed multi-cation architectures coupled with interface-stable electrolytes. Mixed transition-metal olivines provide a tunable platform to balance voltage, kinetics, and safety, while operando characterization will be essential for resolving degradation mechanisms at high potentials. We anticipate that design strategies integrating crystal chemistry, defect control, and interfacial engineering will be decisive in enabling next-generation olivine-based batteries.

CRediT authorship contribution statement

Theodore Azemtsop Manfo: Writing – review & editing, Writing – original draft, Visualization, Validation, Software, Resources, Project administration, Methodology, Investigation, Funding acquisition, Formal analysis, Data curation, Conceptualization. **Hannu Laaksonen:** Supervision, Methodology, Formal analysis.

Funding

This research did not receive any specific grant from funding agencies in the public, commercial, or not-for-profit sectors.

Declaration of competing interest

The authors declare that they have no known competing financial interests or personal relationships that could have appeared to influence the work reported in this paper.

Acknowledgments

The authors are thankful to the Department of Electrical Engineering and Energy Technology, School of Technology and Innovations, University of Vaasa.

Data availability

Data will be made available on request.

References

[1] N. Badi, A.M. Theodore, S.A. Alghamdi, H.A. Al-Aoh, A. Lakhouit, P.K. Singh, M. N.F. Norrrahim, G. Nath, The impact of polymer electrolyte properties on lithium-ion batteries, Polymers 14 (2022) 3101, https://doi.org/10.3390/polym14153101.
[2] A.M. Theodore, A.A. Abbas, P.S. Dhapola, Effect of layered, spinel, and olivine-based positive electrode materials on rechargeable lithium-ion batteries: a review, J. Comput. Mech. 6 (2023) 38–57, https://doi.org/10.46253/jcmps.v6i4.a4.
[3] A.M. Theodore, Promising cathode materials for rechargeable lithium-ion batteries: a review, J. Sustain. Energy 14 (2023) 51–58.
[4] N. Badi, A.M. Theodore, A. Roy, S.A. Alghamdi, A.O.M. Alzahrani, A. Ignatiev, Preparation and characterization of 3D porous silicon anode material for lithium-ion battery application, Int. J. Electrochem. Sci. 17 (2022) 22064, https://doi.org/10.20964/2022.06.29.
[5] A.M. Theodore, Structural, electrical, and electrochemical studies of the olivine $LiMPO_4$ (M = Fe, Co, Cr, Mn, V) as cathode materials for lithium-ion rechargeable batteries based on the intercalation principle, Mater. Open Res. 2 (2023) 11, https://doi.org/10.12688/materialsopenres.17559.1.
[6] A.M. Theodore, M.E. Şahin, Modeling and simulation of a series and parallel battery pack model in MATLAB/Simulink, TEPES 4 (2024) 2–12, https://doi.org/10.5152/tepes.2024.23024.
[7] T.A. Manfo, M.E. Şahin, Intercalation reaction in lithium-ion battery: effect on cell characteristics, IJMET 6 (2023) 70–78.
[8] T.A. Manfo, A comprehensive analysis of material revolution to evolution in lithium-ion battery technology, Turk. J. Mater. 8 (2023) 1–13.
[9] Z.M.S. Elbarbary, P.A. Hoskeri, A.A. Javidparvar, M.M. Alammar, A. Rajakannu, T.A. Manfo, Machine learning approach to the possible synergy between co-doped elements in the case of $LiFePO_4$/C, J. Alloys Compd. 1034 (2025) 181316, https://doi.org/10.1016/j.jallcom.2025.181316.

[10] S. Ghosh, U. Bhattacharjee, S. Bhowmik, S.K. Martha, High-capacity and high-voltage cathodes for next-generation lithium-ion batteries, J. Energy Storage 68 (2023) 107690, https://doi.org/10.1016/j.est.2023.107690.
[11] A. Manthiram, A reflection on lithium-ion battery cathode chemistry, Nat. Commun. 14 (2023) 406, https://doi.org/10.1038/s41467-020-15355-0.
[12] X. Fan, C. Wang, High-voltage liquid electrolytes for Li batteries: progress and perspectives, Chem. Soc. Rev. 50 (2021) 10486–10566, https://doi.org/10.1039/D1CS00450F.
[13] V. Ragupathi, P. Panigrahi, G.S. Nagarajan, Enhanced electrochemical performance of nanopyramid-like $LiMnPO_4$/C cathode for lithium-ion batteries, Appl. Surf. Sci. 495 (2019) 143541, https://doi.org/10.1016/j.apsusc.2019.143541.
[14] J. Ling, C. Karuppiah, S.G. Krishnan, M.V. Reddy, B.V.R. Chowdari, Phosphate poly-anion materials as high-voltage lithium-ion battery cathodes: a review, Energy Fuel 35 (2021) 10428–10450, https://doi.org/10.1021/acs.energyfuels.1c01102.
[15] S. Nag, S. Roy, La-doped $LiMnPO_4$/C cathode material for lithium-ion battery, Chem. Eng. Sci. 272 (2023) 118600, https://doi.org/10.1016/j.ces.2023.118600.
[16] M.S. Akhter, B. Moossa, R. Kahraman, S. Rasul, R.A. Shakoor, Advancements in high voltage, high-energy density lithium-ion cathode materials: a focused review, Appl. Mater. Today 45 (2025) 102827, https://doi.org/10.1016/j.apmt.2025.102827.
[17] S.K. Martha, L. Elias, Nanostructured anode materials for batteries (lithium-ion, Ni-MH, lead-acid, and thermal batteries), in: Nanomaterials for Electrochemical Energy Storage Devices, Elsevier, 2019, p. 3.
[18] J. Jyoti, B.P. Singh, S.K. Tripathi, Recent advancements in development of different cathode materials for rechargeable lithium-ion batteries, J. Energy Storage 43 (2021) 103112, https://doi.org/10.1016/j.est.2021.103112.
[19] L. Xu, C. Huang, Z. Hua, L. Chen, Optimizing D-band center of tube brush-like $CoZn_{13}$/Co/ZnO architecture with multiple heterointerfaces enhancing ion/electron migration toward pseudocapacitive storage, Energy Storage Mater. 61 (2023) 102888, https://doi.org/10.1016/j.ensm.2023.102888.
[20] S. Ko, H. Otsuka, S. Kimura, Y. Takagi, S. Yamaguchi, T. Masuda, A. Yamada, A rapid safety screening realized by accelerating rate calorimetry with lab-scale small batteries, Nat. Energy 10 (2025) 1–8, https://doi.org/10.1038/s41560-025-01751-7.
[21] H. Wan, J. Xu, C. Wang, Designing electrolytes and interphases for high-energy lithium batteries, Nat. Rev. Chem. 8 (2024) 30–44, https://doi.org/10.1038/s41570-023-00557-z.
[22] L. Chang, X. Bi, S. Luo, Y. Liu, Y. Zhang, Insight into structural and electrochemical properties of Mg-doped $LiMnPO_4$/C cathode materials: first-principles calculation and experimental verification, Int. J. Energy Res. 45 (2021) 20715–20728, https://doi.org/10.1002/er.7135.
[23] A.M. Theodore, Progress into lithium-ion battery research, J. Chem. Res. 47 (2023), https://doi.org/10.1177/174751982311833, 17475198231183349.
[24] F. Yu, L. Zhang, Y. Li, Y. An, M. Zhu, B. Dai, Mechanism studies of $LiFePO_4$ cathode material: lithiation/delithiation process, electrochemical modification, and synthetic reaction, RSC Adv. 4 (2014) 54576–54602, https://doi.org/10.1039/C4RA10899J.
[25] A. Eftekhari, $LiFePO_4$/C nanocomposites for lithium-ion batteries, J. Power Sources 343 (2017) 395–411, https://doi.org/10.1016/j.jpowsour.2017.01.080.
[26] C. Delacourt, P. Poizot, M. Morcrette, J.M. Tarascon, C. Masquelier, One-step low-temperature route for the preparation of electrochemically active $LiMnPO_4$ powders, Chem. Mater. 16 (2004) 93–99, https://doi.org/10.1021/cm030347b.
[27] R. Dominko, M. Bele, M. Gaberscek, M. Remskar, D. Hanzel, J.M. Goupil, S. Pejovnik, J. Jamnik, Porous olivine composites synthesized by sol-gel technique, J. Power Sources 153 (2006) 274–280, https://doi.org/10.1016/j.jpowsour.2005.05.033.
[28] J. Yang, J.J. Xu, Synthesis and characterization of carbon-coated lithium transition metal phosphates $LiMPO_4$ (M = Fe, Mn, Co, Ni) prepared via a nonaqueous sol-gel route, J. Power Sources 153 (2006) A716–A723, https://doi.org/10.1149/1.2168410.
[29] Y. Hong, C. Li, J. Ouyang, Q. Hu, X. Wang, Z. Tang, T. Liu, High-yield synthesis of $LiMnPO_4$/C nanoplates as cathode materials for lithium-ion batteries, Scr. Mater. 241 (2024) 115878, https://doi.org/10.1016/j.scriptamat.2023.115878.
[30] Z. Yang, Y. Dai, S. Wang, J. Yu, How to make lithium iron phosphate better: a review exploring classical modification approaches in-depth and proposing future optimization methods, J. Mater. Chem. A 4 (2016) 18210–18222, https://doi.org/10.1039/C6TA05048D.
[31] J. Wang, X. Sun, Olivine $LiFePO_4$: the remaining challenges for future energy storage, Energy Environ. Sci. 8 (2015) 1110–1138, https://doi.org/10.1039/C4EE04016C.
[32] Z. Bi, X. Zhang, W. He, D. Min, W. Zhang, Recent advances in $LiFePO_4$ nanoparticles with different morphology for high-performance lithium-ion batteries, RSC Adv. 3 (2013) 19744–19751, https://doi.org/10.1039/C3RA42601G.
[33] Y. Guo, Q. Zhang, J. Wei, Y. Hu, X. Liu, S. Huang, C. Pang, Advances and industrialization of $LiFePO_4$ cathodes in electric vehicles: challenges, innovations, and future directions, J. Mater. Chem. A 13 (2025) 17271–17283, https://doi.org/10.1039/D5TA00166H.
[34] A.S. Wijareni, J. Karunawan, Z.T. Ichlas, A. Sumboja, M.Z. Mubarok, Recent advances in synthesis and fabrication of $LiFePO_4$ cathode materials: a comprehensive review, Ionics 31 (2025) 7565–7593, https://doi.org/10.1007/s11581-025-06460-5.
[35] G.K. Singh, G. Ceder, M.Z. Bazant, Intercalation dynamics in rechargeable battery materials: general theory and phase-transformation waves in $LiFePO_4$, Electrochim. Acta 53 (2008) 7599–7613, https://doi.org/10.1016/j.electacta.2008.03.083.
[36] Z. Gong, Y. Yang, Recent advances in the research of polyanion-type cathode materials for Li-ion batteries, Energy Environ. Sci. 4 (2011) 3223–3242, https://doi.org/10.1039/C0EE00713G.
[37] G. Jin, W. Zhao, J. Zhang, W. Liang, M. Chen, R. Xu, High-temperature stability of $LiFePO_4$/carbon lithium-ion batteries: challenges and strategies, Sustain. Chem. 6 (2025) 7, https://doi.org/10.3390/suschem6010007.
[38] S. Kraas, A. Vijn, M. Falk, B. Ufer, B. Luerßen, J. Janek, M. Fröba, Nanostructured and nanoporous $LiFePO_4$ and $LiNi_{0.5}Mn_{1.5}O_{4-\delta}$ as cathode materials for lithium-ion batteries, Prog. Solid-State Chem. 42 (2014) 218–241, https://doi.org/10.1016/j.progsolidstchem.2014.04.014.
[39] K. Amine, H. Yasuda, M. Yamachi, Olivine $LiCoPO_4$ as 4.8 V electrode material for lithium batteries, ESL 3 (2000) 178, https://doi.org/10.1149/1.1390994.
[40] M. Hu, X. Pang, Z. Zhou, Recent progress in high-voltage lithium-ion batteries, J. Power Sources 237 (2013) 229–242, https://doi.org/10.1016/j.jpowsour.2013.03.024.
[41] L. Fang, H. Zhang, Y. Zhang, L. Liu, Y. Wang, Design and synthesis of two-dimensional porous Fe-doped $LiCoPO_4$ nano-plates as improved cathode for lithium-ion batteries, J. Power Sources 312 (2016) 101–108, https://doi.org/10.1016/j.jpowsour.2016.02.035.
[42] A. Örnek, An impressive approach to solving the ongoing stability problems of $LiCoPO_4$ cathode: nickel oxide surface modification with excellent core-shell principle, J. Power Sources 356 (2017) 1–11, https://doi.org/10.1016/j.jpowsour.2017.04.074.
[43] Y. Chen, M. Sang, W. Jiang, Y. Wang, Y. Zou, C. Lu, Z. Ma, Fracture predictions based on a coupled chemo-mechanical model with strain gradient plasticity theory for film electrodes of Li-ion batteries, Eng. Fract. Mech. 253 (2021) 107866, https://doi.org/10.1016/j.engfracmech.2021.107866.
[44] Z.S. Ma, Z.C. Xie, Y. Wang, P.P. Zhang, Y. Pan, Y.C. Zhou, C. Lu, Failure modes of hollow core-shell structural active materials during the lithiation–delithiation process, J. Power Sources 290 (2015) 114–122, https://doi.org/10.1016/j.jpowsour.2015.05.008.
[45] Z. Ma, H. Wu, Y. Wang, Y. Pan, C. Lu, An electrochemical-irradiated plasticity model for metallic electrodes in lithium-ion batteries, Int. J. Plast. 88 (2017) 188–203, https://doi.org/10.1016/j.ijplas.2016.10.009.
[46] A. Khan, H. Al Rashid, P.K. Roy, S.I. Chowdhury, S.A. Sathi, Challenges and the way to improve lithium-ion battery technology for next-generation energy storage, Energy Environ. Mater. 8 (2025) e70088, https://doi.org/10.1002/eem2.70088.
[47] A.K. Padhi, K.S. Nanjundaswamy, J.B. Goodenough, Phospho-olivines as positive-electrode materials for rechargeable lithium batteries, JES 144 (1997) 1188, https://doi.org/10.1149/1.1837571.
[48] K. Zaghib, A. Mauger, C.M. Julien, Olivine-based cathode materials, in: Rechargeable Batteries: Materials, Technologies, and New Trends, Springer International Publishing, Cham, 2015, pp. 25–65, https://doi.org/10.1007/978-3-319-15458-9_2.
[49] W. Hwang, J. Kim, S. Kim, E. Ko, S. Lee, M. Kim, S. Yu, Y. Sung, H. Kim, C. Kim, J. Park, Unveiling olivine cathodes for high energy-density lithium-ion batteries: a comprehensive review from the atomic level to the electrode scale, J. Mater. Chem. A 12 (2024) 27800–27824, https://doi.org/10.1039/D4TA02338B.
[50] M. Gianvincenzi, M. Marconi, E.M. Mosconi, C. Favi, F. Tola, Systematic review of battery life cycle management: a framework for European regulation compliance, Sustainability 16 (2024) 10026, https://doi.org/10.3390/su162210026.
[51] H. Liu, F. Nozaki, J. Hwang, K. Matsumoto, Journey of olivine materials from classic to state-of-the-art technologies for next-generation batteries, J. Power Sources 630 (2025) 236172, https://doi.org/10.1016/j.jpowsour.2025.236172.
[52] O. Alsauskas, E. Connelly, A. Daou, A. Gouy, M. Huismans, H. Kim, J.B.L. Marois, S. McDonagh, A. Petropoulos, J. Teter, T. Nomura, Global EV Outlook 2023: Catching Up With Climate Ambitions, International Energy Agency, 2023, pp. 1–142.
[53] M. Armand, J.M. Tarascon, Building better batteries, Nature 451 (2008) 652–657, https://doi.org/10.1038/451652a.
[54] M.S. Whittingham, Y. Song, S. Lutta, P.Y. Zavalij, N.A. Chernova, Some transition metal (oxy) phosphates and vanadium oxides for lithium batteries, J. Mater. Chem. 15 (2005) 3362–3379, https://doi.org/10.1039/B501961C.
[55] T. Chen, M. Li, J. Bae, Recent advances in lithium iron phosphate battery technology: a comprehensive review, Batteries 10 (2024) 424, https://doi.org/10.3390/batteries10120424.
[56] W.F. Howard, R.M. Spotnitz, Theoretical evaluation of high-energy lithium metal phosphate cathode materials in Li-ion batteries, J. Power Sources 165 (2007) 887–891, https://doi.org/10.1016/j.jpowsour.2005.12.046.
[57] C. Delacourt, L. Laffont, R. Bouchet, C. Wurm, J.B. Leriche, M. Morcrette, J. M. Tarascon, C. Masquelier, Toward understanding of electrical limitations (electronic, ionic) in $LiMPO_4$ (M = Fe, Mn) electrode materials, JES 152 (2005) A913, https://doi.org/10.1149/1.1884787.
[58] J. Wolfenstine, J. Allen, $LiNiPO_4$–$LiCoPO_4$ solid solutions as cathodes, J. Power Sources 136 (2004) 150–153, https://doi.org/10.1016/j.jpowsour.2004.05.017.
[59] N.N. Bramnik, K. Nikolowski, C. Baehtz, K.G. Bramnik, H. Ehrenberg, Phase transitions occurring upon lithium insertion–extraction of $LiCoPO_4$, Chem. Mater. 19 (2007) 908–915, https://doi.org/10.1021/cm062246u.
[60] C.V. Ramana, A. Ait-Salah, S. Utsunomiya, U. Becker, A. Mauger, F. Gendron, C. M. Julien, Structural characteristics of lithium nickel phosphate studied using analytical electron microscopy and Raman spectroscopy, Chem. Mater. 18 (2006) 3788–3794, https://doi.org/10.1021/cm061137c.

[61] B. Jin, H.B. Gu, K.W. Kim, Effect of different conductive additives on charge/discharge properties of $LiCoPO_4$/Li batteries, JES 12 (2008) 105–111, https://doi.org/10.1007/s10008-007-0367-4.

[62] (a) C. Delacourt, C. Wurm, P. Reale, M. Morcrette, C. Masquelier, Low-temperature preparation of optimized phosphates for Li-battery applications, Solid State Ion 173 (2004) 113–118, https://doi.org/10.1016/j.ssi.2004.07.061; (b) H. Gabrisch, J.D. Wilcox, M.M. Doeff, Carbon surface layers on a high-rate $LiFePO_4$, Electrochem. Solid-State Lett. 9 (2006) A360, https://doi.org/10.1149/1.2203309.

[63] S.Y. Chung, J.T. Bloking, Y.M. Chiang, Electronically conductive phospho-olivines as lithium storage electrodes, Nat. Mater. 1 (2002) 123–128, https://doi.org/10.1038/nmat732.

[64] A. Manthiram, J.B. Goodenough, Lithium insertion into $Fe_2(SO_4)_3$ frameworks, J. Power Sources 26 (1989) 403–408, https://doi.org/10.1016/0378-7753(89)80153-3.

[65] T. Muraliganth, A. Manthiram, Understanding the shifts in the redox potentials of olivine $LiM_{1-y}M_yPO_4$ (M = Fe, Mn, Co, and Mg) solid solution cathodes, J. Phys. Chem. C 114 (2010) 15530–15540, https://doi.org/10.1021/jp1055107.

[66] A. Mauger, C.M. Julien, Olivine positive electrodes for Li-ion batteries: status and perspectives, Batteries 4 (2018) 39, https://doi.org/10.3390/batteries4030039.

[67] S. Kanungo, A. Bhattacharjee, N. Bahadursha, A. Ghosh, Comparative analysis of $LiMPO_4$ (M = Fe, Co, Cr, Mn, V) as cathode materials for lithium-ion battery applications: a first-principles-based theoretical approach, Nanomaterials 12 (2022) 3266, https://doi.org/10.3390/nano12193266.

[68] Y. Zhang, Y. Sun, Q. Li, J. Wang, Z. Chen, Design strategies and recent advances of olivine-type phosphate cathodes for high-energy lithium-ion batteries, Energy Storage Mater. 63 (2024) 103012, https://doi.org/10.1016/j.ensm.2024.103012.

[69] H. Liu, E. Zhao, Y. Wang, X. Li, G. Chen, High-voltage cathode materials for next-generation lithium-ion batteries: challenges and perspectives, J. Power Sources 560 (2023) 232617, https://doi.org/10.1016/j.jpowsour.2023.232617.

[70] M.S. Islam, C.A. Fisher, Lithium and sodium battery cathode materials: computational insights into voltage, diffusion, and nanostructural properties, Chem. Soc. Rev. 43 (2014) 185–204, https://doi.org/10.1039/c3cs60199d.

[71] Y.S. Meng, M.E. Arroyo-de Dompablo, Recent advances in first principles computational research of cathode materials for lithium-ion batteries, Acc. Chem. Res. 46 (2013) 1171–1180, https://doi.org/10.1021/ar2002396.

[72] M.D. Radin, S. Hy, M. Sina, C. Fang, H. Liu, J. Vinckeviciute, M. Zhang, M. S. Whittingham, Y.S. Meng, A. Van der Ven, Narrowing the gap between theoretical and practical capacities in Li-ion layered oxide cathode materials, Adv. Energy Mater. 7 (2017) 1602888, https://doi.org/10.1002/aenm.201602888.

[73] C. Delmas, C. Fouassier, P. Hagenmuller, Structural classification and properties of the layered oxides, Phys. B + C 99 (1980) 81–85, https://doi.org/10.1016/0378-4363(80)90214-4.

[74] A. Chakraborty, S. Kunnikuruvan, S. Kumar, B. Markovsky, D. Aurbach, M. Dixit, D.T. Major, Layered cathode materials for lithium-ion batteries: review of computational studies on $LiNi_{1-x-y}Co_xMn_yO_2$ and $LiNi_{1-x-y}Co_xAl_yO_2$, Chem. Mater. 32 (2020) 915–952, https://doi.org/10.1021/acs.chemmater.9b04066.

[75] M.S. Whittingham, Lithium batteries and cathode materials, Chem. Rev. 104 (2004) 4271–4302, https://doi.org/10.1021/cr020731c.

[76] M.S. Islam, Recent atomistic modelling studies of energy materials: batteries included, Philos. Trans. R. Soc. A 368 (2010) 3255–3267, https://doi.org/10.1098/rsta.2010.0070.

[77] M.S. Whittingham, Ultimate limits to intercalation reactions for lithium batteries, Chem. Rev. 114 (2014) 11414–11443, https://doi.org/10.1021/cr5003003.

[78] C. Masquelier, L. Croguennec, Polyanionic (phosphates, silicates, sulfates) frameworks as electrode materials for rechargeable Li (or Na) batteries, Chem. Rev. 113 (2013) 6552–6591, https://doi.org/10.1021/cr3001862.

[79] C.M. Julien, A. Mauger, K. Zaghib, H. Groult, Comparative issues of cathode materials for Li-ion batteries, Inorganics 2 (2014) 132–154, https://doi.org/10.3390/inorganics2010132.

[80] L. Zhu, C. Bao, L. Xie, X. Yang, X. Cao, Review of synthesis and structural optimization of $LiNi_{1/3}Co_{1/3}Mn_{1/3}O_2$ cathode materials for lithium-ion batteries applications, J. Alloys Compd. 831 (2020) 154864, https://doi.org/10.1016/j.jallcom.2020.154864.

[81] J.P. Pender, G. Jha, D.H. Youn, J.M. Ziegler, I. Andoni, E.I. Choi, A. Heller, B. S. Dunn, P.S. Weiss, R.M. Penner, C.B. Mullins, Electrode degradation in lithium-ion batteries, ACS Nano 14 (2020) 1243–1295, https://doi.org/10.1021/acsnano.9b04365.

[82] A. Manthiram, A reflection on lithium-ion battery cathode chemistry, Nat. Commun. 11 (2020) 1550, https://doi.org/10.1038/s41467-020-15355-0.

[83] W. Lee, S. Muhammad, C. Sergey, H. Lee, J. Yoon, Y.M. Kang, W.S. Yoon, Advances in the cathode materials for lithium rechargeable batteries, Angew. Chem. Int. Ed. Eng. 59 (2020) 2578–2605, https://doi.org/10.1002/anie.201902359.

[84] N. Baikalov, N. Serik, S. Kalybekkyzy, I. Kurmanbayeva, Z. Bakenov, A. Mentbayeva, High mass-loading sulfur-composite cathode for lithium-sulfur batteries, Front. Energy Res. 8 (2020) 207, https://doi.org/10.3389/fenrg.2020.00207.

[85] S. Yang, Y. Song, P.Y. Zavalij, M.S. Whittingham, Reactivity, stability, and electrochemical behavior of lithium iron phosphates, Electrochem. Commun. 4 (2002) 239–244, https://doi.org/10.1016/S1388-2481(01)00298-3.

[86] A.K. Padhi, K.S. Nanjundaswamy, J.B. Goodenough, Phospho-olivines as positive-electrode materials for rechargeable lithium batteries, J. Energy Storage 144 (1997) 1188, https://doi.org/10.1149/1.1837571.

[87] C. Xu, B. Peng, W. Yang, J. Tian, H. Zhou, High energy density lithium battery systems: from key cathode materials to pouch cell design, Chem. Soc. Rev. 54 (2025) 10245–10303, https://doi.org/10.1039/D5CS00641D.

[88] S.F.L.C. Franger, F. Le Cras, C. Bourbon, H. Rouault, $LiFePO_4$ synthesis routes for enhanced electrochemical performance, ESL 5 (2002) A231, https://doi.org/10.1149/1.1506962.

[89] Q. Wang, H.S. Hu, H. Li, H.-M. Cheng, T. Zhao, C. Zhao, Ionic potential for battery materials, Nat. Rev. Mater. 10 (2025) 697–712, https://doi.org/10.1038/s41578-025-00822-1.

[90] J. Yang, J.S. Tse, Li-ion diffusion mechanisms in $LiFePO_4$: an ab initio molecular dynamics study, J. Phys. Chem. A 115 (2011) 13045–13049, https://doi.org/10.1021/jp205057d.

[91] J. Molenda, A. Kulka, A. Milewska, W. Zając, K. Świerczek, Structural, transport, and electrochemical properties of $LiFePO_4$ substituted in lithium and iron sublattices (Al, Zr, W, Mn, Co, and Ni), Materials 6 (2013) 1656–1687, https://doi.org/10.3390/ma6051656.

[92] A. Andezai, J.O. Iroh, Overview of organic cathode materials in lithium-ion batteries and supercapacitors, Energies 18 (2025) 582, https://doi.org/10.3390/en18030582.

[93] M. Nakayama, S. Yamada, R. Jalem, T. Kasuga, Density functional studies of olivine-type $LiFePO_4$ and $NaFePO_4$ as positive electrode materials for rechargeable lithium and sodium-ion batteries, Solid State Ionics 286 (2016) 40–44, https://doi.org/10.1016/j.ssi.2015.12.019.

[94] M.S. Islam, D.J. Driscoll, C.A. Fisher, P.R. Slater, Atomic-scale investigation of defects, dopants, and lithium transport in the $LiFePO_4$ olivine-type battery material, Chem. Mater. 17 (2005) 5085–5092, https://doi.org/10.1021/cm050999v.

[95] Y. Bi, D. Wang, Revisiting olivine phosphate and blend cathodes in lithium-ion batteries for electric vehicles, in: New Perspectives on Electric Vehicles, IntechOpen, 2021, https://doi.org/10.5772/intechopen.99931.

[96] M.H. Alfaruqi, S. Kim, S. Park, S. Lee, J. Lee, J.Y. Hwang, Y.K. Sun, J. Kim, Density functional theory investigation of mixed transition metals in olivine and tavorite cathode materials for Li-ion batteries, ACS Appl. Mater. Interfaces 12 (2020) 16376–16386, https://doi.org/10.1021/acsami.9b23367.

[97] C. Ouyang, S. Shi, Z. Wang, X. Huang, L. Chen, First-principles study of Li ion diffusion in $LiFePO_4$, Phys. Rev. B 69 (2004) 104303, https://doi.org/10.1103/PhysRevB.69.104303.

[98] K. Kim, J.K. Kim, Comparison of structural characteristics and electrochemical properties of $LiMPO_4$ (M = Fe, Mn, and Co) olivine compounds, Mater. Lett. 176 (2016) 244–247, https://doi.org/10.1016/j.matlet.2016.04.145.

[99] C. Hu, M. Geng, H. Yang, F. Maosong, S. Zhaoqin, Y. Ran, W. Bin, Capacity fade mechanisms and promotion strategies for $LiFePO_4$ batteries, Coatings 14 (2024) 832, https://doi.org/10.3390/coatings14070832.

[100] J.K. Kim, J.W. Choi, G.S. Chauhan, J.H. Ahn, G.C. Hwang, J.B. Choi, H.J. Ahn, Enhancement of electrochemical performance of lithium iron phosphate by controlled sol-gel synthesis, Electrochim. Acta 53 (2008) 8258–8264, https://doi.org/10.1016/j.electacta.2008.06.049.

[101] J.S. Menye, M.-B. Camara, B. Dakyo, Lithium battery degradation and failure mechanisms: a state-of-the-art review, Energies 18 (2025) 342, https://doi.org/10.3390/en18020342.

[102] L.X. Yuan, Z.H. Wang, W.X. Zhang, X.L. Hu, J.T. Chen, Y.H. Huang, J. B. Goodenough, Development and challenges of $LiFePO_4$ cathode material for lithium-ion batteries, Energy Environ. Sci. 4 (2011) 269–284, https://doi.org/10.1039/C0EE00029A.

[103] J. Wang, X. Sun, Understanding and recent development of carbon coating on $LiFePO_4$ cathode materials for lithium-ion batteries, Energy Environ. 5 (2012) 5163–5185, https://doi.org/10.1039/C1EE01263K.

[104] M. Zhang, N. Garcia-Araez, A.L. Hector, Understanding and development of olivine $LiCoPO_4$ cathode materials for lithium-ion batteries, J. Mater. Chem. A 6 (2018) 14483–14517, https://doi.org/10.1039/C8TA04063J.

[105] B. Kang, G. Ceder, Battery materials for ultrafast charging and discharging, Nature 458 (2009) 190–193, https://doi.org/10.1038/nature07853.

[106] R. Malik, F. Zhou, G. Ceder, Kinetics of non-equilibrium lithium incorporation in $LiFePO_4$, Nat. Mater. 10 (2011) 587–590, https://doi.org/10.1038/nmat3065.

[107] H. Liu, F.C. Strobridge, O.J. Borkiewicz, K.M. Wiaderek, K.W. Chapman, P. J. Chupas, C.P. Grey, Capturing metastable structures during high rate cycling of $LiFePO_4$ nanoparticle electrodes, Science 344 (2014) 1252817, https://doi.org/10.1126/science.1252817.

[108] G. Wang, P. Xu, H.G. Desta, B.A. Beshiwork, B. Li, W.G. Adam, B. Lin, Water effect on the electronic properties and lithium-ion conduction in a defect-engineered $LiFePO_4$ electrode, Batteries 10 (2024) 281, https://doi.org/10.3390/batteries10080281.

[109] M.G. Fischer, X. Hua, B.D. Wilts, E. Castillo-Martínez, U. Steiner, Polymer-templated $LiFePO_4$/C nanonetworks as high-performance cathode materials for lithium-ion batteries, ACS Appl. Mater. Interfaces 10 (2018) 1646–1653, https://doi.org/10.1021/acsami.7b12376.

[110] C. Sun, S. Rajasekhara, J.B. Goodenough, F. Zhou, Monodisperse porous $LiFePO_4$ microspheres for a high-power Li-ion battery cathode, JACS 133 (2011) 2132–2135, https://doi.org/10.1021/ja1110464.

[111] Q. Zhang, S.Z. Huang, J. Jin, J. Liu, Y. Li, H.E. Wang, L.H. Chen, B.J. Wang, B. L. Su, Engineering 3D bicontinuous hierarchically macro-mesoporous $LiFePO_4$/C nanocomposite for lithium storage with high-rate capability and long cycle stability, Sci. Rep. 6 (2016) 25942, https://doi.org/10.1038/srep25942.

[112] Y. Liu, J. Gu, J. Zhang, F. Yu, L. Dong, N. Nie, W. Li, Metal-organic frameworks derived porous lithium iron phosphate with continuous nitrogen-doped carbon

networks for lithium-ion batteries, J. Power Sources 304 (2016) 42–50, https://doi.org/10.1016/j.jpowsour.2015.11.022.
[113] H. El-Shinawi, E.J. Cussen, S.A. Corr, Morphology-directed synthesis of $LiFePO_4$ and $LiCoPO_4$ from nanostructured $Li_{1+2x}PO_{3+x}$, Inorg. Chem. 58 (2019) 6946–6949, https://doi.org/10.1021/acs.inorgchem.9b00517.
[114] S. Ju, T. Liu, H. Peng, G. Li, K. Chen, A facile synthesis route for porous spherical $LiFePO_4$/C microscale secondary particles, Mater. Lett. 93 (2013) 194–198, https://doi.org/10.1016/j.matlet.2012.11.083.
[115] N. Bai, K. Xiang, W. Zhou, H. Lu, X. Zhao, H. Chen, $LiFePO_4$/carbon nanowires with 3D nano-network structure as potential high-performance cathode for lithium-ion batteries, Electrochim. Acta 191 (2016) 23–28, https://doi.org/10.1016/j.electacta.2016.01.019.
[116] D. Xu, P. Wang, B. Shen, Synthesis and characterization of sulfur-doped carbon decorated $LiFePO_4$ nanocomposite as high-performance cathode material for lithium-ion batteries, Ceram. Int. 42 (2016) 5331–5338, https://doi.org/10.1016/j.ceramint.2015.12.064.
[117] M. Minakshi, P. Singh, D. Appadoo, D.E. Martin, Synthesis and characterization of olivine $LiNiPO_4$ for aqueous rechargeable battery, Electrochim. Acta 56 (2011) 4356–4360, https://doi.org/10.1016/j.electacta.2011.01.017.
[118] A. Yamada, Y. Takei, H. Koizumi, N. Sonoyama, R. Kanno, K. Itoh, M. Yonemura, T. Kamiyama, Electrochemical, magnetic, and structural investigation of the $Li_x(Mn_yFe_{1-y})PO_4$ olivine phases, Chem. Mater. 18 (2006) 804–813, https://doi.org/10.1021/cm051861f.
[119] M. Yonemura, A. Yamada, Y. Takei, N. Sonoyama, R. Kanno, Comparative kinetic study of olivine $LixMPO_4$ (M = Fe, Mn), JES 151 (2004) A1352, https://doi.org/10.1149/1.1773731.
[120] X. Rui, X. Zhao, Z. Lu, H. Tan, D. Sim, H.H. Hng, R. Yazami, T.M. Lim, Q. Yan, Olivine-type nanosheets for lithium-ion battery cathodes, ACS Nano 7 (2013) 5637–5646, https://doi.org/10.1021/nn401588p.
[121] X. Wang, Morphological and orientational diversity of $LiFePO_4$ crystallites: remarkable reaction path dependence in hydrothermal/solvothermal syntheses, CrystEngComm 16 (2014) 10112–10122, https://doi.org/10.1039/C4CE01397B.
[122] F. Cheng, S. Wang, A.H. Lu, W.C. Li, Immobilization of nanosized $LiFePO_4$ spheres by 3D coralloid carbon structure with large pore volume and thin walls for high-power lithium-ion batteries, J. Power Sources 229 (2013) 249–257, https://doi.org/10.1016/j.jpowsour.2012.12.036.
[123] Y. Jiang, S. Liao, Z. Liu, G. Xiao, Q. Liu, H. Song, High-performance $LiFePO_4$ microsphere composed of nanofibers with an alcohol-thermal approach, J. Mater. Chem. A 1 (2013) 4546–4551, https://doi.org/10.1039/C3TA01566A.
[124] N. Zhou, H.Y. Wang, E. Uchaker, M. Zhang, S.Q. Liu, Y.N. Liu, G. Cao, Additive-free solvothermal synthesis and Li-ion intercalation properties of dumbbell-shaped $LiFePO_4$/C mesocrystals, J. Power Sources 239 (2013) 103–110, https://doi.org/10.1016/j.jpowsour.2013.03.136.
[125] H. Ghafarian-Zahmatkesh, M. Javanbakht, M. Ghaemi, Ethylene glycol- assisted hydrothermal synthesis and characterization of bow-tie-like lithium iron phosphate nanocrystals for lithium-ion batteries, J. Power Sources 284 (2015) 339–348, https://doi.org/10.1016/j.jpowsour.2015.02.157.
[126] Z. Zheng, W.K. Pang, X. Tang, D. Jia, Y. Huang, Z. Guo, Solvothermal synthesis and electrochemical performance of hollow $LiFePO_4$ nanoparticles, J. Alloys Compd. 640 (2015) 95–100, https://doi.org/10.1016/j.jallcom.2015.04.007.
[127] J. Song, L. Wang, G. Shao, M. Shi, Z. Ma, G. Wang, W. Song, S. Liu, C. Wang, Controllable synthesis, morphology evolution, and electrochemical properties of $LiFePO_4$ cathode materials for Li-ion batteries, Phys. Chem. Chem. Phys. 16 (2014) 7728–7733, https://doi.org/10.1039/C7RA10112K.
[128] Y. Wang, B. Zhu, Y. Wang, F. Wang, Solvothermal synthesis of $LiFePO_4$ nanorods as high-performance cathode materials for lithium-ion batteries, Ceram. Int. 42 (2016) 10297–10303, https://doi.org/10.1016/j.ceramint.2016.03.165.
[129] R. Tian, G. Liu, H. Liu, L. Zhang, X. Gu, Y. Guo, H. Wang, L. Sun, W. Chu, Very high power and superior rate capability $LiFePO_4$ nanorods hydrothermally synthesized using tetra glycol as surfactant, RSC Adv. 5 (2015) 1859–1866, https://doi.org/10.1039/C4RA09776A.
[130] L. Wang, H. Chen, Y. Zhang, J. Liu, L. Peng, Research progress in strategies for enhancing the conductivity and conductive mechanism of $LiFePO_4$ cathode materials, Molecules 29 (2024) 5250, https://doi.org/10.3390/molecules29225250.
[131] Y. Qiu, Y. Geng, N. Li, X. Liu, X. Zuo, Nonstoichiometric $LiFePO_4$/C nanofibers by electrospinning as cathode materials for lithium-ion batteries, Mater. Chem. Phys. 144 (2014) 226–229, https://doi.org/10.1016/j.matchemphys.2013.12.022.
[132] D. Shao, J. Wang, X. Dong, W. Yu, G. Liu, F. Zhang, L. Wang, Electrospinning fabrication and electrochemical properties of $LiFePO_4$/C composite nanofibers, J. Mater. Sci.: Mater. Electron. 14 (24) (2013) 4263–4269, https://doi.org/10.1007/s10854-013-1395-8.
[133] H.Y. Lin, S.M. Yeh, J.S. Chen, Physical and electrochemical properties of $LiFePO_4$/C nanofibers synthesized by electrospinning, Int. J. Electrochem. Sci. 9 (2014) 6936–6948, https://doi.org/10.1016/S1452-3981(23)10942-4.
[134] O. Toprakci, L. Ji, Z. Lin, H.A. Toprakci, X. Zhang, Fabrication and electrochemical characteristics of electrospun $LiFePO_4$/carbon composite fibers for lithium-ion batteries, J. Power Sources 196 (2011) 7692–7699, https://doi.org/10.1016/j.jpowsour.2011.04.031.
[135] D. Shao, J. Wang, X. Dong, W. Yu, G. Liu, F. Zhang, L. Wang, Preparation and electrochemical performances of $LiFePO_4$/C composite nanobelts via facile electrospinning, J. Mater. Sci.: Mater. Electron. 25 (2014) 1040–1046, https://doi.org/10.1007/s10854-013-1684-2.
[136] L.L. Chen, X.Q. Shen, M.X. Jing, S.W. Zhu, Z.C. Pi, J.Q. Li, H.A. Zhai, K.S. Xiao, Electrospun $LiFePO_4$/C composite fiber membrane as a binder-free, self-standing cathode for power lithium-ion battery, JNN 18 (2018) 4720–4727, https://doi.org/10.1166/jnn.2018.15319.
[137] L. Bao, G. Xu, X. Sun, H. Zeng, R. Zhao, X. Yang, G. Shen, G. Han, S. Zhou, Monodispersed $LiFePO_4$@ C core-shell [001] nanorods for a high-power Li-ion battery cathode, J. Alloys Compd. 708 (2017) 685–693, https://doi.org/10.1016/j.jallcom.2017.03.052.
[138] L. Boqiao, W. Zhao, C. Zhang, Z. Yang, F. Dang, Y. Liu, F. Jin, X. Chen, Monodispersed $LiFePO_4$@C core-shell nanostructures for a high-power Li-ion battery cathode, J. Mater. 246 (2014) 696–702, https://doi.org/10.1155/2020/2607017.
[139] H. Yuan, X. Wang, Q. Wu, H. Shu, H.X. Yang, Effects of Ni and Mn doping on physicochemical and electrochemical performances of $LiFePO_4$/C, J. Alloys Compd. 675 (2016) 187–194, https://doi.org/10.1016/j.jallcom.2016.03.065.
[140] K. Saravanan, J.J. Vittal, M.W. Reddy, B.V.R. Chowdari, P. Balaya, Storage performance of $LiFe_{1-x}Mn_xPO_4$ nanoplates (x = 0, 0.5, and 1), J. Mater. Chem. 19 (2009) 605–610, https://doi.org/10.1039/B817242K.
[141] K. Saravanan, M.V. Reddy, P. Balaya, H. Gong, B.V.R. Chowdari, J.J. Vittal, Storage performance of $LiFePO_4$ nanoplates, J. Mater. Chem. 19 (2009) 605–610, https://doi.org/10.1039/B817242K.
[142] K. Saravanan, P. Balaya, M.V. Reddy, B.V.R. Chowdari, J.J. Vittal, Morphology-controlled synthesis of $LiFePO_4$/C nanoplates for Li-ion batteries, Energy Environ. Sci. 3 (2010) 457–463, https://doi.org/10.1039/B923576K.
[143] R. Schmuch, R. Wagner, G. Hörpel, T. Placke, M. Winter, Performance and cost of materials for lithium-based rechargeable automotive batteries, Nat. Energy 3 (2018) 267–278, https://doi.org/10.1038/s41560-018-0107-2.
[144] P. Benedek, N. Wenzler, M. Yarema, V.C. Wood, Low-temperature hydrothermal synthesis of battery-grade lithium iron phosphate, RSC Adv. 7 (2017) 17763–17767, https://doi.org/10.1039/C7RA00463J.
[145] V. Ramar, P. Balaya, Nanostructured olivine-based cathode materials for lithium-ion batteries, Mater. Matters 11 (2016) 23.
[146] V. Ramar, K. Saravanan, S.R. Gajjela, S. Hariharan, P. Balaya, The effect of synthesis parameters on the lithium storage performance of $LiMnPO_4$/C, Electrochim. Acta 105 (2013) 496–505, https://doi.org/10.1039/B817242K.
[147] V. Ramar, P. Balaya, Enhancing the electrochemical kinetics of high voltage olivine $LiMnPO_4$ by isovalent co-doping, Phys. Chem. Chem. Phys. 15 (2013) 17240–17249, https://doi.org/10.1039/C3CP52311J.
[148] C. Wang, J. Hong, Ionic/electronic conducting characteristics of $LiFePO_4$ cathode materials: the determining factors for high-rate performance, Electrochem. Solid-State Lett. 10 (2007) A65, https://doi.org/10.1149/1.2409768.
[149] C.S. Sun, Z. Zhou, Z.G. Xu, D.G. Wang, J.P. Wei, X.K. Bian, J. Yan, Improved high-rate charge/discharge performances of $LiFePO_4$/C via V-doping, J. Power Sources 193 (2009) 841–845, https://doi.org/10.1016/j.jpowsour.2009.03.061.
[150] D. Morgan, A. Van der Ven, G. Ceder, Li conductivity in Li_xMPO_4 (M = Mn, Fe, Co, Ni) olivine materials, Electrochem. Solid-State Lett. 7 (2003) A30, https://doi.org/10.1149/1.1633511.
[151] M.F. Sgroi, R. Lazzaroni, D. Beljonne, D. Pullini, Doping $LiMnPO_4$ with cobalt and nickel: a first-principle study, Batteries 3 (2017) 11, https://doi.org/10.3390/batteries3020011.
[152] K. Wang, R. Cai, T. Yuan, X. Yu, R. Ran, Z. Shao, Process investigation, electrochemical characterization, and optimization of $LiFePO_4$/C composite from mechanical activation using sucrose as carbon source, Electrochim. Acta 54 (2009) 2861–2868, https://doi.org/10.1016/j.electacta.2008.11.012.
[153] E.S. Lee, A. Huq, A. Manthiram, Understanding the effect of synthesis temperature on the structural and electrochemical characteristics of layered-spinel composite cathodes for lithium-ion batteries, J. Power Sources 240 (2013) 193–203, https://doi.org/10.1016/j.jpowsour.2013.04.010.
[154] L. Chen, X. Fan, E. Hu, X. Ji, J. Chen, S. Hou, T. Deng, J. Li, D. Su, X. Yang, C. Wang, Achieving high energy density through increasing the output voltage: a highly reversible 5.3 V battery, Chem 5 (2019) 896–912, https://doi.org/10.1016/j.chempr.2019.02.003.
[155] W. Yan-Zhuang, C. Ren-Fei, Y. Jin-Xing, W. Xiao-Hui, Progress in high-performance lithium iron phosphate for lithium ion batteries, Adv. Ceram. 45 (2024) 74–99, https://doi.org/10.16253/j.cnki.37-1226/tq.2024.01.006.
[156] S. Ji, J. Wang, Y. Zhao, B. Du, L. Xu, M. Guan, P. Lou, S. Tang, S. Cheng, Y. Cao, Recent advances of $LiFe_{1-y}Mn_yPO_4$ ($0 < y < 1$) cathode materials on performance optimization and sustainable preparation, Energy Mater. 5 (2025) 500013, https://doi.org/10.20517/energymater.2024.37.
[157] H. Guo, C. Wu, L. Liao, J. Xie, S. Zhang, P. Zhu, G. Cao, X. Zhao, Performance improvement of lithium manganese phosphate by controllable morphology tailoring with acid-engaged nanoengineering, Inorg. Chem. 54 (2015) 667–674, https://doi.org/10.1021/ic5026075.
[158] F. Yu, L. Zhang, M. Zhu, Y. An, L. Xia, X. Wang, B. Dai, Overwhelming microwave irradiation assisted synthesis of olivine-structured $LiMPO_4$ (M = Fe, Mn, Co, and Ni) for Li-ion batteries, Nano Energy 3 (2014) 64–79, https://doi.org/10.1016/j.nanoen.2013.10.011.
[159] D. Choi, J. Xiao, Y.J. Choi, J.S. Hardy, M. Vijayakumar, M.S. Bhuvaneswari, J. Liu, W. Xu, W. Wang, Z. Yang, G.L. Graff, Thermal stability and phase transformation of electrochemically charged/discharged $LiMnPO_4$ cathode for Li-ion batteries, Energy Environ. Sci. 4 (2011) 4560–4566, https://doi.org/10.1039/C1EE01501J.
[160] T. Ohzuku, Y. Makimura, Layered lithium insertion material of $LiCo_{1/3}Ni_{1/3}Mn_{1/3}O_2$ for lithium-ion batteries, Chem. Lett. 30 (2001) 642–643, https://doi.org/10.1246/cl.2001.642.
[161] H.J. Noh, S. Youn, C.S. Yoon, Y.K. Sun, Comparison of the structural and electrochemical properties of layered $Li[Ni_xCo_yMn_z]O_2$ (x = 1/3, 0.5, 0.6, 0.7,

0.8, and 0.85) cathode material for lithium-ion batteries, J. Power Sources 233 (2013) 121–130, https://doi.org/10.1016/j.jpowsour.2013.01.063.
[162] N. Tolganbek, Y. Yerkinbekova, S. Kalybekkyzy, Z. Bakenov, A. Mentbayeva, Current state of high voltage olivine structured $LiMPO_4$ cathode materials for energy storage applications: a review, J. Alloys Compd. 882 (2021) 160774, https://doi.org/10.1016/j.jallcom.2021.160774.
[163] L.H. Hu, F.Y. Wu, C.T. Lin, A.N. Khlobystov, L.J. Li, Graphene-modified $LiFePO_4$ cathode for lithium-ion battery beyond theoretical capacity, Nat. Commun. 4 (2013) 1–7, https://doi.org/10.1038/ncomms2705.
[164] V. Aravindan, J. Gnanaraj, Y.S. Lee, S. Madhavi, $LiMnPO_4$—a next-generation cathode material for lithium-ion batteries, J. Mater. Chem. A 1 (2013) 3518–3539, https://doi.org/10.1039/C2TA01393B.
[165] J. Liu, X. Liu, T. Huang, A. Yu, Synthesis of nano-sized $LiMnPO_4$ and in situ carbon coating using a solvothermal method, J. Power Sources 229 (2013) 203–209, https://doi.org/10.1016/j.jpowsour.2012.11.093.
[166] C.L. Hu, H.H. Yi, F.X. Wang, S.Y. Xiao, Y.P. Wu, D. Wang, D.L. He, Boron doping at P-site to improve electrochemical performance of $LiMnPO_4$ as cathode for lithium-ion battery, J. Power Sources 255 (2014) 355–359, https://doi.org/10.1016/j.jpowsour.2013.12.040.
[167] H. Ji, G. Yang, H. Ni, S. Roy, J. Pinto, X. Jiang, General synthesis and morphology control of $LiMnPO_4$ nanocrystals via microwave-hydrothermal route, Electrochim. Acta 56 (2011) 3093–3100, https://doi.org/10.1016/j.electacta.2011.01.079.
[168] H. Xu, J. Zong, F. Ding, Z.W. Lu, W. Li, X.J. Liu, Effects of Fe^{2+} ion doping on $LiMnPO_4$ nanomaterial for lithium-ion batteries, RSC Adv. 6 (2016) 27164–27169, https://doi.org/10.1039/C6RA02977A.
[169] B.N. Rao, P.R. Kumar, O. Padmaraj, M. Venkateswarlu, N. Satyanarayana, Rapid microwave-assisted hydrothermal synthesis of porous α-Fe_2O_3 nanostructures as stable and high-capacity negative electrodes for lithium and sodium-ion batteries, RSC Adv. 5 (2015) 34761–34768, https://doi.org/10.1039/C5RA03238E.
[170] B.N. Rao, O. Padmaraj, D. Narsimulu, M. Venkateswarlu, N. Satyanarayana, AC conductivity and dielectric properties of spinel $LiMn_2O_4$ nanorods, Ceram. Int. 41 (2015) 14070–14077, https://doi.org/10.1016/j.ceramint.2015.07.026.
[171] J. Wang, J. Tu, H. Lei, H. Zhu, The effect of graphitization degree of carbonaceous material on the electrochemical performance for aluminum-ion batteries, RSC Adv. 9 (2019) 38990–38997, https://doi.org/10.1039/C9RA07234A.
[172] R.M. German, S.J. Park, Handbook of Mathematical Relations in Particulate Materials Processing: Ceramics, Powder Metals, Cermets, Carbides, Hard Materials, and Minerals vol. 3, John Wiley & Sons, 2008, https://doi.org/10.1002/9780470370087.
[173] N.H. Kwon, H. Yin, T. Vavrova, J.H. Lim, U. Steiner, B. Grobéty, K.M. Fromm, Nanoparticle shapes of $LiMnPO_4$, Li^+ diffusion orientation, and diffusion coefficients for high volumetric energy Li^+ ion cathodes, J. Power Sources 342 (2017) 231–240, https://doi.org/10.1016/j.jpowsour.2016.11.111.
[174] B. Zhao, R. Ran, M. Liu, Z. Shao, A comprehensive review of $Li_4Ti_5O_{12}$-based electrodes for lithium-ion batteries: the latest advancements and future perspectives, Mater. Sci. Eng. R. Rep. 98 (2015) 1–71, https://doi.org/10.1016/j.mser.2015.10.001.
[175] T. Doi, S. Yatomi, T. Kida, S. Okada, J.I. Yamaki, Liquid-phase synthesis of uniformly nanosized $LiMnPO_4$ particles and their electrochemical properties for lithium-ion batteries, Cryst. Growth Des. 9 (2009) 4990–4992, https://doi.org/10.1021/cg900452a.
[176] S. Zhang, F.L. Meng, Q. Wu, F.L. Liu, H. Gao, M. Zhang, C. Deng, Synthesis and characterization of $LiMnPO_4$ nanoparticles prepared by a citric acid-assisted sol-gel method, Int. J. Electrochem. Sci. 8 (2013) 6603–6609, https://doi.org/10.1016/S1452-3981(23)14790-0.
[177] T.A. Wani, G. Suresh, A comprehensive review of $LiMnPO_4$ based cathode materials for lithium-ion batteries: current strategies to improve its performance, J. Energy Storage 44 (2021) 103307, https://doi.org/10.1016/j.est.2021.103307.
[178] M. Massot, K. Zaghib, A. Mauger, F. Gendron, C.M. Julien, Characterization of the carbon-coating of $LiFePO_4$ by transmission electron microscopy and Raman spectroscopy, OPL 972 (2006), https://doi.org/10.1557/PROC-0972-AA13-07, 0972-AA13.
[179] M.L. Trudeau, D. Laul, R. Veillette, A.M. Serventi, A. Mauger, C.M. Julien, K. Zaghib, In situ high-resolution transmission electron microscopy synthesis observation of nanostructured carbon-coated $LiFePO_4$, J. Power Sources 196 (2011) 7383–7394, https://doi.org/10.1016/j.jpowsour.2011.04.003.
[180] N. Ravet, M. Gauthier, K. Zaghib, M.A. Goodenough, A. Mauger, F.J. Gendron, Mechanism of the Fe^{3+} reduction at low temperature for $LiFePO_4$ synthesis from a polymeric additive, Chem. Mater. 19 (2007) 2595–2602, https://doi.org/10.1021/cm070485r.
[181] Y. Mizuno, M. Kotobuki, H. Munakata, K. Kanamura, Effect of carbon source on electrochemical performance of carbon-coated $LiMnPO_4$ cathode, JCS Jpn. 117 (2009) 1225–1228, https://doi.org/10.2109/jcersj2.117.1225.
[182] L.E. Li, J. Liu, L. Chen, H. Xu, J. Yang, Y. Qian, Effect of different carbon sources on the electrochemical properties of rod-like $LiMnPO_4$–C nanocomposites, RSC Adv. 3 (2013) 6847–6852, https://doi.org/10.1016/j.jallcom.2014.06.050.
[183] J. Fan, Y. Yu, Y. Wang, Q.H. Wu, M. Zheng, Q. Dong, Nonaqueous synthesis of nano-sized $LiMnPO_4$@C as a cathode material for high-performance lithium-ion batteries, Electrochim. Acta 194 (2016) 52–58, https://doi.org/10.1016/j.electacta.2016.02.090.
[184] S. Moon, P. Muralidharan, D.K. Kim, Carbon coating by high-energy milling and electrochemical properties of $LiMnPO_4$ obtained in polyol process, Ceram. Int. 38 (2012) S471–S475, https://doi.org/10.1016/j.ceramint.2011.05.042.
[185] J. Liu, D. Hu, T. Huang, A. Yu, Synthesis of flower-like $LiMnPO_4$/C with precipitated $NH_4MnPO_4{\cdot}H_2O$ as precursor, J. Alloys Compd. 518 (2012) 58–62, https://doi.org/10.1016/j.jallcom.2011.12.134.
[186] S. Aono, K. Urita, H. Yamada, I. Moriguchi, Rapid synthesis, and charge–discharge properties of $LiMnPO_4$ nanocrystallite-embedded porous carbons, Chem. Lett. 41 (2012) 162–164, https://doi.org/10.1246/cl.2012.162.
[187] T.N.L. Doan, I. Taniguchi, Cathode performance of $LiMnPO_4$/C nanocomposites prepared by a combination of spray pyrolysis and wet ball-milling followed by heat treatment, J. Power Sources 196 (2011) 1399–1408, https://doi.org/10.1016/j.jpowsour.2010.08.067.
[188] F. Wang, J. Yang, P. Gao, Y. NuLi, J. Wang, Morphology regulation and carbon coating of $LiMnPO_4$ cathode material for enhanced electrochemical performance, J. Power Sources 196 (2011) 10258–10262, https://doi.org/10.1016/j.jpowsour.2011.08.090.
[189] M. Zhao, Y. Fu, N. Xu, G. Li, M. Wu, X. Gao, High-performance $LiMnPO_4$/C prepared by a crystallite size control method, J. Mater. Chem. A 2 (2014) 15070–15077, https://doi.org/10.1039/C4TA03311F.
[190] Y. Yu, H. Zhao, Y. Chen, Z.K. Feng, X. Liu, H. Yang, Double carbon coated $LiCoPO_4$ nano composite as high-performance cathode for lithium-ion batteries, Trends Renew. Energy 6 (2020) 1–11, https://doi.org/10.17737/tre.2020.6.1.00108.
[191] Y. Maeyoshi, S. Miyamoto, Y. Noda, H. Munakata, K. Kanamura, Effect of organic additives on characteristics of carbon-coated $LiCoPO_4$ synthesized by hydrothermal method, J. Power Sources 337 (2017) 92–99, https://doi.org/10.1016/j.jpowsour.2016.10.106.
[192] A. Örnek, Influences of different reaction mediums on the properties of high-voltage $LiNiPO_4$@ C cathode material in terms of dielectric heating efficiency, Electrochim. Acta 258 (2017) 524–534, https://doi.org/10.1016/j.electacta.2017.11.095.
[193] A. Örnek, M.Z. Kazancioglu, A novel and effective strategy for producing core-shell $LiNiPO_4$/C cathode material for excellent electrochemical stability using a long-time and low-level microwave approach, Scr. Mater. 122 (2016) 45–49, https://doi.org/10.1016/j.scriptamat.2016.05.022.
[194] Y. Zhang, Y. Pan, J. Liu, G. Wang, D. Cao, Synthesis and electrochemical studies of carbon-modified $LiNiPO_4$ as the cathode material of Li-ion batteries, Chem. Res. Chin. Univ. 31 (2015) 117–122, https://doi.org/10.1007/s40242-015-4261-9.
[195] V. Koleva, E. Zhecheva, R. Stoyanova, A new phosphate-formate precursor method for the preparation of carbon-coated nano-crystalline $LiFePO_4$, J. Alloys Compd. 476 (2009) 950–957, https://doi.org/10.1016/j.jallcom.2008.09.144.
[196] S.M. Oh, S.W. Oh, C.S. Yoon, B. Scrosati, K. Amine, Y.K. Sun, High-performance carbon-$LiMnPO_4$ nanocomposite cathode for lithium batteries, Adv. Funct. Mater. 20 (2010) 3260–3265, https://doi.org/10.1002/adfm.201000469.
[197] V. Koleva, R. Stoyanova, E. Zhecheva, Nano-crystalline $LiMnPO_4$ prepared by a new phosphate–formate precursor method, Mater. Chem. Phys. 121 (2010) 370–377, https://doi.org/10.1016/j.matchemphys.2010.01.043.
[198] K. Su, F. Liu, J. Chen, Preparation of high-performance carbon-coated $LiMnPO_4$ nanocomposite by an acetate-assisted antisolvent precipitation method, J. Power Sources 232 (2013) 234–239, https://doi.org/10.1016/j.jpowsour.2013.01.054.
[199] H.C. Dinh, S.I. Mho, Y. Kang, I.H. Yeo, Large discharge capacities at high current rates for carbon-coated $LiMnPO_4$ nanocrystalline cathodes, J. Power Sources 244 (2013) 189–195, https://doi.org/10.1016/j.jpowsour.2013.01.191.
[200] Y. Hong, Z. Tang, S. Wang, W. Quan, Z. Zhang, High-performance LiMnPO4 nanorods synthesized via a facile EG-assisted solvothermal approach, Mater. Chem. A 3 (2015) 10267–10274, https://doi.org/10.1039/C5TA01218J.
[201] B. Huang, X. Zheng, X. Fan, G. Song, M. Lu, Enhanced rate performance of nano–micro structured $LiFePO_4$/C by improved process for high-power Li-ion batteries, Electrochim. Acta 56 (2011) 4865–4868, https://doi.org/10.1016/j.electacta.2011.02.118.
[202] Y. Wang, P. He, H. Zhou, Olivine $LiFePO_4$: development and future, Energy Environ. Sci. 4 (2011) 805–817, https://doi.org/10.1039/C0EE00176G.
[203] C.A. Fisher, V.M.H. Prieto, M.S. Islam, Lithium battery materials $LiMPO_4$ (M = Mn, Fe, Co, and Ni): insights into defect association, transport mechanisms, and doping behavior, Chem. Mater. 20 (2008) 5907–5915, https://doi.org/10.1021/cm801262x.
[204] S. Yufeng, S. Cheng, F. Yi-Bin, L. Zhi-Pan, G. Xin-Gao, Y. Ji-Hui, Diffusion behaviors of lithium ions at the cathode/electrolyte interface from a global neural network potential, J. Mater. Chem. A 12 (2024) 33808–33817, https://doi.org/10.1039/D4TA05530F.
[205] J. Molenda, W. Ojczyk, K. Świerczek, W. Zając, F. Krok, J. Dygas, R.S. Liu, Diffusional mechanism of deintercalation in $LiFe_{1-y}Mn_yPO_4$ cathode material, Solid State Ionics 177 (2006) 2617–2624, https://doi.org/10.1016/j.ssi.2006.03.047.
[206] C.A. Fisher, M.S. Islam, Surface structures and crystal morphologies of $LiFePO_4$: relevance to electrochemical behavior, J. Mater. Chem. A 18 (2008) 1209–1215, https://doi.org/10.1039/B715935H.
[207] K. Dokko, S. Koizumi, H. Nakano, K. Kanamura, Particle morphology, crystal orientation, and electrochemical reactivity of $LiFePO_4$ synthesized by the hydrothermal method at 443 K, J. Mater. Chem. A 17 (2007) 4803–4810, https://doi.org/10.1039/B711521K.
[208] M.S. Islam, A.J.F. Craig, Lithium and sodium battery cathode materials: computational insights into voltage, diffusion and nanostructural properties, Chem. Mater. 26 (2014) 471–482, https://doi.org/10.1039/C3CS60199D.
[209] G. Liang, K. Park, J. Li, R.E. Benson, D. Vaknin, J.T. Markert, M.C. Croft, Anisotropy in magnetic properties and electronic structure of single-crystal $LiFePO_4$, Phys. Rev. B 77 (2008) 064414, https://doi.org/10.1103/PhysRevB.77.064414.

[210] R. Amin, P. Balaya, J. Maier, Anisotropy of electronic and ionic transport in $LiFePO_4$ single crystals, Electrochem. Solid-State Lett. 10 (2006) A13, https://doi.org/10.1149/1.2388240.
[211] (a) S. Aggarwal, J. Töpfer, T.L. Tsai, R. Dieckmann, Point defects and transport in binary and ternary, non-stoichiometric oxides, Solid State Ion 101 (1997) 321–331, https://doi.org/10.1016/S0167-2738(97)84048-9;
(b) K. Ullrich, K.D. Becker, Kinetics and diffusion of defects in fayalite, Fe_2SiO_4, Solid State Ionics 141 (2001) 307–312, https://doi.org/10.1016/S0167-2738(01)00796-2.
[212] C. Delacourt, C. Wurm, L. Laffont, J.B. Leriche, C. Masquelier, Electrochemical and electrical properties of Nb- and/or C-containing $LiFePO_4$ composites, Solid State Ionics 177 (2006) 333–341, https://doi.org/10.1016/j.ssi.2005.11.003.
[213] N. Ravet, A. Abouimrane, M. Armand, On the electronic conductivity of phospho-olivines as lithium storage electrodes, Nat. Mater. 2 (2003) 702, https://doi.org/10.1038/nmat1009a.
[214] P.S. Herle, B. Ellis, N. Coombs, L.F. Nazar, Nano-network electronic conduction in iron and nickel olivine phosphates, Nat. Mater. 3 (2004) 147–152, https://doi.org/10.1038/nmat1063.
[215] B.L. Ellis, K.T. Lee, L.F. Nazar, Positive electrode materials for Li-ion and Li-batteries, Chem. Mater. 22 (2010) 691–714, https://doi.org/10.1021/cm902696j.
[216] G.C. Mather, M.S. Islam, F.M. Figueiredo, Atomistic study of a $CaTiO_3$-based mixed conductor: defects, nanoscale clusters, and oxide-ion migration, Adv. Funct. Mater. 17 (2007) 905–912, https://doi.org/10.1002/adfm.200600632.
[217] J.R. Tolchard, P.R. Slater, M.S. Islam, Insight into doping effects in apatite silicate ionic conductors, Adv. Funct. Mater. 17 (2007) 2564–2571, https://doi.org/10.1002/adfm.200600789.
[218] J. Wolfenstine, Electrical conductivity of doped $LiCoPO_4$, J. Power Sources 158 (2006) 1431–1435, https://doi.org/10.1016/j.jpowsour.2005.10.072.
[219] X.Y. Chang, Z.X. Wang, X.H. Li, L. Zhang, H.J. Guo, W.J. Peng, Synthesis and performance of $LiMn_{0.7}Fe_{0.3}PO_4$ cathode material for lithium-ion batteries, Mater. Res. Bull. 40 (2005) 1513–1520, https://doi.org/10.1016/j.materresbull.2005.04.020.
[220] C.M. Burba, R. Frech, Local structure in the Li-ion battery cathode material $Li_x(Mn_yFe_{1-y})$ PO_4 for $0 < x \leq 1$ and $y = 0.0$, 0.5 and 1.0, J. Power Sources 172 (2007) 870–876, https://doi.org/10.1016/j.jpowsour.2007.05.075.
[221] A. Nytén, J.O. Thomas, A neutron powder diffraction study of $LiCo_xFe_{1-x}PO_4$ for $x = 0$, 0.25, 0.40, 0.60, and 0.75, Solid State Ion 177 (2006) 1327–1330, https://doi.org/10.1016/j.ssi.2006.05.019.
[222] J. Chen, M.J. Vacchio, S. Wang, N. Chernova, P.Y. Zavalij, M.S. Whittingham, The hydrothermal synthesis and characterization of olivines and related compounds for electrochemical applications, Solid State Ionics 178 (2008) 1676–1693, https://doi.org/10.1016/j.ssi.2007.10.015.
[223] G. Chen, J.D. Wilcox, T.J. Richardson, Improving the performance of lithium manganese phosphate through divalent cation substitution, Electrochem. Solid-State Lett. 11 (2008) A190, https://doi.org/10.1149/1.2971169.
[224] M.R. Roberts, G. Vitins, J.R. Owen, High-throughput studies of $Li_{1-x}Mg_{x/2}FePO_4$ and $LiFe_{1-y}Mg_yPO_4$ and the effect of carbon coating, J. Power Sources 179 (2008) 754–762, https://doi.org/10.1016/j.jpowsour.2008.01.034.
[225] J. Maier, R. Amin, Defect chemistry of $LiFePO_4$, J. Electrochem. Soc. 155 (2008) A339, https://doi.org/10.1149/1.2839626.
[226] G. Butt, N. Sammes, G. Tompsett, A. Smirnova, O. Yamamoto, Raman spectroscopy of superionic Ti-doped $Li_3Fe_2(PO_4)_3$ and $LiNiPO_4$ structures, J. Power Sources 134 (2004) 72–79, https://doi.org/10.1016/j.jpowsour.2004.01.053.
[227] D.H. Snydacker, C. Wolverton, Transition-metal mixing and redox potentials in $Li_x(M_{1-y}M'_y)PO_4$ (M, M′ = Mn, Fe, Ni) olivine materials from first-principles calculations, J. Phys. Chem. C 120 (2016) 5932–5939, https://doi.org/10.1021/acs.jpcc.6b00575.
[228] M. Köntje, M. Memm, P. Axmann, M. Wohlfahrt-Mehrens, Substituted transition metal phospho olivines $LiMM'PO_4$ (M = Mn, M′ = Fe, Co, Mg): optimisation routes for $LiMnPO_4$, Prog. Solid State Chem. 42 (2014) 106–117, https://doi.org/10.1016/j.progsolidstchem.2014.04.005.
[229] N. Bai, C. Li, H. Lu, K. Xiang, H. Chen, $LiFePO_4$/C composite with a three-dimensional foam structure constructed via evaporative self-assembly assisted by polyethylene glycol and its improved electrochemical performance, Mater. Lett. 137 (2014) 237–240, https://doi.org/10.1016/j.matlet.2014.09.009.
[230] R. Malik, D. Burch, M. Bazant, G. Ceder, Particle size dependence of the ionic diffusivity, Nano Lett. 10 (2010) 4123–4127, https://doi.org/10.1021/nl1023595.
[231] P.P. Prosini, M. Lisi, D. Zane, M. Pasquali, Determination of the chemical diffusion coefficient of lithium in $LiFePO_4$, Solid State Ionics 148 (2002) 45–51, https://doi.org/10.1016/S0167-2738(02)00134-0.
[232] D. Fujimoto, N. Kuwata, Y. Matsuda, J. Kawamura, F. Kang, Fabrication of solid-state thin-film batteries using $LiMnPO_4$ thin films deposited by pulsed laser deposition, Thin Solid Films 579 (2015) 81–88, https://doi.org/10.1016/j.tsf.2015.02.041.
[233] D. Choi, D. Wang, I.T. Bae, J. Xiao, Z. Nie, W. Wang, V.V. Viswanathan, Y.J. Lee, J.G. Zhang, G.L. Graff, Z. Yang, $LiMnPO_4$ nanoplate grown via solid-state reaction in molten hydrocarbon for Li-ion battery cathode, Nano Lett. 10 (2010) 2799–2805, https://doi.org/10.1021/nl1007085.
[234] N.H. Kwon, T. Drezen, I. Exnar, I. Teerlinck, M. Isono, M. Graetzel, Enhanced electrochemical performance of mesoparticulate $LiMnPO_4$ for lithium-ion batteries, Electrochem. Solid-State Lett. 9 (2006) A277, https://doi.org/10.1149/1.2191432.
[235] A.V. Murugan, T. Muraliganth, P.J. Ferreira, A. Manthiram, Dimensionally modulated, single-crystalline $LiMPO_4$ (M = Mn, Fe, Co, and Ni) with nano-thumblike shapes for high-power energy storage, Inorg. Chem. 48 (2009) 946–952, https://doi.org/10.1021/ic8015723.
[236] K. Amine, H. Yasuda, M. Yamachi, Olivine $LiCoPO_4$ as 4.8 V electrode material for lithium batteries, Electrochem. Solid-State Lett. 3 (2000) 178, https://doi.org/10.1149/1.1390994.
[237] J. Xie, N. Imanishi, T. Zhang, A. Hirano, Y. Takeda, O. Yamamoto, Li-ion diffusion kinetics in $LiCoPO_4$ thin films deposited on NASICON-type glass-ceramic electrolytes by magnetron sputtering, J. Power Sources 192 (2009) 689–692, https://doi.org/10.1016/j.jpowsour.2009.03.001.
[238] F. Zhou, M. Cococcioni, K. Kang, G. Ceder, The Li intercalation potential of $LiMPO_4$ and $LiMSiO_4$ olivines with M = Fe, Mn, Co, Ni, Electrochem. Commun. 6 (2004) 1144–1148, https://doi.org/10.1016/j.elecom.2004.09.007.
[239] L. Dimesso, C. Spanheimer, W. Jaegermann, Effect of the Mg-substitution on the graphitic carbon foams—$LiNi_{1-y}Mg_yPO_4$ composites as possible cathode materials for 5 V applications, Mater. Res. Bull. 48 (2013) 559–565, https://doi.org/10.1016/j.materresbull.2012.11.050.
[240] L. Dimesso, D. Becker, C. Spanheimer, W. Jaegermann, Investigation of graphitic carbon foams/$LiNiPO_4$ composites, J. Solid State Electrochem. 16 (2012) 3791–3798, https://doi.org/10.1007/s10008-012-1817-1.
[241] M.B. Bechir, A.B. Rhaiem, K. Guidara, Ac conductivity and dielectric study of $LiNiPO_4$ synthesized by the solid-state method, Bull. Mater. Sci. 37 (2014) 473–480, https://doi.org/10.1007/s12034-014-0685-y.
[242] N. Membreño, K. Park, J.B. Goodenough, K.J. Stevenson, Electrode/electrolyte interface of composite α-$Li_3V_2(PO_4)_3$ cathodes in a nonaqueous electrolyte for lithium-ion batteries and the role of the carbon additive, Chem. Mater. 27 (2015) 3332–3340, https://doi.org/10.1021/acs.chemmater.5b00447.
[243] X. Rui, Q. Yan, M. Skyllas-Kazacos, T.M. Lim, Li_3V_2 $(PO_4)_3$ cathode materials for lithium-ion batteries: a review, J. Power Sources 258 (2014) 19–38, https://doi.org/10.1016/j.jpowsour.2014.01.126.
[244] S.C. Yin, H. Grondey, P. Strobel, M. Anne, L.F. Nazar, Electrochemical property: structure relationships in monoclinic $Li_{3-y}V_2$ $(PO_4)_3$, J. Am. Chem. Soc. 125 (2003) 10402–10411, https://doi.org/10.1021/ja034565h.
[245] X.H. Rui, N. Ding, J. Liu, C. Li, C.H. Chen, Analysis of the chemical diffusion coefficient of lithium ions in Li_3V_2 $(PO_4)_3$ cathode material, Electrochim. Acta 55 (2010) 2384–2390, https://doi.org/10.1016/j.electacta.2009.11.096.
[246] S.W. Kim, J. Kim, H. Gwon, K. Kang, Phase stability study of $Li_{1-x}MnPO_4$ ($0 \leq x \leq 1$) cathode for Li rechargeable battery, JES 156 (2009) A635, https://doi.org/10.1149/1.3138705.
[247] V. Aravindan, J. Gnanaraj, Y.S. Lee, S. Madhavi, $LiMnPO_4$—a next-generation cathode material for lithium-ion batteries, J. Mater. Chem. A 1 (2013) 3518–3539, https://doi.org/10.1039/C2TA01393B.
[248] A. Yamada, Y. Kudo, Y.K. Liu, Phase diagram of $Li_x(Mn_yFe_{1-y})$ PO_4 ($0 \leq x, y \leq 1$), JES 148 (2001) A1153, https://doi.org/10.1149/1.1401083.
[249] C. Delacourt, P. Poizot, M. Morcrette, J.M. Tarascon, C. Masquelier, One-step low-temperature route for the preparation of electrochemically active $LiMnPO_4$ powders, Chem. Mater. 16 (2004) 93–99, https://doi.org/10.1021/cm030347b.
[250] S.P. Ong, V.L. Chevrier, G. Ceder, Comparison of small polaron migration and phase separation in olivine $LiMnPO_4$ and $LiFePO_4$ using hybrid density functional theory, PRB 83 (2011) 075112, https://doi.org/10.1103/PhysRevB.83.075112.
[251] W. Li, B. Song, A. Manthiram, High-voltage positive electrode materials for lithium-ion batteries, Chem. Soc. Rev. 46 (2017) 3006–3059, https://doi.org/10.1039/c6cs00875e.
[252] L. Liao, H. Wang, H. Guo, P. Zhu, J. Xie, C. Jin, S. Zhang, G. Cao, T. Zhu, X. Zhao, Facile solvothermal synthesis of ultrathin $LiFe_xMn_{1-x}PO_4$ nanoplates as advanced cathodes with long cycle life and superior rate capability, J. Mater. Chem. A 3 (2015) 19368–19375, https://doi.org/10.1039/C5TA05358G.
[253] X. Chen, C. Xusen, L. Xihao, Q. Dongmei, L. Jin-Hang, H. Yan, Z. Changchao, Z. Hang, Yun Gao, X. Yao Xiao, Suppressing Jahn-Teller distortion and accelerating ion kinetics via heterostructure engineering for stable aqueous zinc-ion batteries, Chem. Eng. J. 526 (2025) 170760, https://doi.org/10.1016/j.cej.2025.170760.
[254] Y. Chen, X. Hu, X. Chen, J.H. Liu, Y. Huang, D. Cao, Trimetallic-organic framework-derived Ni-doped MnO/PC as cathodes for high-performance aqueous zinc-ion batteries, Chem. Eng. J. 478 (2023) 147411, https://doi.org/10.1016/j.cej.2023.147411.
[255] X. Hu, Y. Chen, X.Y. Chen, Z. Li, Y. Huang, L. Deng, D. Cao, Synergistic H^+/Zn^{2+} co-insertion mechanism in vanadium trioxide composited on carbon nanotubes cathode for aqueous zinc ion batteries, J. Alloys Compd. 945 (2023) 169271, https://doi.org/10.1016/j.jallcom.2023.169271.
[256] X. Chen, X. Hu, Y. Chen, X. Cao, Y. Huang, H. Zhang, J.H. Liu, Y. Wang, S.L. Chou, D. Cao, Ultrastable hydrated vanadium dioxide cathodes for high-performance aqueous zinc ion batteries with H^+/Zn^{2+} co-insertion mechanism, J. Mater. Chem. A 10 (2022) 22194–22204, https://doi.org/10.1039/D2TA07101K.
[257] Y. Wang, Y. Fan, X. Chen, J.H. Liu, Y. Gao, X. Lin, Y. Huang, H. Jiang, C. Zhan, H. Zhang, X. Cao, Synergistic effects of structural and electronic dual engineering for ultra-stable aqueous zinc-ion batteries, InfoMat 7 (2025) e70055, https://doi.org/10.1002/inf2.70055.
[258] T.A. Hamdalla, A.M. Aboraia, V.V. Shapovalov, A.A. Guda, N.V. Kosova, O. A. Podgornova, A.A.A. Darwish, S.A. Al-Ghamdi, S. Alfadhli, A.M. Alatawi, A. Soldatov, Synchrotron-based operando X-ray diffraction and X-ray absorption spectroscopy study of $LiCo_{0.5}Fe_{0.5}PO_4$ mixed d-metal olivine cathode, Sci. Rep. 13 (2023) 2169, https://doi.org/10.1038/s41598-023-28951-z.
[259] A.P. Black, A. Sorrentino, F. Fauth, I. Yousef, L. Simonelli, C. Frontera, A. Ponrouch, D. Tonti, M.R. Palacín, Synchrotron radiation-based operando

characterization of battery materials, Chem. Sci. 14 (2023) (2023) 1641–1665, https://doi.org/10.1039/D2SC04397A.
[260] H. Bian, Q. Ge, H. Xu, A. Wang, Q. Zhao, D. Li, D. Sun, Synergistic H^+/Zn^{2+} insertion mechanism in N/Co co-doped $H_xV_2O_5$ film electrodes for aqueous zinc-ion batteries, J. Alloys Compd. 1053 (2026) 186128, https://doi.org/10.1016/j.jallcom.2026.186128.
[261] W. Dachraoui, R. Erni, In situ liquid-cell transmission electron microscopy insights into lithium-ion battery materials degradation: challenges and emerging solutions, Adv. Sci. 0 (2026) e21842, https://doi.org/10.1002/advs.202521842.
[262] S. Awasthi, S. Moharana, V. Kumar, N. Wang, E. Chmanehpour, A.D. Sharma, S. K. Tiwari, V. Kumar, Y.K. Mishra, Progress in doping and crystal deformation for polyanions cathode based lithium-ion batteries, Nano Mater. Sci. 6 (2024) 504–535, https://doi.org/10.1016/j.nanoms.2024.01.004.
[263] M. Ma, M. Zhang, B. Jiang, Y. Du, B. Hu, C. Sun, A review of all-solid-state electrolytes for lithium batteries: high-voltage cathode materials, solid-state electrolytes and electrode-electrolyte interfaces, Mater. Chem. Front. 7 (2023) 1268–1297, https://doi.org/10.1039/D2QM01071B.
[264] I. Kurmanbayeva, L. Rakhymbay, K. Korzhynbayeva, A. Adi, D. Batyrbekuly, A. Mentbayeva, Z. Bakenov, Tetrapropylammonium hydroxide as a zinc dendrite growth suppressor for rechargeable aqueous battery, Front. Energy Res. 8 (2020) 1–10, https://doi.org/10.3389/fenrg.2020.599009.
[265] R. Kate, H. Jadhav, Ujjwala V. Kawade, Kaustav Bhattacharjee, Milind V. Kulkarni, R.J. Deokate, Bharat B. Kale, R. Kalubarme, Critical review of the recent progress and challenges of polyanion $Na_3V_2(PO_4)_3$ cathode materials in rechargeable sodium-ion batteries, J. Mater. Chem. A 12 (2024) 7418–7451, https://doi.org/10.1039/D3TA07545A.
[266] S. Kalybekkyzy, A. Mentbayeva, Y. Yerkinbekova, N. Baikalov, M.V. Kahraman, Z. Bakenov, Electrospun 3D structured carbon current collector for Li/S batteries, Nanomaterials Basel Switz. 10 (2020) 745, https://doi.org/10.3390/nano10040745.
[267] S. Kalybekkyzy, A. Mentbayeva, M.V. Kahraman, Y. Zhang, Z. Bakenov, Flexible S/DPAN/KB nanofiber composite as binder-free cathodes for Li-S batteries, J. Electrochem. Soc. 166 (2019) A5396–A5402, https://doi.org/10.1149/2.0571903jes.
[268] S. Kalybekkyzy, A.F. Kopzhassar, M.V. Kahraman, A. Mentbayeva, Z. Bakenov, Fabrication of UV-crosslinked flexible solid polymer electrolyte with pdms for Li-ion batteries, Polymers Basel 23 (2021) 1–12, https://doi.org/10.3390/polym13010015.
[269] N. Tolganbek, A. Mentbayeva, N. Serik, N. Batyrgali, M. Naizakarayev, K. Kanamura, Z. Bakenov, Design and preparation of thin film gel polymer electrolyte for 3D Li-ion battery, J. Power Sources 493 (2021) 229686, https://doi.org/10.1016/j.jpowsour.2021.229686.
[270] N. Tolganbek, A. Mentbayeva, B. Uzakbaiuly, K. Kanamura, Z. Bakenov, $Li_{1+x}Al_xTi_{2-x}(PO_4)_3$, NASICON-type solid electrolyte fabrication with different methods, Mater. Today Proc. 25 (2019) 97–100, https://doi.org/10.1016/j.matpr. 2019.12.279.
[271] N. Tolganbek, Y. Yerkinbekova, A. Khairullin, Z. Bakenov, K. Kanamura, A. Mentbayeva, Enhancing purity and ionic conductivity of NASICON-typed $Li_{1.3}Al_{0.3}Ti_{1.7}(PO_4)_3$ solid electrolyte, Ceram. Int. (2021) 1–8, https://doi.org/10.1016/j.ceram.